Cell blebbing in Confined Microfluidic Environments

by

Markela Ibo

A dissertation submitted to the Johns Hopkins University in conformity with the requirements for the degree of Doctor of Philosophy of Chemical and Biomolecular Engineering

Baltimore, Maryland

March 2017

ABSTRACT

Migrating cells can extend their leading edge by forming myosin-driven blebs and F-actin driven pseudopods. When coerced to migrate in resistive environments, *Dictyostelium* cells switch from using predominately pseudopods to blebs. Bleb formation has been shown to be chemotactic and can be influenced by the direction of the chemotactic gradient. In this study, we determine the blebbing responses of developed cells of *Dictyostelium discoideum* to cAMP gradients of varying steepness produced in microfluidic channels with different confining heights, ranging between 1.7 μm and 3.8 μm. We show that microfluidic confinement height, gradient steepness, buffer osmolarity and Myosin II activity are important factors in determining whether cells migrate with blebs or with pseudopods. *Dictyostelium* cells were observed migrating within the confines of microfluidic gradient channels. When the cAMP gradient steepness is increased from 0.7 nM/μm to 20 nM/μm, cells switch from moving with a mixture of blebs and pseudopods to moving only using blebs when chemotaxing in channels with confinement heights less than 2.4 μm. Furthermore, the size of the blebs increases with gradient steepness and correlates with increases in myosin-II localization at the cell cortex. Reduction of intracellular pressure by high osmolarity buffer or inhibition of myosin-II by blebbistatin leads to a decrease in bleb formation and bleb size. Together, our data reveal that the protrusion type formed by migrating cells can be influenced by the channel height and the steepness of the cAMP gradient, and suggests that a combination of confinement-induced myosin-II localization and cAMP-regulated cortical contraction leads to increased intracellular fluid pressure and bleb formation.

Thesis Committee:

Dr. Zachary Gagnon (Thesis Advisor)

Dr. Douglas Robinson

Dr. Konstantinos Konstantopoulos

Dr. Sharon Gerecht

Dr. Anthony Shoji Hall

Dr. Marc Ostermeier

ACKNOWLEDGEMENTS

First and foremost, I would like to express my deepest gratitude to my advisor, Dr. Zachary Gagnon, for giving me the unprecedented opportunity to work in his laboratory. Considering that I was the first Ph.D. student in his lab, our advisor-student relationship was an experiment that nobody had previously tried so I am tremendously grateful for the results we achieved together. Dr. Gagnon provided me with the all-important guidance, support, encouragement, and resources, but perhaps more crucial to my research pursuits, independence and freedom. At this final juncture of my Hopkins life, I would warmly like to express my deep thanks to him for setting me up on the road to my post-graduate career.

In addition, I was privileged to collaborate with Dr. Douglas Robinson and his former Ph.D. student, Vasudha Srivastava, without whose help and generous support this dissertation would not have been possible. Dr. Robinson is one of the best professors in the 'Dicty world', and I feel blessed that I could work with him. Therefore, I would like to give special thanks to him for his constructive suggestions, valuable guidance, for being a member of my thesis committee, and for his insightful feedback at my annual review presentations. I also would like to thank all the other members of my GBO and thesis committee: Dr. Konstantinos Konstantopoulos, Dr. Sharon Gerecht, Dr. Anthony Shoji Hall, and Dr. Marc Ostermeier.

To the department chair and Professor Konstantinos Konstantopoulos, I am eternally indebted for accepting me into the Ph.D. program in the department of Chemical and

Biomolecular Engineering at Johns Hopkins University. This was a life altering position that I under took very seriously. I also would like to express my sincere gratitude to Dr. Konstantopoulos for his generous support overall. I will always be thankful to two other professors, Dr. Denise Sarigiannis and Dr. Stergios Yantsios, for believing in me and encouraging me to peruse a Ph.D. degree. They have played a pivotal role in my life, which I will always remember. Those two professors are a source of inspiration for me and I hope one day I will be able to emulate their traits, assisting other up and coming students as they did with me. Generally, I would like to express my profound and cordial thanks to them from the bottom of my heart.

I thank my current lab members, Dr. Xiaotong Fu, Nicholas Mavrogiannis, Francesca Crivellari, and Joshua Cole, for their valuable feedback on my research projects during our lab meeting presentations. I also would like to thank Dr. Michael Bevan, Dr. Sharon Gerecht, and Dr.Marc Ostermeier for allowing me to use their lab equipment during my graduate time in our department. Moreover, I convey my gratitude to my tutor here at Hopkins Denise Link-Farajali, for helping me every time that I needed her assistance and for going out of her way to provide support whenever she could.

During my graduate career at Hopkins, I have had the good fortune to build incredible and strong friendships that I hope will last for a lifetime. These include, Ivie Aifua, Brad Rupp, Abdul Majeed Mohammed, Alexandros Afthinos, John Zenk, and Nikki Neibloom. I would like to give special thanks to my dearest friends, Ivie and Brad, for all the time that we spent discussing each other's problems and offering warm support and encouragement to one another.

My deepest gratitude and love belong to my parents, Ferzilet and Kujtim, who have sacrificed immeasurably to be able to send me to college. I am also indebted to my parents for their love, unconditional support, and encouragement throughout my life. Special thanks goes to my brother, Klajdi, and my godparents, Artemis and Ioannis Katraki, for believing in me when I decided to go to graduate school. Last but not least, I would like to express my gratitude and love to my partner, Matt Murphy, who has offered me tremendous support and encouragement since the first day I met him. I thank Matt for filling the journey toward my destination with countless pleasant memories and excitement. Finally, I would like to thank the Murphy family for offering up their home and sharing their love with me.

TABLE OF CONTENTS

LIST OF FIGURES

LIST OF TABLES

CHAPTER 1: INTRODUCTION

1.1 Cell motility

Cell motility is a complex process that refers to diverse pathological and physiological processes that involve the translocation of cells from one region to another. Many cells have the capacity to migrate directionally in response to external environmental signals. In particular, the biased movement of cells along a chemoattractant gradient, commonly defined as chemotaxis, plays a critical role in cancer metastasis, wound healing, immune response and embryogenesis (Vicente-Manzanares et al., 2005). Two examples illustrate this clearly. First of all, malignant cancer cells invade adjacent tissues and escape from the primary tumor to colonize other organs (Bravo-Cordero et al., 2012; Wirtz et al., 2011). Secondly, the neutrophils hunt and kill the pathogens during inflammatory immune response (Kolaczkowska and Kubes, 2013). As another example, the keratinocytes in wound healing proliferate and migrate to repair the wound (Martin and Parkhurst, 2004). Moreover, during embryonic development, the stem cells migrate to distant targets to generate new structures and organs (Richardson and Lehmann, 2010). During all these biological processes the cells have to overcome a barrier of resistance to their movement in that they must migrate through very small spaces which are referred to as resistive environments.

1.1.1 Cell migration cycle

Eukaryotic cell locomotion occurs in the form of crawling, which contains three distinct activities: protrusion of the leading edge, adhesion of the newly formed protrusion, and retraction of the trailing edge of the cell (Lauffenburger and Horwitz, 1996). Each of these stages is driven by internal forces generated by distinctive components of the cytoskeleton. This internal filament network that extends throughout the cytoplasm enables the cells to adopt various shapes, interact with the external environment, divide, and generate the required forces for motility. The cytoskeleton is a highly dynamic structure, composed of three unique protein filaments: intermediate filaments, microtubules, and actin filaments (Fletcher and Mullins, 2010). Intermediate filaments are not involved in cell movement, and they provide mechanical strength to cells (Goldman et al., 1996). The microtubules provide platforms for intracellular transport including the movement of vesicles and organelles, and they are involved in various other processes such as mitosis. Lastly, the actin cytoskeleton is essential for cell crawling, phagocytosis, and cell division. During cell locomotion, actin generates significant force, through actin polymerization and cross-linking, for membrane deformation at the leading edge of the cell (Fig 1) (Chhabra and Higgs, 2007; Fujiwara et al., 2002). Actin filaments are also crucial in order for a cell to produce actomyosin contractility. A motor protein known as myosin II binds to actin filaments and moves them in the opposite direction (Fig 1) (Vicente-Manzanares et al., 2009).

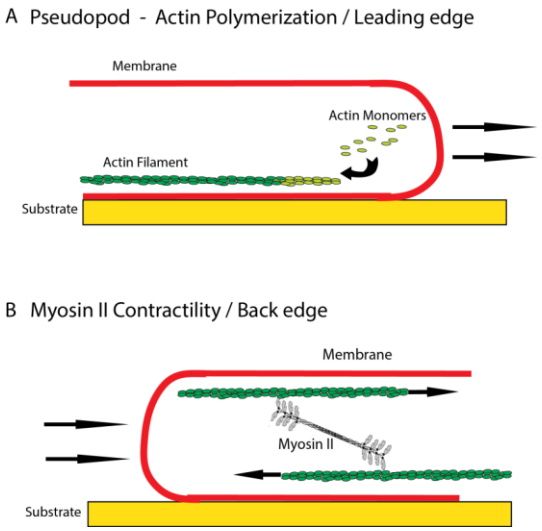

Figure 1: The role of actin filaments. In panel A, actin monomers polymerize to form a pseudopod at the front of the cell. In panel B, myosin II slides actin filaments over each other to produce actomyosin contractility at the back edge of the cell.

Directed cell locomotion is a fundamental phenomenon initiated when cells are stimulated by external cues such as chemical gradients, shear stresses, and electrical fields. The key step of the locomotory mechanism is the expansion of the leading edge of the migrating cell. During this phase, a protrusion is generated at the leading edge of the cell and pushes the cell membrane in the direction of movement. There are two distinct types of protrusions that can be generated: pseudopods and blebs. The second step of the motility cycle is the adhesion of the protrusion to the substrate over which the cell is crawling. This attachment inhibits the extended leading edge from retracting, and as the cell crawls, the adhesion contacts at the back of the cell are released. Finally, myosin II contracts at the trailing edge of the cell by sliding actin filaments in the opposite directions, which results in the movement of the cell body forward (Fig 2) (Ananthakrishnan and Ehrlicher, 2007).

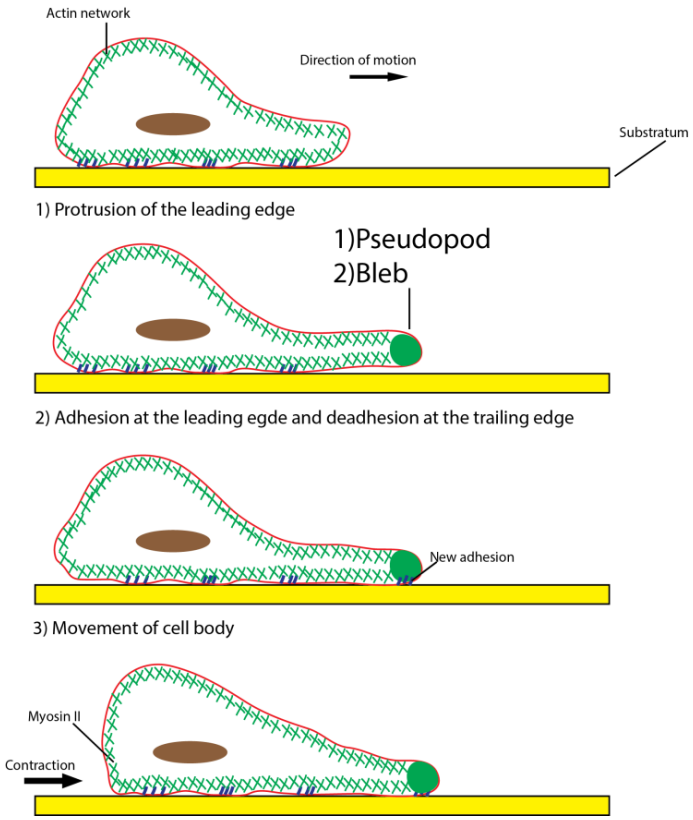

Figure 2: Schematic depicts the process of cell movement.

1.1.2 Actin-based motility

In response to environmental determinants, motile cells dynamically modulate their morphology and protrusive activity. Individual cells can migrate by using two different migration modes known as mesenchymal (Roussos et al., 2011) and amoeboid (Lammermann et al., 2008). In both cases in order to translocate, cells incorporate various types of protrusive structures at their leading edge, such as pseudopods or blebs. The most predominant mode is the pseudopod, whose protrusions are formed by actin polymerization at the leading edge of the cell. Actin filaments can be organized into bundles or a branched network, which gives rise to two alternate types of pseudopods: Lamellipodia and filopodia (Fig 3). Lamellipodia are broad, flat protrusions,

which contain branched and crosslinked networks of actin filaments (Pollard and Borisy, 2003). Cells can also form filopodia, which are fingerlike structures that contain a core of long actin filaments (Faix et al., 2009).

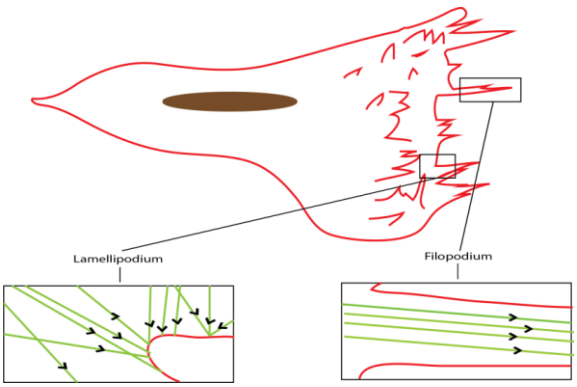

Figure 3: Schematic shows details of the arrangement of actin filaments in lamellipodia and filopodia. Lamellipodia are sheet-like protrusions that contain a crosslinked mesh of actin filaments. Filopodia are long, thin protrusions that contain a loose bundle of actin filaments.

Both lamellipodia and filopodia are generated by actin polymerization at the leading edge of the cells, and they push the membrane out without tearing it (Fig 4). During actin formation and growth, the monomeric globular (G)-actin polymerizes into F-actin filaments, and this process is catalyzed by ATP hydrolysis. An actin filament consists of two strands with a right handed twist repeating every 37 nm with two different ends called barbed and pointed (Pollard and Borisy, 2003). The formation and growth of actin filaments is assisted by various proteins that bind to the pointed end of the filament and promote polymerization. A complex of actin related proteins 2 and 3 (Arp 2/3 complex) is one of the set of proteins that carry out this process (Pollard and Beltzner, 2002). These proteins bind to the existing acting filaments and nucleate the growth of a new

filament, forming branched junctions. The depolymerizing protein dissociate actin monomers from the barbed end, and the capping proteins will protect the filaments from further assembly or disassembly at the front of the protrusion (Pollard and Borisy, 2003).

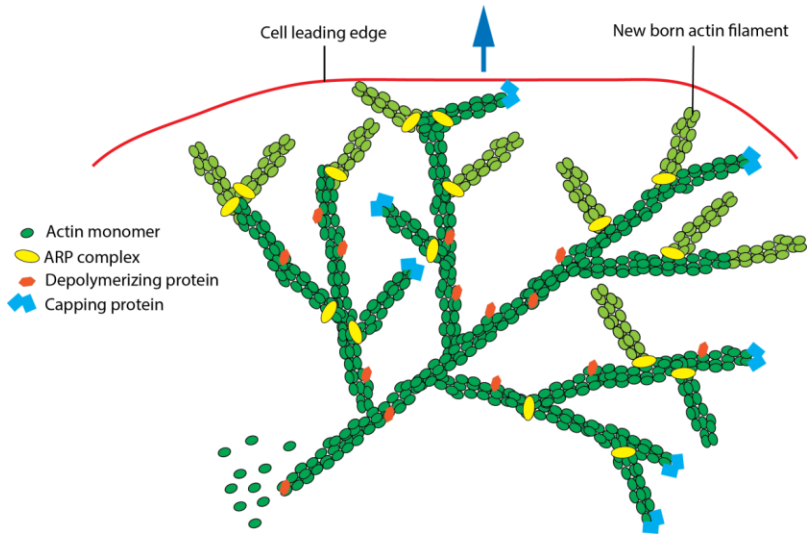

Figure 4: Assembly of branched actin network in a lamellipodium assisted by various accessories proteins.

1.1.3 Myosin II structure and function in Dictyostelium

Dictyostelium cells express one conventional two-headed myosin II as compared to the eukaryotic cells that have multiple members of the motor protein. Myosin II in Dictyostelium cells is composed of two myosin heavy chains (MHC), two essential light chains (ELC), and two regulatory light chains (RLC) (Fig5). Each myosin II molecule consists of two identical myosin strands that are held together by their tails; it has two globular heads attached to a coiled-coil tail. When a myosin II heavy chain tail is unphosphorylated, then myosin II filaments will spontaneously assemble into bipolar filaments (de la Roche and Cote, 2001). Consequently, the bipolar filaments will bind

and crosslink actin filaments to form the actomyosin complex. The resulting actomyosin complex after the phosphorylation of the regulatory light chain produces contraction by myosin II sliding actin filaments in the opposite direction, in the course of which ATP is hydrolyzed (Fig 5) (Bosgraaf and van Haastert, 2006).

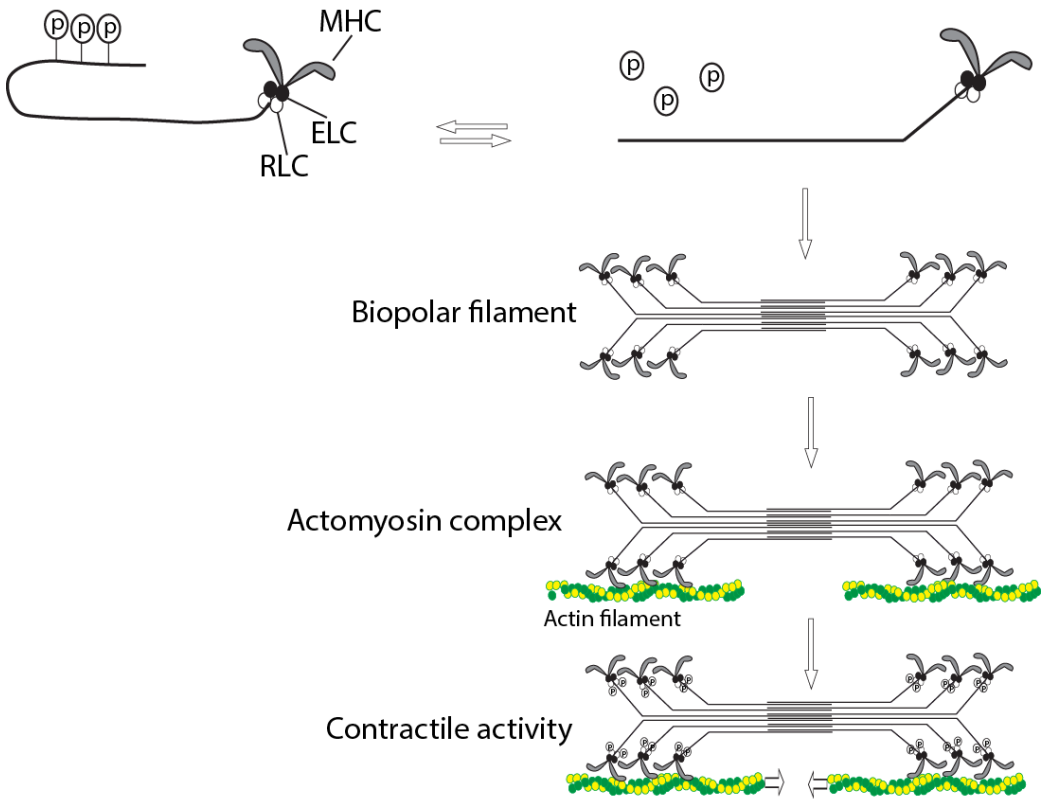

Figure 5: Schematic diagram of the structure and motor activity action of myosin II in Dictyostelium cells.

Myosin II has two modes of action; it increases cortical integrity and produces actomyosin contractility. Both actions of myosin II are important for cell migration in resistive environments. Under normal circumstances, the plasma membrane is tightly bound to the cell cortex, a layer of actin, myosin, and associated proteins (Fig 6) (Salbreux et al., 2012). The mechanoenzyme myosin II increases cortical integrity when

bipolar filaments bind and crosslink actin filaments. In addition, myosin II motor protein contracts cortical actin which leads to an increase in the cortical tension (Luo et al., 2013). The elevated cortical tension increases the hydrostatic pressure in the cytoplasm. Cells lacking a myosin II heavy chain (mhcA$^-$) are not able to chemotax under a layer of agarose as the cortical integrity is not sufficient to resist the external applied force from the layer of agarose or migrate underneath it. Moreover the cell will fragment because it is not capable of retracting its trailing edge in the absence of myosin II (Laevsky and Knecht, 2003).

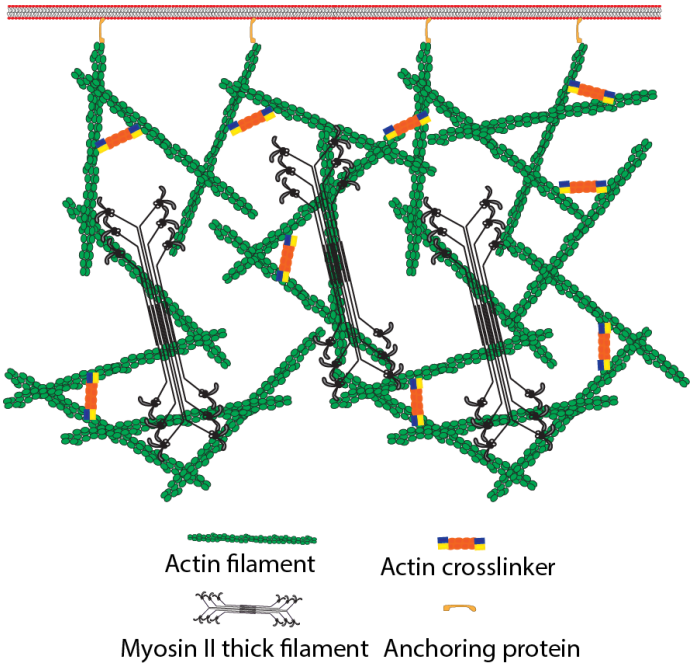

Figure 6: Schematic of the cell cortex - plasma membrane complex.

1.1.4 Bleb-driven motility

Cell blebs are rapidly extended spherical membrane protrusions that are produced by hydrostatic pressures that propagate through the cytoplasm and are generally thought to originate from actomyosin contractility (Charras et al., 2005). Pseudopodia, on the

other hand, are actin-rich projections of the membrane where cell locomotion is driven by actin polymerization (Insall, 2010). As compared to pseudopodia, blebs differ significantly in their life cycle time, size, and shape. During the life cycle of a bleb, initially, the increased intracellular pressure causes the membrane to locally delaminate from the cortex (Charras et al., 2005) or to locally rupture the actin cortex (Charras and Paluch, 2008). Sequentially, cytoplasm flows into the bleb neck, inducing further tearing of the bilayer from the cortex. Finally, reconstruction of the actin cortex within the bleb completes the protrusion (Fig7) (Charras and Paluch, 2008). Cell blebbing has been observed in many diverse physiological and pathological processes, including during cytokinesis (Stewart et al., 2011), cell spreading (Gauthier et al., 2011), apoptosis (Mills et al., 1998), and cell movement (Sahai and Marshall, 2003; Trinkaus, 1973) . More importantly, blebs drive the movement of certain motile cancer cell lines upon inhibition of their proteolytic activity, especially when these cells are invading 3D matrices or migrating through tissues (Wolf et al., 2003). This amoeboid motility of cancer cells is very similar to the migration of leukocytes and *Dictyostelium* cells. In addition, migration plasticity is correlated with the ability of the cells to dynamically modulate their morphology and protrusive activity as a function of the environment that they are encountering. It has been reported that under conditions of low adhesion and high confinement, cells switch from f-actin driven motility to bleb-driven migration (Liu et al., 2015).

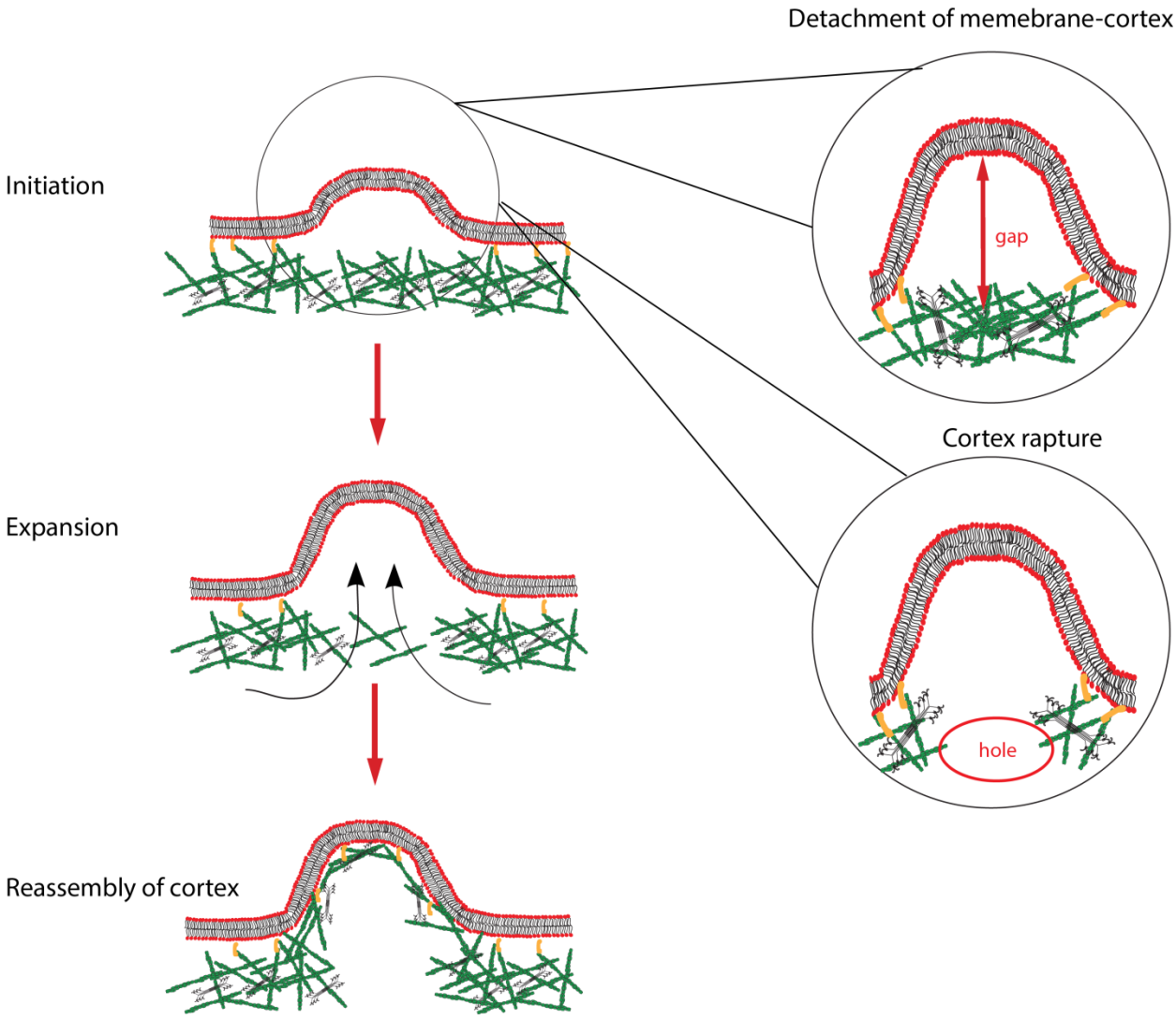

Figure 7: Schematic diagrams of the bleb life cycle.

Under physiological conditions, *Dictyostelium* cells can form two distinct types of cell surface protrusions: pseudopods and blebs (Yoshida and Soldati, 2006). Their study was the first scientific report showing the contribution of blebs to cell motility in *Dictyostelium* cells. Another scientific group from Dr. Rob Kay's lab at the University of Cambridge used the under agarose assay to study blebbing of *Dictyostelium* cells in resistive environments. They reported that the blebbing increases as agarose stiffness in the overlay increases (Zatulovskiy et al., 2014). Lastly, a uniform treatment of

developed Dictyostelium cells with cAMP has been shown to induce a transient phase of blebbing (Langridge and Kay, 2006).There are different factors that contribute to bleb formation. However, the main three parameters are (Table1): Actomyosin contractility, actin polymerization, and substrate adhesiveness (Paluch and Raz, 2013; Tinevez et al., 2009; Zatulovskiy et al., 2014).

Table 1: Parameters that control the type of protrusions migrating cells form.

Factors controlling bleb formation	**Experimental perturbation**	**Drugs or cell mutants**	**Observed effect**
Actomyosin contractility	Inhibition of contractility	Blebbistatin, Y27632 Myosin II null cells	Decrease in blebbing
Actin polymerization	Decreasing actin polymerization	Inhibition of Arp2/3 activity	Increase in blebbing
Cortical tension	Decrease in cortical tension	Blebbistatin Y27632	Decrease in blebbing
Membrane tension	Increase membrane	Wheat germ agglutinin (WGA)	Decrease in blebbing
Membrane – cortex adhesion	Decrease in membrane-cortex adhesion	Erzin/Radixin/Moesin mutants	Increase in blebbing
Substrate adhesiveness	Low adhesion	Non adhesive coating	Increase in blebbing
Osmolarity	Increase in osmolarity	Sorbitol, Sucrose	Decrease in blebbing
Degree of cellular confinement	Increase cellular confinement	Stiffness of agarose layer, microfluidic	Increase in blebbing

		channel height	

1.2 Dictyostelium discoideum as a model organism

The social amoeba Dictyostelium discoideum, first discovered in 1935, is the most studied species of the cellular slime molds. The single cell organism Dictyostelium, live in forest soil and feed on bacteria. The cells, approximately 10 μm in diameter, are a little smaller than the average mammalian cell and can move as fast as 10-15 μm/min. Dictyostelium discoideum is a powerful model organism for studying chemotaxis, cell motility, cytokinesis, phagocytosis, signal transduction, and cell differentiation during development.

1.2.1 The life cycle of Dictyostelium cells

The life cycle of Dictyostelium discoideum cells consists of two strictly separated stages: vegetative and developmental cycles. In the vegetative state, the cells live a solitary life by consuming bacteria or other nutrients and divide mitotically every 4-12 h. Upon depletion of their food source, the cells enter a developmental cycle to protect themselves from dying. The starved cells initially undergo an aggregative state which relies heavily upon chemotaxis. During this stage, cells synthesize and secrete the chemottractant, 3',5'-cyclic adenosine monophosphate (cyclic-AMP), to communicate with each other. The starved cells detect the cAMP gradients and gather at one point, which leads to the formation of aggregates containing 10^5 amoebae in a process taking approximately 8 hours under most laboratory conditions. After the aggregation period, cells differentiate and rearrange themselves to form a fruiting body that behaves as a multicellular entity (Fig 8). This fruiting body is constructed by a mass of spores that are

held up by dead stalk cells. When the spores are transported to new feeding sites, the cells are capable of entering the growth phase. The entire developmental cycle takes about 24 h, and to begin development in the laboratory, we remove the source of nutrients (Bozzaro, 2013).

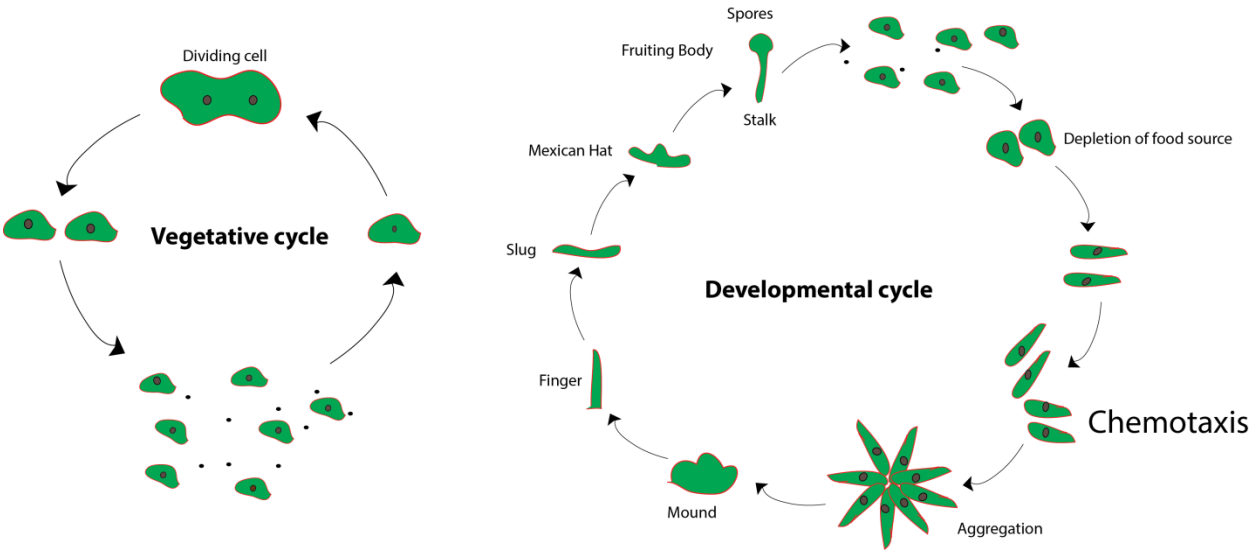

Figure 8: Dictyostelium discoideum life cycles. In the vegetative cycle, cells feed on bacteria and proliferate. Starvation leads to development, and the different morphological stages that take place during this cycle are depicted.

1.2.2 Advantages of Dictyostelium as a model organism

Dictyostelium discoideum is a popular model for investigating fundamental aspects of various eukaryotic functions. Dictyostelium cells display strong chemotactic responses and they employ similar mechanisms with other motile cells such as leukocytes during the detection of the chemoattractant, the signal transduction pathways, and the rearrangement of the different cytoskeleton components. Some advantages of this ideal model include (Bozzaro, 2013; Manahan et al., 2004):

a) *Easily grown*. Dictyostelium cells can grow on bacteria or axenic culture media in plastic Petri dishes or shaking suspension. Large amounts of cells can be cultured easily and cheaply at room temperature (22 ˚C) and under atmospheric CO_2 levels. The latter results in the capability of imaging the cells with various microscopy techniques without the need for controlling temperature and CO2 levels.

b) Small and compact genome. The Dictyostelium haploid genome is organized into six chromosomes, and it has been completely sequenced (Eichinger et al., 2005). Dictyostelium cells often contain only one gene for molecules that are present in multiple isoforms in mammalian cells. For instance, Dictyostelium has only one conventional myosin (myosin II) gene in contrast with the other eukaryotic cells, which contain three myosin genes: myosin II A, myosin II B, and myosin II C.

c) Genetically manipulated. It is relatively easy to genetically manipulate Dictyostelium cells. In addition, there are genetic tools that can be used to overexpress or to fluorescently tag a gene of interest. Moreover, a wide selection of mutants, plasmids, and cell strains are publicly available in the Dictyostelium stock center (www.dictybase.org).

d) No extracellular matrix is required. Dictyostelium cells can crawl on flat substrates without the need for the deposition of an extracellular matrix on the

substrate. Lastly, these cells move more quickly than the cultured mammalian cells.

1.2.3 Chemotaxis of Dictyostelium cells

Chemotaxis or directed cell migration is a mechanism by which motile cells sense and respond to chemical gradients by migrating towards higher concentrations. During vegetative growth, Dictyostelium cells rely on chemotaxis to find food. Specifically, the cells naturally chemotaxes towards higher concentrations of folic acid, which is a chemical released by bacteria. As part of its developmental life cycle, Dictyostelium respond to the chemoattractant cAMP by crawling towards the high end of the gradient. Chemotaxis is a dynamic process that consists of three distinct modules: directional sensing, cell polarity, and motility (Swaney et al., 2010).

In the absence of a chemoattractant gradient, the cells extend psueodopods in all directions, which results in their random migration (Li et al., 2008). However, when a gradient has been established, the cells have an internal compass that allows them to detect the gradient and extend pseudopods in the direction of the applied gradient (Huang et al., 2013). The molecular mechanism that enables the cells to detect the gradient, through a specific intracellular localization of different molecules, is referred to as directional sensing.

Under starvation conditions, cells gain an elongated morphology and obtain a defined front and trailing edge; therefore, during development, cells become polarized. Polarity leads to the localization of specific proteins to each cell pole, and cell polarization can occur in uniform chemoattractant or in a gradient. Polar cells extend pseudopods only at

their leading edge (Fig 9); however, non-polar cells extend protrusions from all different parts: front, back, and sides (Fig 9) (Swaney et al., 2010).

Cell motility is referred to as the translocation of cells from one location to another. Directional sensing, cell polarity, and motility are all independent from each other. Unpolarized cells can sense the gradient by using their internal compass, and they can go on random walks. Polarized cells have a well defined leading and back edge; they are able to detect the chemoattractant gradient and migrate in the direction of the gradient (Vorotnikov, 2011).

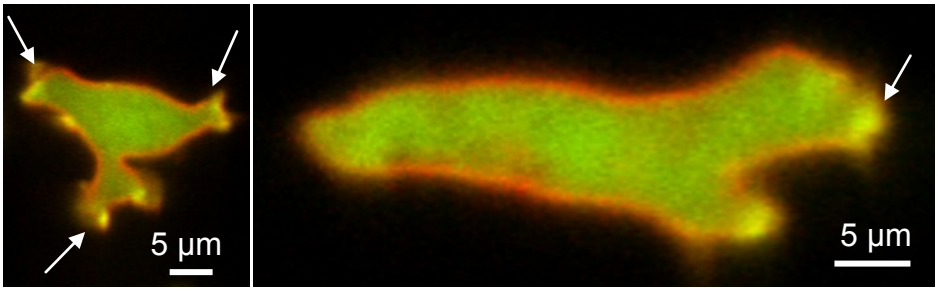

Figure 9: Non-polar and polar Dictyostelium cells. Arrows depict pseudopod formation. The first image shows a cell extending pseudopods in all directions, which leads to random migration, while the second picture shows a polarized elongated cell chemotaxing towards the high end of the gradient, which is pointing to the right.

1.2.4 Signaling pathways mediating chemotaxis

During chemotaxis, the cells are able to sense and respond to the chemical gradient by displaying a directed migration. Specifically, Dictyostelium cells secret cAMP upon starvation and through the activation of signal transduction pathways, they are able to receive, process, and respond. The process through which the cells sense and translate the extracellular stimuli into a biochemical signal that elicit specific cellular responses is

referred to as signal transduction (Kay et al., 2008). Initially, an environmental signal activates a cell surface receptor and the activated membrane receptor transfers information from the environment to the interior of the cell. The environmental signal from the exterior of the cell is converted into a biochemical signal in the interior of the cell. The second stage of signal transduction is the activation of a second messenger which will continue the signal inside the cell. The signal is often amplified before eliciting a physiological response (Fig 10) (Hamill and Martinac, 2001).

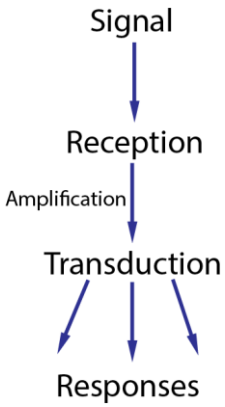

Figure 10: Principles of signal transduction.

Starved Dictyostelium cells synthesize and secret the chemoattractant cAMP, neighboring cells sense and chemotaxes towards each other. The activation of the chemotactic signal starts when cAMP binds and activates the seven transmembrane domain receptors, cARs, which are localized at the surface of the cell. Dictyostelium cells have four cAMP receptors (cAR1-4). cAR1 is the key receptor in early development and is coupled to a heterotrimeric G protein which consists of α, β, and γ subunits. cAR1 and G protein are uniformly expressed on the cell surface and remain evenly distributed on the plasma membrane when cells are exposed to a cAMP gradient. When the cAMP binds to cAR1, the G protein gets activated and dissociates

into G_{α} and $G_{\beta\gamma}$ subunits (Fig 10). The last one transmits the signal to downstream effectors such as Ras, which localizes at the leading edge of the cell when it is in a gradient. This leads to the activation of PI3K, which converts $PI(3,4)P_2$ to $PI(3,4,5)P_3$ at the leading edge of the cell. The PIP3 has binging sites for proteins that contain the Pleckstrin Homology (PH) domain and those proteins (Rac GEF, SCAR, Arp 2/3) lead to actin polymerization at the front. PTEN, a negative regulator of PI3K, localizes at the lateral sides and back edge of the cell. The presence of PIP2 at the back of the cells prohibits the localization of proteins and molecules that are related to actin polymerization; therefore, PTEN suppresses the pseudopod formation at the lateral sides and back edge of the cell (Willard and Devreotes, 2006).

The presence of myosin II at the lateral sides and back edge of the cell inhibits pseudopod formation as well as promotes contraction of the trailing edge. The chemoattractants cAMP and folic acid stimulate the synthesis of cGMP, which regulates chemotaxis by regulating the phosphorylation and localization of myosin II. The cGMP activates GbpC/GbpD proteins, which switch on the myosin heavy chain kinase A (MHCK-A). The activation of MHCK-A leads to the phosphorylation of the regulatory light chain (RLC), which increases the ATPase activity of myosin II. After chemotactic stimulation, the myosin heavy chain tail is phosphorylated, and this leads to the recruitment of myosin II to the cytoskeleton (Fig 12). Therefore, cGMP activates a signaling pathway which leads to the phosphorylation of RLC and MHC (Bosgraaf et al., 2002).

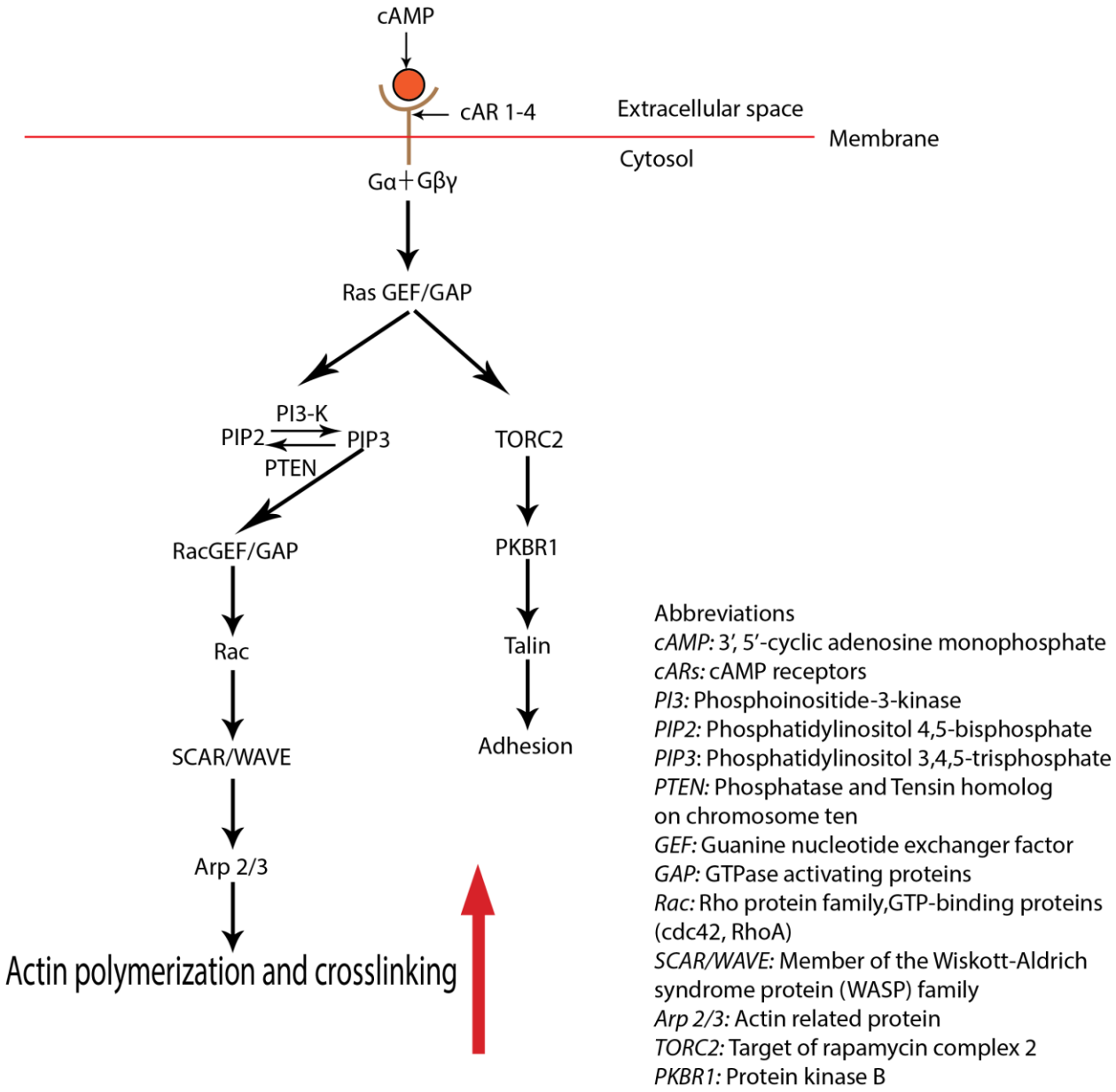

Figure 11: Signal Transduction of Actin Polymerization in Dictyostelium cells.

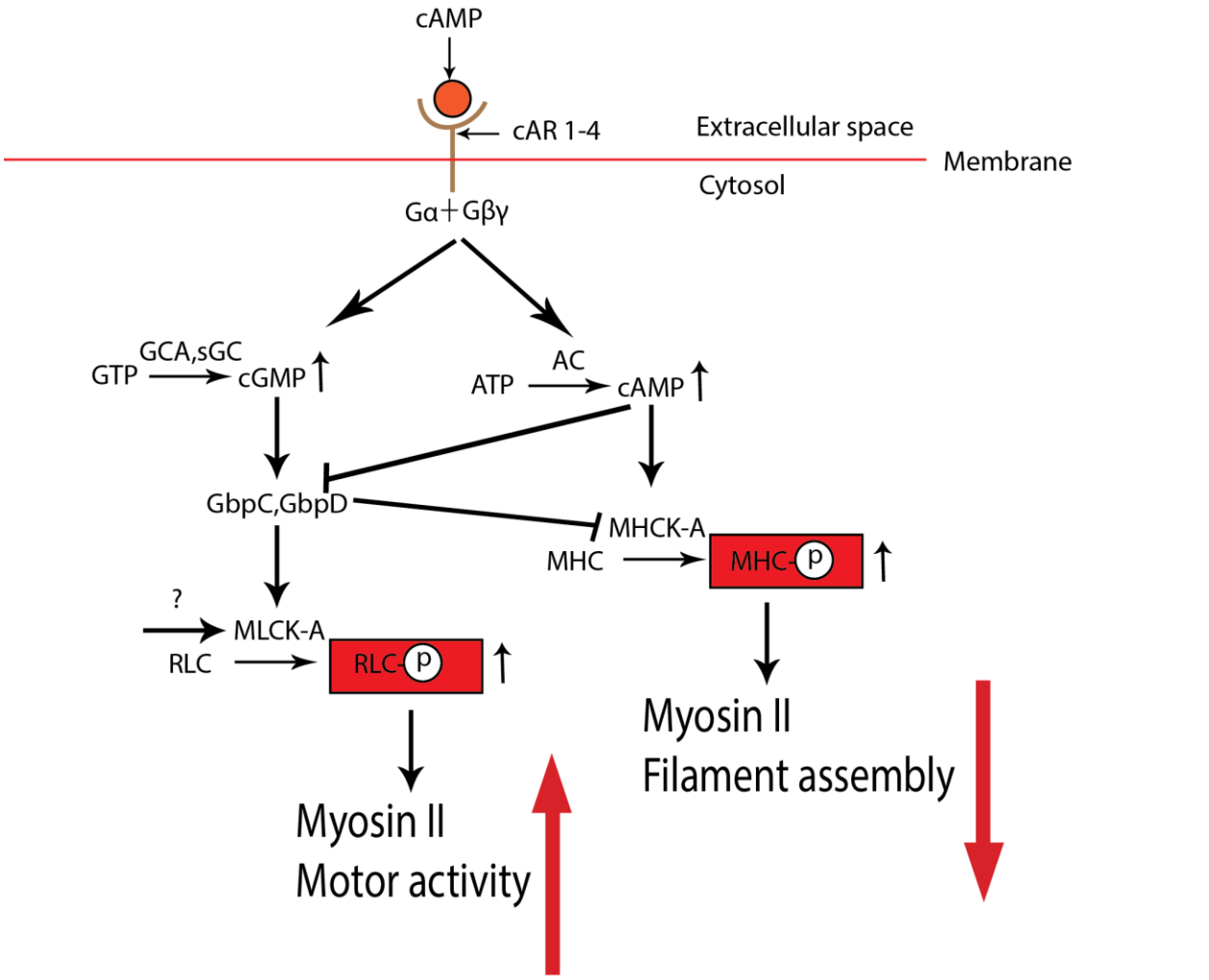

Abbreviations
cGMP: 3′, 5′-cyclic guanosine monophosphate
GCA: Guanylyl cyclase A
sGC: Soluble guanylyl cyclase
GbpC,GbpD: Two large muti-domain proteins
MLCK-A: Myosin light chain kinase
RLC: Regulatory light chain
AC: Adenylate cyclase
MHCK-A: Myosin heavy chain kinase
ATP: Adenosine triphosphate
GTP: Guanosine-5'-triphosphate

Figure 12: Signal transduction regulating myosin II in Dictyostelium.

1.3 Engineered confined environments

1.3.1 Microfluidic device versus under agarose assay

Cell migration can be studied *in vivo* where cells confront their physiological relevant 3D environments, but it is technically difficult to study in a controlled manner (Cavanagh and Weninger, 2008). Therefore, several *in vitro* experimental systems have been developed to replicate the resistive environment that the cells encounter in order to image and quantify chemotactic motility. Most of the *in vitro* assays, such as the Boyden chamber, transwell assay, extracellular matrix gels, and under agarose chemotaxis assay (Laevsky and Knecht, 2001; Laevsky and Knecht, 2003; Zatulovskiy et al., 2014), however, suffer from various drawbacks; namely, they provide only end point data, lack of well-defined chemotactic gradients, or exhibit a variability of structures and densities of ECM (Keenan and Folch, 2008).

In addition, with the under agarose technique before the arrival of cells, the agarose is in direct contact with the plastic surface of the petri dish. Thereafter, the cells squeeze underneath the agarose and become deformed by it. As the cells move underneath agarose, they locally deform or move it upward. Cells thus face variations in the height of their microenvironments and, to add to that, the leading edge of cells has to lift up the agarose in order to move towards the gradient. As a result, the front part of the cell is always more confined than the rest of the cell.

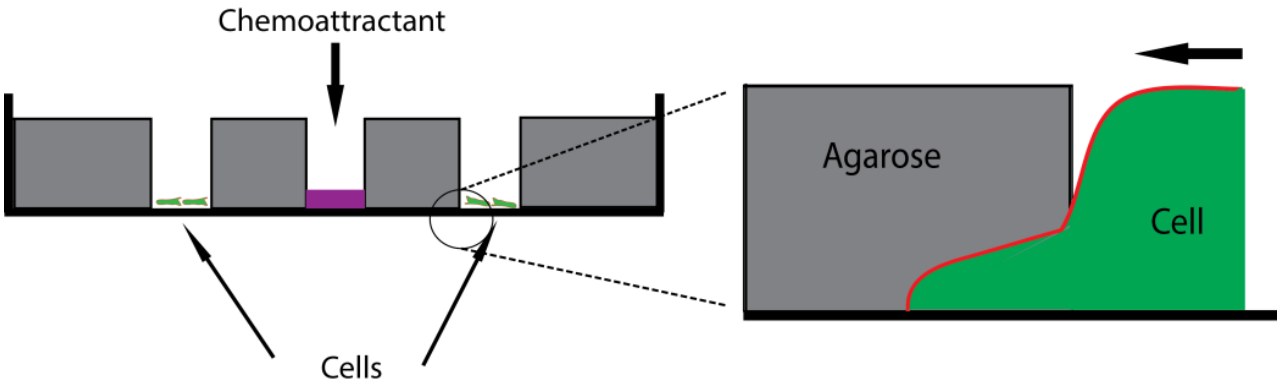

Figure 13: Under agarose assay. During migration the cell deforms the agarose upward. The front of the cell is always more confined than the rest of the cell.

This experimental platform cannot be used to configure well-controlled gradients because the chemoattractant gradient degrades with time. In brief, the under agarose chemotaxis assay suffers from not having a constant height of the resistive environment and from lacking a stable gradient. Finally, quantification of cell migration at the single cell level is difficult, making the comparison between conditions less precise.

To address the issues of the conventional agarose assays and to generate a resistive environment which is physiologically relevant, polydimethylsiloxane (PDMS)-based microfluidic channels have been developed (Li and Lin, 2011). Microfluidics and microfabrication provide an experimental platform to study individual cell migration under better controlled chemoattractant gradients and environmental conditions (Kim et al., 2010). Moreover, this small scale offers cost effectiveness, low consumption of reagents, and repeatable structures between preparations of PDMS.

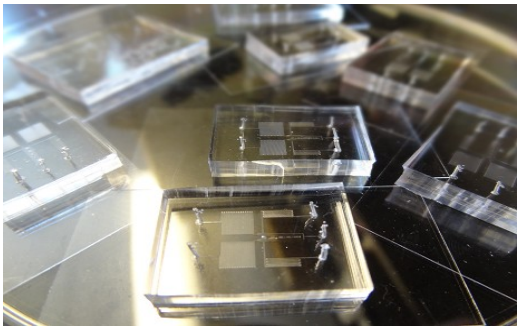

Figure 14: The PDMS device utilized to study cell migration in resistive environments.

CHAPTER 2: MATERIALS AND METHODOS

2.1 Protocols for different solutions

2.1.1 1L 1.5X HL-5 Media

1. Pour 600 mL Milli-Q water into a glass container.
2. Dissolve the following while stirring with a stir bar:

   15 g Proteose Peptone 0.13 g Na_2HPO_4-$7H_2O$

   3.9 g Bacto-Yeast Extract 0.13 g KH_2PO_4

   3.0 g Glucose
3. Add Milli-Q water to bring final volume to 1L.
4. Autoclave at 250˚F for 40 min, when autoclave is cold.

2.1.2 Penicillin/Streptomycin (PEN/STREP)

1. Pour 78 mL Milli-Q water into a glass container.
2. Dissolve while stirring with a stir bar:

   0.5 g Penicillin G * (stored at room temp)

   0.78 g Streptomycin sulfate (stored at 4°C)
3. Filter sterilize and aliquot.
4. Store in -20˚C freezer.

2.1.3 G418

Want 100mg/mL stock solution. Working concentration 15 µg/mL.

1. Dissolve 0.5 g G418 in 5 mL Milli-Q water.

2. Filter sterilize.
3. Aliquot 1 mL into microtubes.
4. Store in -20°C freezer.

2.1.4 Hygromycin B

Want 50 mg/mL stock solution. Working concatenation 40 µg/mL.

1. Dissolve 0.250 g Hygromycin B in 5 mL Milli-Q water.
2. Filter sterilize.
3. Aliquot 1 mL into microtubes.
4. Store in 2°C refrigerator.

Sometimes a 50 mg/mL stock solution of Hygromycin B was bought from Gemini Bio-Products.

2.1.5 Media for Dictyostelium Discoideum cells

1. 500 mL 1.5X HL-5 Media.
2. Add 43 mL FM to 1.5X HL-5 media to make enriched media.
3. Add 1 mL Pen/Strep.
4. Add 81.6 µL 100 mg/mL G418 to 500 ml enriched media, so the final concentration of G418 is 15 µg/mL.
5. Add 435 µl 50 mg/mL Hygromycin B to 500Ml enriched media, so the final concentration of Hygromycin B is 40 µg/mL.

Added G418 and Hygromycin B only when I had double mutant cells for instance:

AX2:: GFP-LimEΔcoil, mCherry-cAR1.

For wild type cells no drugs are needed.

2.1.6 1L FM

1. 1 L Milli-Q water
2. Dissolve 19.3 g FM

2.1.7 Development buffer (DB) (Protocol adapted from www.Dictybase.org)

DB contains:

1. 5 mM $Na_2PO_4 \cdot 7\ H_2O$
2. 5 mM KH_2PO_4
3. 1 mM $CaCl_2$
4. 2 mM $MgCl_2 \cdot 6\ H_2O$

2.1.8 1L 10X Phosphate solution

3. 1 L Milli-Q water
4. Dissolve 6.8 g KH_2PO_4 .
5. Dissolve 13.4 g $Na_2PO_4 \cdot 7\ H_2O$.
6. Autoclave the phosphate solution at 250 ˚F for 50 min.

2.1.9 1 M $CaCl_2$

1. 250 mL Milli-Q water.
2. Dissolve 27.2g $CaCl_2$.
3. Autoclave solution at 250 ˚F for 50 min.

2.1.10 1 M MgCl2 ·6 H2O

1. 500 mL Milli-Q water.
2. 101.65 g $MgCl_2 \cdot 6\ H_2O$.
3. Autoclave solution at 250 ˚F for 50 min.

2.1.11 1 L DB

1. 900 mL Milli-Q water.
2. Add 100 mL of 10x Phosphate solution to reach a final concentration of 5 mM $Na_2PO_4 \cdot 7\ H_2O$ and 5 mM KH_2PO_4.
3. Add 1 mL of 1M $CaCl_2$ solution to reach final concentration 1 mM $CaCl_2$.
4. Add 2 mL of 1M $MgCl_2 \cdot 6\ H_2O$ solution to reach final concentration 2 mM $MgCl_2 \cdot 6\ H_2O$.
5. Adjust pH to 6.5 and store in 2°C refrigerator.

2.2 Protocols for growth and maintenance of Dictyostelium cells

2.2.1 Freezing *Dictyostelium* cells

Freeze mix: 10% DMSO in Bis-Tris HL-5 pH 6.7. Dr.Robinson's lab provided Bis-Tris to us.

1. Have a bucket of ice.
2. Prepare 2 mL of freeze mix per confluent plate.
3. Put the freeze mix on ice for at least 15 min.
4. Each plate of cells makes 4 aliquots to freeze.
5. Pour media off of plates.
6. Take 2 mL of freeze mix and resuspend cells quickly.
7. Add 0.5 mL aliquots to 1.5 mL tubes and immediately put on ice.
8. Store cells in -80°C freezer.

2.2.2 Thaw Dictyostelium cells

1. Remove tube from -80°C freezer.

2. Warm in hand till it becomes liquid.

4. Add contents into a Petri dish that contains 10mL of media.

5. Take 1 mL off and add to new plate with 9mL media to dilute DMSO 10-fold.

2.2.3 Transformation into *Dictyostelium* cells

1. Have ready a petri dish of parent strain cells and a bucket of ice. Add cuvette on ice.
2. Add 9 mL of enriched and Pen/Strep 1.5X HL-5 media into a petri dish and place it in 2°C refrigerator.
3. Take 12 mL E-Pore buffer per petri dish and place it on ice. Dr. Robison's lab provided E-Pore buffer to us.
4. Resuspend parent strain cells and place the content into a 50 mL conical tube.
5. Mix gently the cells, take 15 µL of them and count.
6. Centrifuge the content of the 50 mL conical tube at 2000 rpm for 5 min.
7. Decant supernatant and resuspend pellet in 10 mL ice-cold E-Pore buffer.
8. Spin down cells at 2000 rpm for 5 min.
9. Multiply cell count by total mL of the 50 mL conical tube to get total cell count.

   a (cells/mL) · b (mL in the conical tube) = total cells
10. Perform calculations below:

Total cells/ 10^7 = X

X · 0.35 mL = Y amount of E-Pore buffer that we need to resuspend the cells.

11. Resuspend in calculated amount of ice-cold E-Pore buffer. (Must have 10^7 cells per 350 µL E-Pore buffer).
12. Keep the above on ice. The cells should not stay in the E-Pore buffer for long time.
13. Add appropriate amount of plasmid to each cuvette. (1-4 µg)

The plasmid had a concentration of 200 ng/µL. 200 (ng/µL) · K = 1 µg, K= 5 µL.

Add 5 µL of the plasmid to cuvette.

14. Add the cells with the E-Pore buffer to the cuvette that contains the plasmid.
15. To electroporate cells: Set cap knob to 3.0 set voltage at 1.3 kV. Hold down both red buttons until hear a beep, release buttons. Time constant should be between 1.5 – 2.0.
16. Pour content of the cuvette into petri dish that contains no-drug media. Let them grow overnight.
17. The next day put them in drug media. Do not resuspend, just change the media.
18. Keep changing the media every 2-3 days until you will have some nice colonies. After that you can split them.

2.2.4 Growth of Dictyostelium cells in 1.5X HL-5 Media (Protocol adapted from www.Dictybase.org)

1. Add 10 mL of the cell medium in a 100 mm petri dish.
2. Add 10^4 cells/mL in the petri dish that contains the cell medium.

3. Cells will attach to the plastic surface and be observed with a standard microscope.
4. Grow cells in the incubator at 22°C.
5. Passage cells when they reach a density of $5 \cdot 10^6$ cells/mL, which takes 2-3days. Make a 1:100 dilution into fresh medium and add to a new dish.

All the protocols are adopted from Dr.Robinson's lab, if they have not been stated otherwise.

2.2.5 Determination of cell density

The cell density is calculated by counting an aliquot of the cell culture in a hemocytometer. A 15 µl of the cell suspension will be enough to fill the hemocytometer chamber. The hemocytometer carries nine squares but only the four squares at the corners will be used. Count cells that are located in four red squares (Fig 15). Dived the total cell number by four and multiply it by 10^4 to obtain the cell density in cells per ml. It is recommended to dilute the cell suspension when the cell density of the culture is too high, approximately approaches 1 x 10^7 cells ml^{-1}.

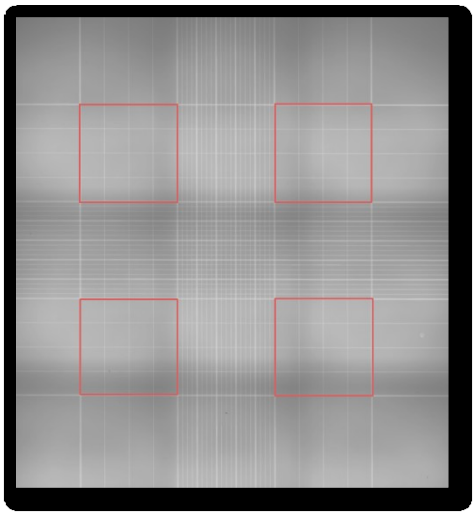

Figure 15: Large image of the hemocytometer gridlines. The hemocytometer diagram indicating the four red squares that should be used for cell counting.

2.2.6 Development of Dictyostelium cells. (Protocols adapted from Dr. Devreotes' lab)

Dictyostelium cells can be developed on DB agar plates or in suspension. For the cell migration experiments we developed cells in suspension.

Wash cells from cell medium

1. Grow cells on petri dishes. Usually I had to make 6 petri dishes and used 4 of them for development and the other two petri dishes to passage cells.
2. Detach cells from the petri dish.
3. Put the cell suspension in a 50 mL conical tube.
4. Centrifuge at 500 g for 4 min.
5. Pour off the supernatant.
6. Wash cells by resuspending the pellet in ½ volume of DB.
7. Repeat the wash twice for a total of three washes.
8. Determine the cell density before the final wash by using a hemicytometer.
9. A 15 µL sample will be enough to fill the hemocytometer. C_1 = number of cells · 10^7/ 4000 (cells/mL).
10. After the final wash resuspend the cells at a density of $2 \cdot 10^7$ cells/mL DB.

2.2.7 DB agar plates

1. Dissolve 1.5 g of agar into 100 mL DB.
2. Autoclave solution at 250 °F for 50 min.
3. Store it at room temperature.
4. Before experiment: Microwave the agar solution in order to liquefy it. Pour 5 to 10 mL of the agar solution to a petri dish.
5. Place the petri dish that contains the agar solution in the refrigerator for at least 30 min.
6. After the final wash resuspend the cells in DB to a concentration of 10^7 cells/mL.
7. Use 1 mL of the cell suspension and spread the cells evenly over the surface of the DB agar plate.
8. Let the cells for 5 min to adhere on the agar surface and then carefully remove the DB buffer from the plate.
9. Incubate cells at 22°C for the desire time period, usually 4 to 5 hr.
10. After development use 1 mL DB to detach cells from the agar surface.

2.2.8 Development in suspension

1. After the final wash resuspend the cells at a density of $2 \cdot 10^7$ cells/mL DB.
2. Place the cell suspension in a 50 mL flask.
3. Shake it at 180 rpm for 4 hr and keep temperature at 22°C.
4. Start pulsing cAMP after the first hour of shaking.
5. Program the pump to deliver 100 µL cAMP solution during a 5 s pulse every 6 min. So it should deliver 1 mL of the solution over one hour.

6. The concentration of the cAMP solution must have a value which will result in a 100 nM cAMP in the cells at the beginning of pulsing.
7. For instance, to develop 2 mL of cell suspension add 10 µL of 10 mM cAMP stock solution to 50 mL DB. To develop 4 mL of cell suspension add 20 µL of 10 mM cAMP stock solution to 50 mL DB. Lastly, to develop 6 mL of cell suspension add 30 µL of 10 mM cAMP stock solution to 50 mL DB.
8. After the 4 hr development put 1 mL of the cell suspension into a 1.5 mL eppendorf tube. Pipette the cell suspension to break the aggregates.
9. Take 100 µL of the cell suspension from the eppendorf tube and load it into the microfluidic device.

2.3 Protocols for various microfluidic techniques

2.3.1 Fabrication of the microfluidic gradient generation chamber

The microfluidic gradient generator was fabricated using the technique of photolithography and soft lithography. Two masks were designed using AutoCAD and printed out on transparency films. A silicon wafer was patterned with the design for the gradient generation channels (mask #1) using SU-8 2002 photoresist (Fig 16a). It was spin-coated at 5000 rpm for 35 sec, 300 rpm/sec to achieve a thickness of 1.7 µm and after spin-coating wafer was baked at 95 °C for 2 min; exposed to UV light (80mJ /cm^2), baked on hot plate at 95 °C for 2 min. The wafer was developed using SU-8 developer and then microchannels of 1.7 µm height and 150 µm in length from top to bottom were generated (Fig 16b). The alignment keys were covered with scotch tape and a second layer of SU8-3050 was spin-coated on the wafer at 2000 rpm for 40 sec to achieve a

thickness of 83 μm. Mask #2 was aligned perpendicularly to the first layer of microchannels, exposed to UV light (250mJ /cm^2) (Fig 16c), baked at 95 °C for 7 min and processed with SU-8 developer to generate the two layer mold (Fig 16d). Finally the wafer was baked at 200°C for 4 hr. A mixure of Poly(dimethyl siloxane)(PDMS) and curing agents (10:1) was used to obtain the three dimension topography of the patterned, solid surface by replica molding (Fig 17a). The Flow inlets and outlets of the device were created by using 0.7 mm and 1.2 mm diameter hole punchers. The PDMS replica was then treated with oxygen plasma using hand - held Tesla coil to be converted to a hydrophilic surface and irreversibly sealed to a rectangular cover glass (Fig 17b and 17c).

Two more molds were generated in the same way. Briefly, a 2.4 μm tall layer of SU-8 2002 photoresist was spin coated on a bare silicon wafer at 1500 rpm for 35 sec, 300 rpm/sec. The fist layer of the third mold was fabricated by spinning a 3.8 μm tall layer of SU-8 2002 photoresist at 580 rpm, for 35 sec, 300 rpm/sec. The second layer of both molds was fabricated as described above in the fabrication of the fist mold.

We wanted to investigate the impacts of the different levels of confinements on blebbing so we fabricated a three layer mold. On this mold the gradient generation channels consist of two different alternating heights. The entrance and the exit part of each channel has a height of 1.9 μm and the middle part of the it has a height of 23 μm. For this purpose three masks were drawn using AutoCAD and printed on transparency films. The fabrication procedure of the 1.9 μm and the 83 μm channels is the same as the two layer mold. So, first we created the 1.9 μm parts of the gradient channels using the S1813 photoresist and then we spin-coated the SU8-2025 photoresist at 3500 rpm

for 1 min to create the middle part of the gradient channel with a 23 µm height. The wafer was exposed to UV light(200 mJ /cm^2),baked on hot plate at 95 °C for 7 min and developed using SU-8 developer. Followed hard bake of the wafer at 200°C for 4 hr. Finally we spin-coated the third layer of SU8-3050 photoresist which represents the precursor for DB,CAMP and cell seeding channels.

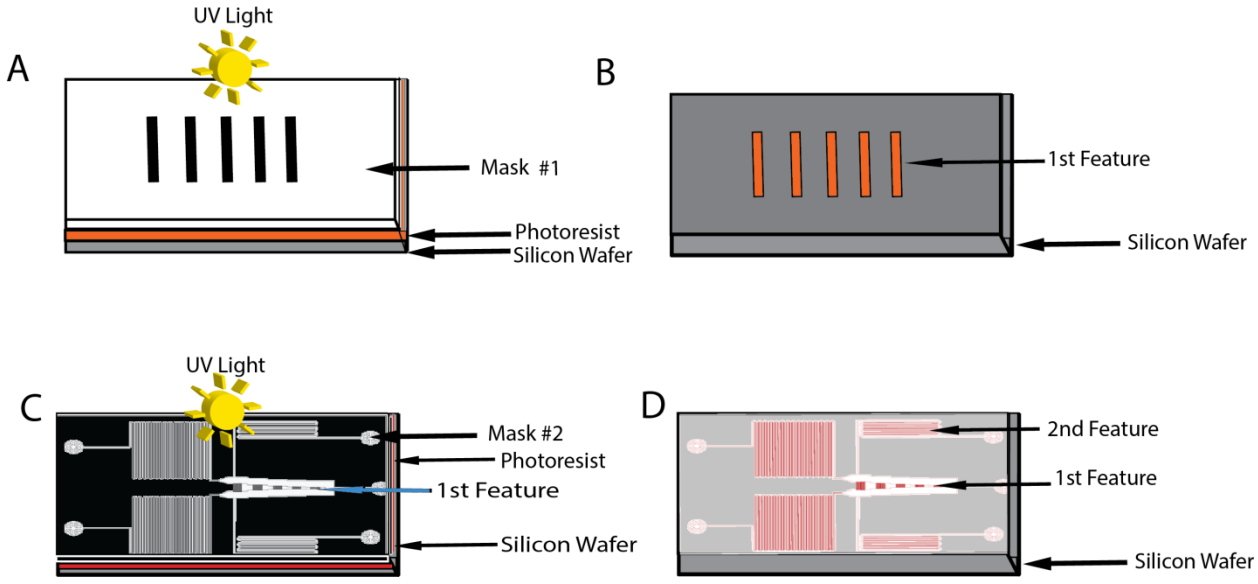

Figure 16: Schematic representation of the lithographic process. (A) SU-8 photoresist is spin-coated on a bare wafer and exposed to ultraviolet light through mask #1. (B) Exposed SU-8 photoresist is developed to define channel patterns of the fist layer. (C) A second layer of SU-8 photoresist is spin-coated on top of the 1st feature and exposed to ultraviolet light through mask #2. (D) The second layer of SU-8 is developed to create the pattern of the microfluidic device.

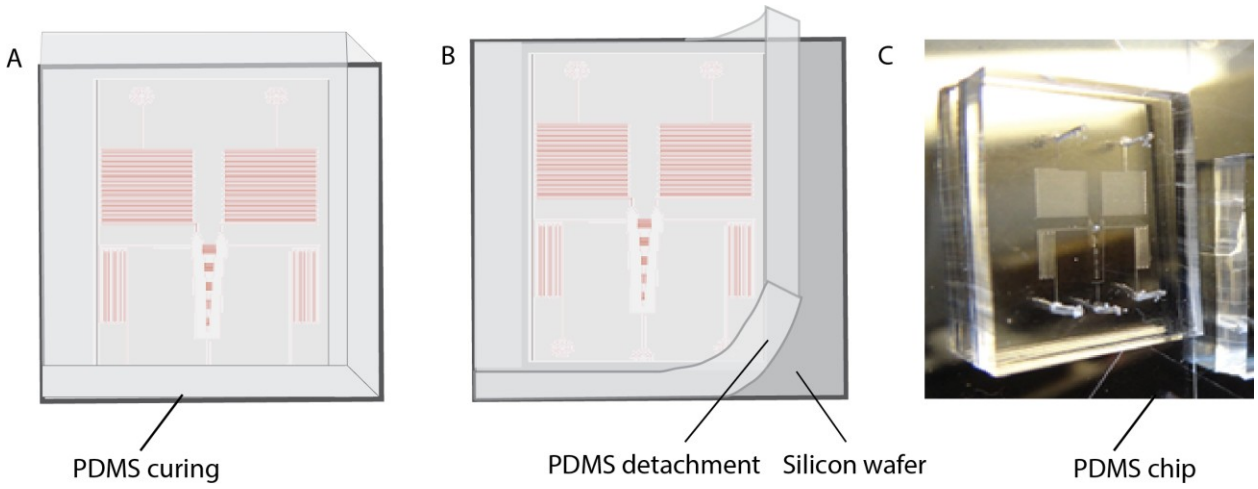

Figure 17: Photolithography procedure. (A) A mixture of Polydimethylsiloxane (PDMS) and cross-linking agent with a 10:1 ratio is poured on top of the patterned wafer and left to cure. (B) Cured PDMS is peeled off from the wafer. (C) The device is trimmed, the inlets and outlets of the chip are opened and the channels are sealed by bonding the PDMS device to a cover glass.

2.3.2 Cell loading into the microfluidic device

Initially, PDMS device was primed by using development buffer in the two main inlets. During this time the cell inlet, outlet, and the outlet of the device were closed. When all the gradient channels were filled with development buffer and there was no air inside of them, the two main inlets were closed. Next, the cells were loaded into the microfluidic device by applying a negative pressure at the cell outlet. A pipette tip which contained the cells was plugged into the cell inlet and tubing that had a syringe connected to the other end was plugged into the cell outlet. The syringe plunger was removed and there was 2 ml of development buffer inside the syringe. The syringe was hold at a height lower than the cell outlet, in this way a negative pressure was applied at the cell outlet, in order to drug the cells into the thick channels (Fig 18). After cell loading was done,

the cell inlet and outlet were closed and the cells were left to settle on the substrate for 5 min. Lastly, the main outlet of the device was opened and we flowed development buffer through the left inlet and cAMP solution on the right inlet. Gradient was generated at the thin channels by molecular diffusion. The concentrations of cAMP that we used to create the different gradients are the following: 0-0.1 μM (0.7 nM/μm), 0-0.5 μM (3.3 nM/μm), 0-2μM (13.3 nM/μm), and 0-3 μM (20 nM/μm). The flow at the two inlets of the device was turned on during the study of the migration of cells through the gradient channels.

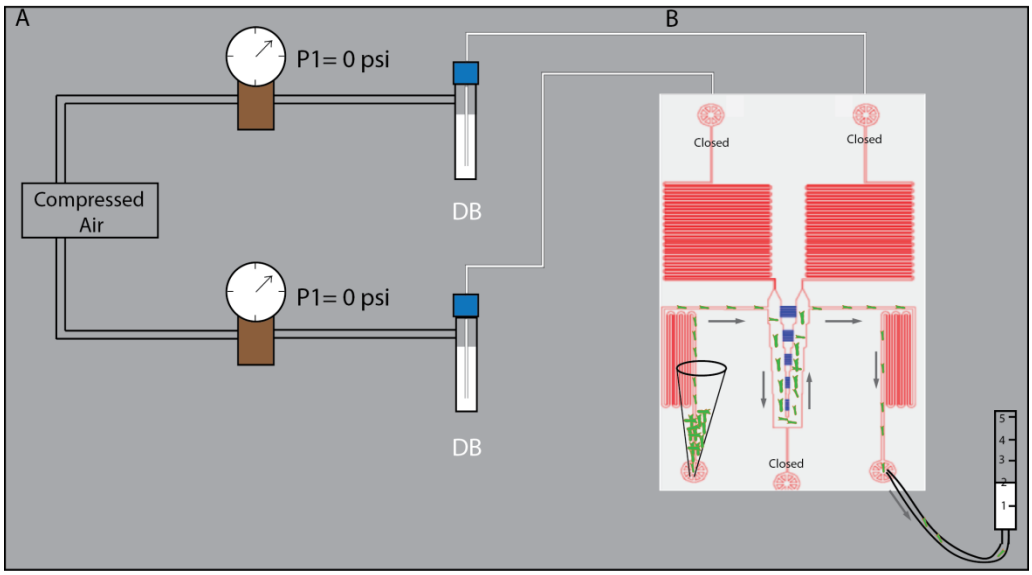

Figure 18: Schematic of the experimental set up. The first part of the schematic is an illustration of the external pressure system and the second part depicts the procedure that we used to load the cell suspension into the microfluidic chip.

2.4 Live cell imaging

Measurements were performed with a Nikon Eclipse Ti swept field confocal microscope (70 μm confocal slit, Nikon/Prairie Technologies) equipped with an Andor iXon 897

camera, four 50 mW solid-state lasers for excitation, a 60x oil objective (NA 1.49), which produced a 1.1 µm-thick optical slice. Protrusion activity was verified using brightfield microscopy to ensure that the thickness of the confocal optical slice was adequate to capture all blebs across the cell cross section. Cell imaging was performed in DB buffer and cells were seeded into the microfluidic chamber at a concentration of 2.5 x 10^5 cells/mL. Cell activity was captured in 4 minute increments. Cell speed was determined by dividing total distance of the cell trajectory by 4 min and the chemotactic velocity was calculated by dividing the net distance cells travel towards the cAMP source by 4 min. The chemotaxis index was obtained by dividing the net distance towards the source by the total migration distance. These calculations were performed using ImageJ (Fiji) with the MtrackJ plugin. Cell trajectorieswere calculated using the ImageJ chemotaxis plugin. Lastly, the bleb surface area was calculated based on measurments obtained with two dimensional confocalmicrographs; we measured the perimeter of each cell bleb and converted this data into a 2D surface area.

Results of blebbing for different microchannel heights were compared using one way ANOVA and unpaired Student's *t*-tests.

Differences were considered significant at $P < 0.05$. Each experiment was performed with between 20-50 cells from several microfluidics gradient channels.

2.5 Human fetal foreskin fibroblast cells (NUFF)

2.5.1 Materials

1. 0.5 ml (0.1 µm) Filters

2. DMEM (11965092 Dulbecco's Modified Eagle Medium (D-MEM) (1X), liquid, high glucose) is a widely used basal medium for supporting the growth of many different mammalian cells. Cells successfully cultures in DMEM include primary fibroblast, neurons, lial cells, HUVECs, and smooth muscle cells, as well as cell lines such as HeLa, 293, Cos-7, and PC-12.
3. HI FBS (Heat Inactivation of Fetal Bovine Serum).
4. Pen/Strep (Penicillin Streptomycin is an antibiotic that can help eliminate or control cell culture contamination.
5. Dulbecco's Phosphate-Buffered Saline (D-PBS) (1X), liquid (phosphate buffer saline provides exactly what the name implies (so that the pH stays approximately constant) and just as many ions per unit volume as the inside of the cell (so that the cells do not swell or shrink)(without Ca^{2+} and Mg^{2+}).
6. Trypsin, 0.25% (1X) with EDTA 4Na, liquid (it is a dissociation reagent, detach the cell from the flask).
7. 150 sq cm Flasks

2.5.2 Passaging cells

1. Filter DMEM, Pen/Strep, and HI FBS. Change media every 2-3 days.
2. Grow in DMEM 11965 supplemented with 10% HiFBS.
3. Pre-warm culture media, DPBS and Trypsin to 37°C in water bath (it takes approximately for 15 min).
4. Remove the cells from incubator (37°C, 5% CO_2, 80% humidity and O_2), observe under the microscope and aspire off the media.

5. Wash the flask with 5 ml DPBS and aspirate. This wash removes any trace of serum, calcium and magnesium that would inhibit the action of trypsin.
6. Remove and discard the wash solution from the flask.
7. Add 7 ml Trypsin in the flask.
8. Incubate the cells at 37°C for 2-3 min.
9. Remove the cells from the incubator and observe under microscope for detachment.
10. Transfer the 7 ml content of the flask into a 45 ml conical tube and add 8 ml fresh media.
11. Centrifuge them at 1,000xg for 5 minutes.
12. Aspirate the content from the conical tube keeping only the cell pellet on the bottom.
13. Resuspend (pipetting) the cell pellet in a 5 ml media.
14. Move 1 ml from the conical tube into the flask.
15. Dilute the cell suspension adding 19 ml media in the flask.
16. Return the cells to the incubator.
17. Information on the flask
    a) Name of the cells
    b) Passage number
    c) Passage rate: 5:1
    d) Date of changing the media
    e) Researcher's name

2.5.3 Freezing of adherent cells

Freeze cells down in 10% DMSO and regular media. Store 5 ml (cells, regular media, and DMSO).

1. Do all the steps of passaging the cells.
2. Resuspend the pellet in 2.5 ml of media.
3. Make 20% DMSO in media (freezing media). 2.5 ml of media and DMSO- 0.5 ML DMSO and 2 ml media.
4. Add 500 µl of cells to cryovial (label cell name, passage number, ration, your name and date).
5. Add 500 µl of freezing media to cells in cryovial. Now you will have a 10% DMSO concentration at the end.
6. Place cells in Mr.Frosty for the moment and then pace in -80°C for overnight storage.
7. Cells must subsequently be placed in liquid nitrogen for long term storage.

2.5.4 Thawing cells

1. Remove the cells from liquid Nitrogen.
2. Pu the cells for few minutes in the water bath (leave a small ball of ice in the cells).
3. Transfer the cells in a 15 ml conical tube.
4. Add 9 ml media (add 8 ml media directly in the conical tube which contains the cells and 1 ml in the cryovial and after that transfer th e1 ml from the cryovila to the conical tube). So in the conical tube we have 10 ml of cells and media.

5. Centrifuge them for 5 min at 1000 rpm.
6. Aspirate the media from the conical tube.
7. Resuspend the cells in 1 ml media.
8. Add 19 ml media in a flask.
9. Finally, move the cells into the flask.

All the protocols related to NUFF cells are adapted from Professor Sharon Gerecht' lab.

CHAPTER 3: AIM OF THE PROJECT

3.1 Introduction

During migration, motile cells must restrict protrusive activity to their periphery if they are to migrate efficiently, and during chemotaxis, these projections must be controlled by the chemotactic gradient. Migrating cells move by extending their leading edge using two main types of protrusions: pseudopods (or lamellipods) driven by actin polymerization, and from pressure-driven membrane blebs (Charras and Paluch, 2008; Ridley, 2011). Blebs are rapidly expanding rounded membrane protrusions that form when the cell membrane separates from the cortex. They grow as a result of intracellular pressure created by myosin II-mediated cortical contraction (Charras et al., 2005; Maugis et al., 2010; Trinkaus, 1973). Blebbing occurs during cytokinesis (Stewart et al., 2011), cell spreading (Gauthier et al., 2011) and apoptosis ; however, recent work demonstrates that blebs also play a role as leading edge protrusions in restrictive three-dimensional environments (Bergert et al., 2012; Gadea et al., 2007; Lammermann and Sixt, 2009; Sahai, 2005; Sahai and Marshall, 2003; Tozluoglu et al., 2013; Wolf et al., 2003).

Dictyostelium amoebae can also move using blebs (Langridge and Kay, 2006; Tyson et al., 2014; Yoshida and Soldati, 2006; Zatulovskiy et al., 2014). *Dictyostelium discoideum* is a fast-moving genetically accessible single cell organism, and has become an ideal model for studying basic aspects of cell motility (Friedl et al., 2002; King and Insall, 2009). When starved, *Dictyostelium* cells undergo a developmental process where signaling proteins are upregulated, and after a few hours, they develop a

polarized morphology as well as the ability to sense and chemotax towards sources of cyclic adenosine 3',5'-monophosphate (cAMP). Oscillatory pulses of cAMP coordinate and recruit chemotaxing cells to form multicellular structures and these cells make a natural transition from moving individually on a planar surface to moving within confined three-dimensional aggregates (Bozzaro, 2013).

In this work, we offer insight into the role that confined environments can play in promoting the formation of blebs during chemotaxis. In particular, we make use of microfluidics to create confining microchannels with stable linear cAMP gradients. Dictyostelium cells are loaded into non-confined microchannel chambers and coerced to migrate through confined channels with a fixed width (50 μm) and varying height (1.7, 2.4, or 3.8 μm). Because bleb-driven movement is chemotactic (Langridge and Kay, 2006) and triggered by applied mechanical resistance, this raises further questions about how cAMP gradient steepness influences bleb formation and how this influences the balance between actin polymerization and myosin contractility to produce blebs.

Therefore, the questions that we aimed to answer in this study are the following:

- How does the height of the gradient microchannels influence the type of protrusions that the cells utilize at their leading edge in order to migrate?
- How does the cAMP gradient steepness impact the blebbing frequency when the height of the gradient channel is constant?
- How does the microfluidic confinement influence the localization of mechanoenzyme myosin II?
- How does the activity of myosin II changes with increasing the gradient steepness?

- How will myosin II-null cells, blebbistatin, and sorbitol treated cells behave?

3.2 Experimental procedures

3.2.1 Microfluidic gradient generator

A major disadvantage of utilizing agarose overlays for observing migrating cell populations is that they do not incorporate well-controlled chemical and mechanical constraints. During migration, cells must squeeze and move underneath the agarose. During this process they locally detach the overlay and move it upward. Cells therefore face spatial variations in height and mechanical resistance since the cell must deform and lift the agarose off the substrate surface to move forward. Therefore, the cell's leading edge is more confined. The chemical gradient is also difficult to control since is not stable and continues to change over time (Song et al., 2006b). Furthermore, under agarose environments do not allow for the removal of any chemicals released by the cells, which can influence their environment and the cAMP gradient. As an alternative to agarose, we studied the influence of cell confinement and gradient steepness on blebbing in a microfluidic environment. Unlike agarose overlays, cells can be controllably coerced into precisely controlled microchannels containing stable linear chemical gradients. The degree of mechanical resistance can be varied by simply changing the height of the microchannels that cells migrate through (Liu et al., 2015). So far, under agarose assays have shown that *Dictyostelium* cells use blebs to migrate in resistive confined environments. However, the influence of gradient steepness on blebbing has not been investigated. Microfluidics has been used to produce stable gradients for *in vitro* cell migration studies. Moreover, many different types of gradient

geometries have been used to study migrating cell populations both on 2D and 3D substrates (Atencia et al., 2012; Breckenridge et al., 2010; Heuze et al., 2011; Huang et al., 2011; Irimia et al., 2006; Irimia and Toner, 2009; Jeon et al., 2000; Jowhar et al., 2010; Long and Ford, 2009). Microfluidic gradients have been used to examine the migration of tumor cells (Irimia and Toner, 2009; Saadi et al., 2006; Tong et al., 2012; Wang et al., 2015), neutrophils (Lin et al., 2004), and the localization of internal molecules at high resolution in *Dictyostelium* (Skoge et al., 2010). However, these devices have not been extended to analyzing the influence of chemical gradient steepness on cell protrusion type.

All microfluidic devices were made of PDMS (Momentive, RTV 615A) using standard soft lithographic methods. Briefly, a 1:10 mixture of PDMS elastomer and curing agent was poured atop a lithographically fabricated polymer mold, cured, and gently peeled off. Fluid ports were punched into the PDMS using a 0.75 mm biopsy punch (Ted Pella, Inc.), the microfluidic device and coverslip were exposed to oxygen plasma (Jelight, Model 42A) and immediately aligned and sealed under an inverted microscope, and the assembled device was baked at 90 ˚C for 2 hours to ensure strong bonding. Buffer solutions (DB and DB + cAMP) were delivered to each microfluidic inlet at a flow rate of 1.5 μL/min using a low-cost external pressure driven flow controller (Mavrogiannis et al., 2016). A solution of Alexa Fluor 647 hydrazide (Invitrogen) was dissolved in the cAMP buffer to characterize the concentration profile of cAMP because of their comparable molecular weight.

To create regions of controlled microfluidic cell confinement, we fabricated “thin” gradient channels orthogonal to “thick” buffer channels using a two-step soft-lithography

process inspired from previous chemotaxis work conducted by (Skoge et al., 2010). First, the “thin” confinement channels were patterned on a silicon wafer using a low viscosity photoresist. A second “thick” photoresist was spin-coated onto the wafer and patterned to create non-confining gradient side-channels and cell-seeding chambers. Once the microchannel mold was completed, PDMS elastomer was poured atop and cured. The final cured PDMS slab was peeled off the wafer and bonded to a glass slide using a brief oxygen plasma treatment to form the completed gradient device. The final device consisted of confining gradient chambers orthogonally-aligned with two larger main channels. These channels were designed with a length L = 150 μm and width W = 50 μm, with various microchannel heights H ranging from 1.7 to 3.8 μm (Figs 19a and 19b). To prevent shallow channels from collapsing during fabrication, we installed small pillars at each confined microchannel entrance and exit. The pillars or the PDMS did not impede cell invasion or impact the formation of the passive gradient as *Dictyostelium* cells can form actin foci on both surfaces, glass and PDMS (Skoge et al., 2010) and their adhesion is not affected by surface hydrophobicity (Loomis et al., 2012).

Two inlets upstream of the gradient chambers served as loading ports for buffer and chemoattractant, while the two downstream inlets were used for cell seeding into the device. The gradient generator operated using constant pressure-driven flow. The upstream inlets were pressurized at equal pressures using an external constant pressure source to deliver cell buffer (0 μM cAMP) to one side of the device and chemoattractant to the other side. The concentration of cAMP solutions used to generate the gradients were 0.1 μM cAMP, 0.5 μM cAMP, 2 μM cAMP, and 3 μM cAMP. Because the microfluidic design is symmetric and the fluid pressures are equal,

no fluid flow is produced across the two main flow channels and stable gradients of chemoattractant are generated within the confinement chambers through molecular diffusion between these two flow channels. To visualize the diffusion-driven gradient (Fig 19b), fluorescent Alexa Fluor 488 and Alexa Fluor 647 dyes were introduced into the buffer and chemoattractant streams, respectively. The gradient was rapidly established across the confinement slots and maintained indefinitely due to the continuous passive molecular diffusion between the two flowing buffer chemoattractant reservoir streams (Fig 19c).

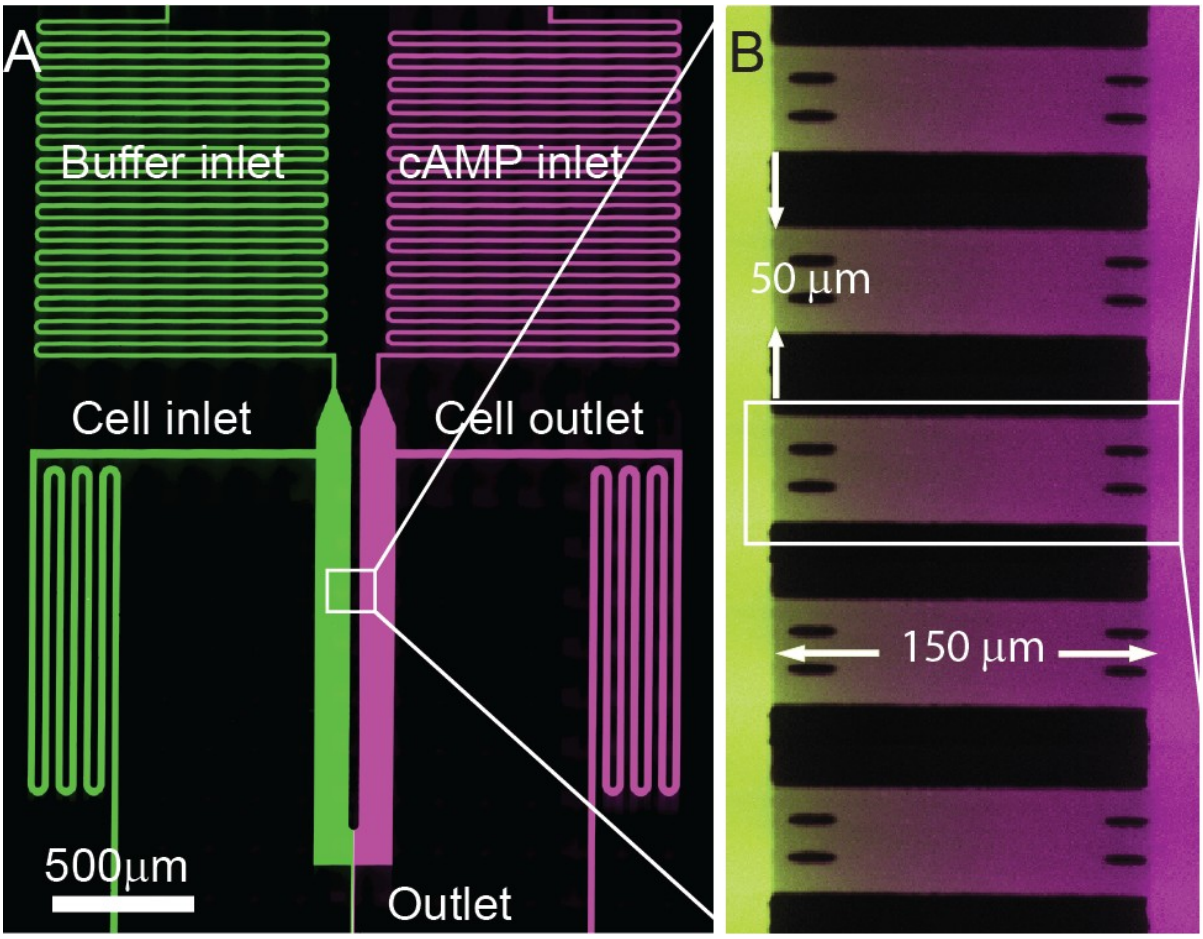

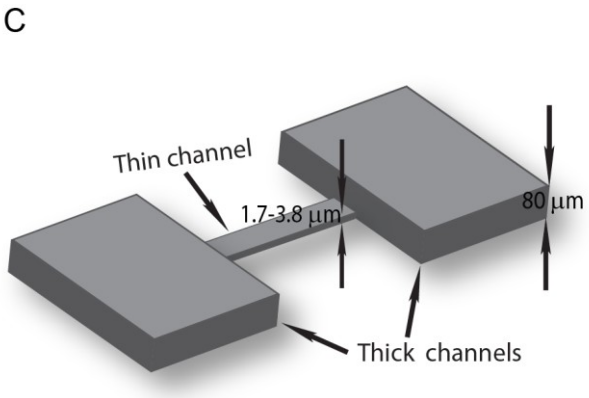

Figure 19: Microfluidic device for studying cell blebbing in confinement. (A) Confocal micrograph of the microfluidic gradient generator. The device consists of an array of microchannel gradient channels aligned perpendicular to main flow channels. Buffer is introduced through “Buffer inlet” (shown in green), and buffer with cAMP is introduced through “cAMP inlet” (shown in purple). Cells are loaded into the device by flowing a cell suspension into the “Cell inlet”. (B) Linear concentration profiles in gradient channels are established through molecular diffusion between the two main flow channels. Each gradient channel has a length of 150 µm and a width of 50 µm. (C) The “thin” confinement channels are between 1.7 and 3.8 µm in height connected to the main “thick” flow channels that are 80 µm in height.

3.2.2 Fluorescence markers for bleb identification

Cells were derived from the axenic strain Ax2 of *D. discoideum*. Cells were grown in 1.5X HL-5 medium with glucose (FORMEDIUM Ltd.)(1L H2O, 15 g proteose peptone, 3.9 g bacto-yeast extract, 3.0 g glucose, 0.13 g Na_2HPO_4-$7H_2O$, 0.13 g KH_2PO_4), and all experiments were performed at 22^{o}C. Ax2 was transformed with markers for F-actin (GFP-LimEΔcoil), the plasma membrane (cAR1-mCherry, kindly provided by P.N

Devreotes) (Fig 20). Transformed cell lines were selected with G418 and Hygromyocin B. When exponentially growing cells reached a concentration of 2-4 x 10^6 cells/mL, they were washed free of growth medium in development buffer (DB; 5 mM $KHPO_4$, 5 mM Na_2HPO_4, 1 mM $CaCl_2$, 2 mM $MgCl_2$ pH 6.4) and resuspended in DB buffer at a concentration of 2 x 10^7 cells/mL. Cells were then starved by shaking at 180 rpm for 4 h with pulses of 100 nM cAMP added every 6 min after the first hour.

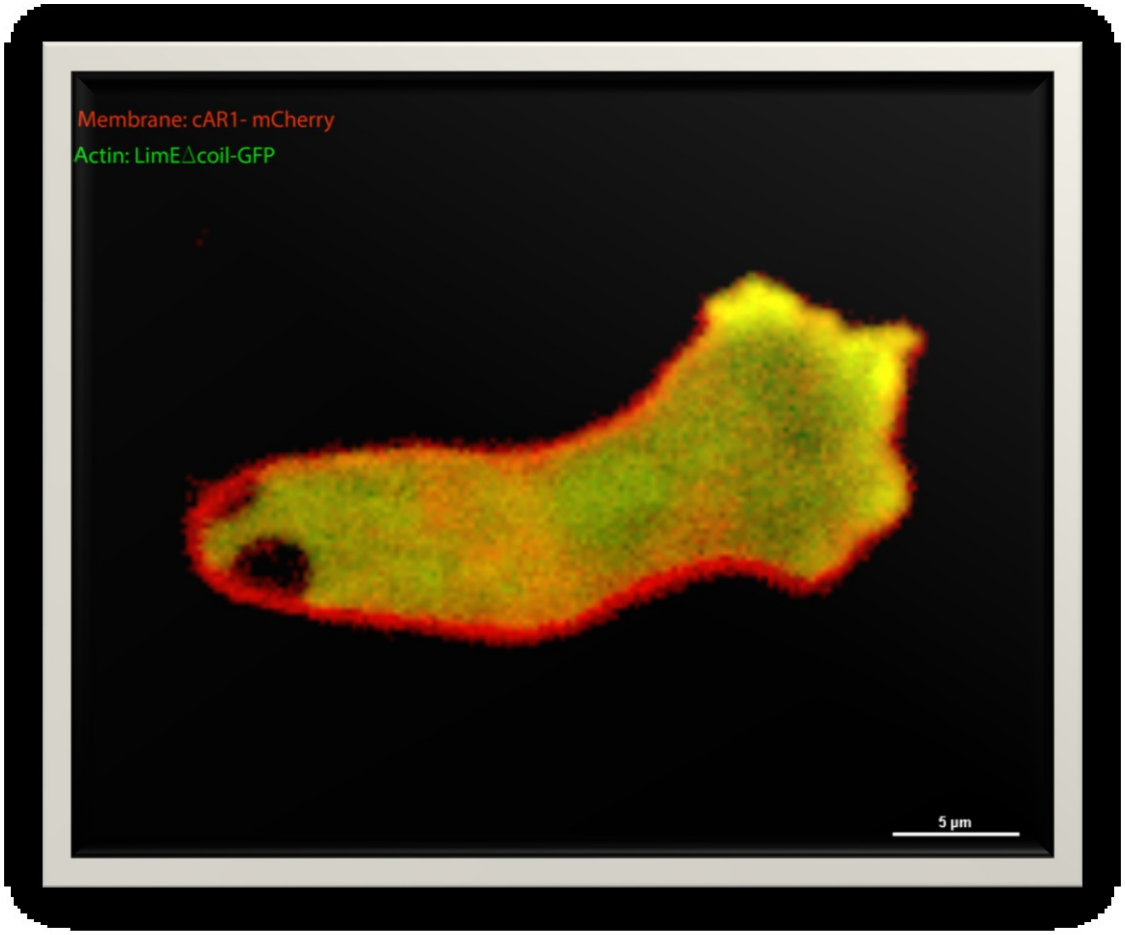

Figure 20: Fluorescence markers. Membrane was labeled red by tagging the cAMP receptor cAR1 with mCherry and actin was labeled green by tagging the actin binding protein(LimEΔcoil) with green fluorescence protein (GFP).

3.2.3 Experimental setup

To perform our experiments we used a low cost external pressure system to deliver the liquid solutions to the inlets of the PDMS device at a flow rate of 1.5 µl/min. Initially, we delivered development buffer to the two main inlets of the device, this way we were able to remove all the air that was in the microfluidic channels. Next, we loaded the 4 hr starved cells by flowing the cell suspension through the cell inlet. Lastly, we establish a linear gradient through in the gradient microchannels by flow development buffer through one inlet and cAMP with development buffer through the other main inlet. The cells were able to detect the gradient and move toward the entrance of the gradient microchannels. When Dictyostelium cells traverse through the gradient channels they experienced the same cAMP gradient throughout the channels. However, the cells encounter a higher concentration of cAMP as they were getting closer to the outlet of the channel (Fig 21).

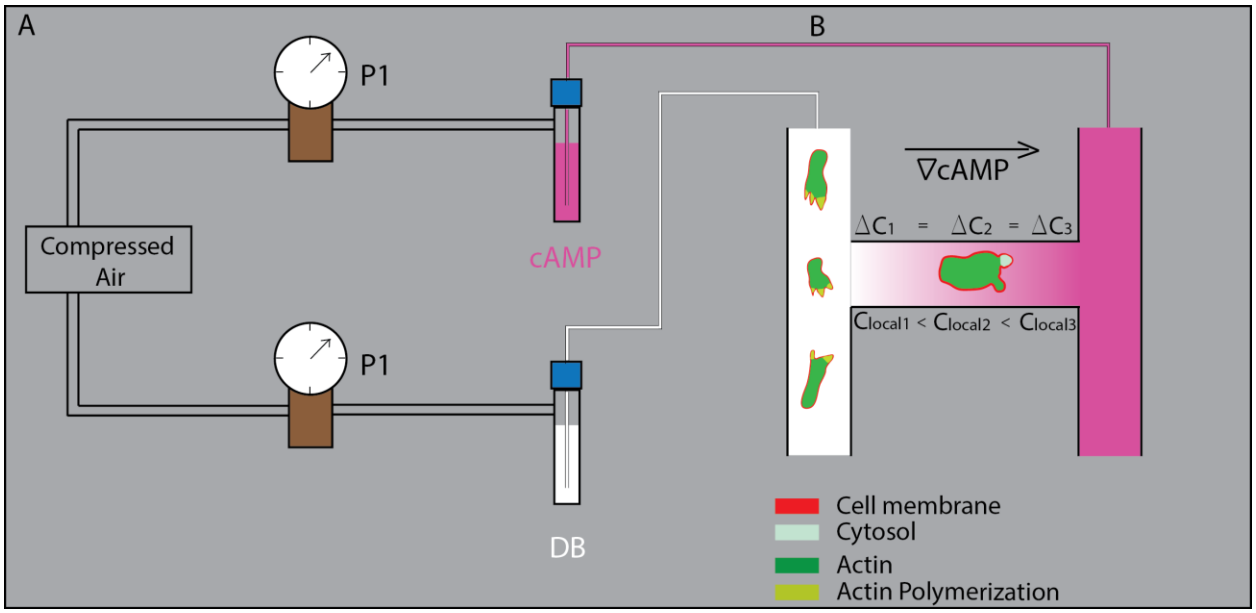

Figure 21: Illustration of the experimental set up. (**A**) Constant pressure system for delivering development buffer and cAMP solutions to the microfluidic device. (**B**) Depiction of microfluidic gradient generator device used to study chemotactic *Dictyostelium* cells migrating under confinement. A linear gradient produces constant relative cAMP concentration over the entire channel length while the local cAMP concentration is low at the inlet of the gradient channel and approaches the concentration of the cAMP solution used to form the gradient at the outlet.

Dictyostelium cells of 10 μm in diameter, initially not confined at a 80 μm tall channel sense the cAMP gradient and migrate toward the entrance of the gradient channels by using pseudopods (Fig 22). The gradient channels represent the resistive environments since the channel height is smaller than the natural height of the cell when left unconfined. When cells arrive at the entrance of the gradient channels enter by flattening and forming mostly pseudopods. In the next chapters we are presenting the data related to the migration of the cells in the resistive microfluidic environments.

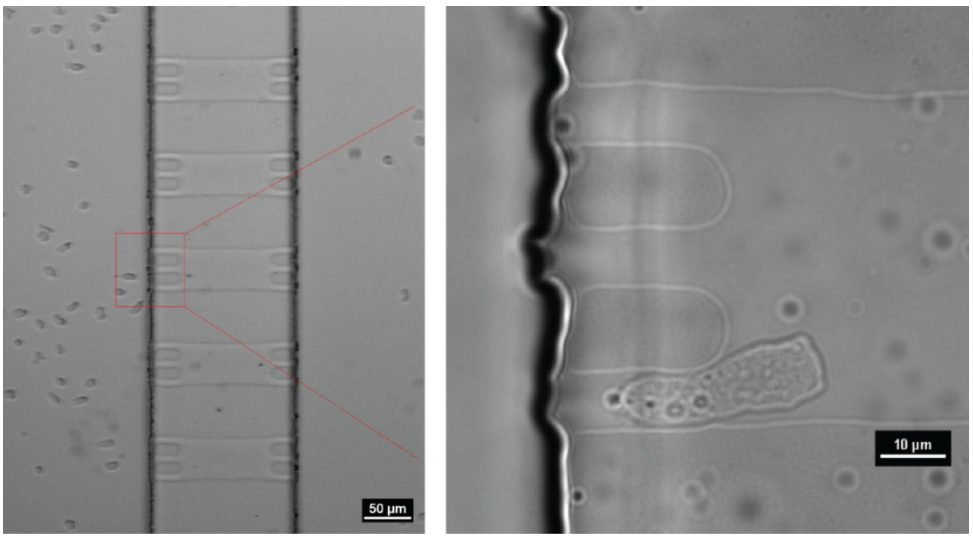

Figure 22: Brightfield micrographs of the PDMS microfluidic device.

CHAPTER 4: BLEB-DRIVEN MOTILITY UNDER MICROFLUIDIC CONFINEMENT

4.1 Introduction

During chemotaxis under buffer, *Dictyostelium* move mainly using F-actin-driven pseudopods, but switch to using blebs when migrating through mechanically resistant environments (Zatulovskiy et al., 2014). This behavior is usually observed using an elastic overlay, such as agarose, where cells are coerced to migrate underneath and deform the overlay to continue towards a nearby well containing cAMP. Cells passing under the agarose exert mechanical force on the overlay and in doing so experience mechanical resistance from it. The degree of mechanical resistance can be controlled using different agarose concentrations. Previous work has shown that when the stiffness of the agarose is increased, cell blebbing increases (Zatulovskiy et al., 2014).

Blebbing was previously observed in *Dictyostelium* cells as they migrated under agarose towards a nearby well containing cAMP (Zatulovskiy et al., 2014). The proportion of blebs compared with total cellular projections increased from 20% under buffer and approached upwards of 100% in cells moving under overlays with more than 1% agarose. As might be expected, cells were observed to flatten when moving under the agarose, with the cell height decreasing with increasing agarose stiffness. When non-confined under buffer, for example, cells migrated with an average height of ~ 8 μm, while at an agarose concentration above 1% cells were flattened and migrated with a height of ~ 3.5 μm. Based on the confined cell height under agarose, we fabricated microfluidic confinement chambers for quantifying cell protrusion activity, and

determined the equivalent microchannel height where blebbing was shown to play a significant role in motility.

4.2 Results

4.2.1 Developed cells undergo chemotaxis in microfluidic channels

To investigate the influence of microfluidic confinement on cell blebbing, we examined *Dictyostelium* cells migrating through channels of varying height. For each case, wild-type Ax2 cells were coerced to migrate on glass through a confinement channel using a stable linear gradient of cAMP. The channel height was controlled using standard soft lithography techniques, and the cAMP gradients were imaged using confocal microscopy (Fig 19a). To illustrate the microfluidic gradient, buffers were labeled with two different Alexa Fluor fluorescent dyes. Cells were loaded and seeded into the device by flowing a cell suspension through the cell inlet and outlet channels. The cAMP gradient was created using positive pressure to deliver continuous and equal flow rates through two microfluidic inlets, one (shown in green) containing development buffer (DB) and a second (purple) with a fixed concentration of cAMP in DB. Confinement channels of varying micron-scale heights were fabricated across the DB and DB/cAMP inlets. A gradient was quickly established by passive diffusion from one fluidic inlet to the other across these channels (Fig 19b). Cells were then imaged as they migrated from 80-μm “thick” buffer channels across a “thin” confinement channel 150 μm in length and into the adjacent cAMP/DB channel (Fig 19c).

We first performed experiments to investigate the influence of microchannel height on the formation of cell blebs and observed the migration of confined *Dictyostelium* cells

through a thin microfluidic channel containing a controlled cAMP gradient (Fig 23a). A solution of Alexa Fluor 647 hydrazide (Invitrogen) was dissolved in the cAMP buffer to characterize the concentration profile of cAMP because of their comparable molecular weights. We followed cell protrusion activity and formation by transforming cells with a construct that generates Green Fluorescent Protein (GFP) linked to a protein domain that specifically binds to F-actin (LimEΔcoil) (Fig 23b). The position of the cortex was simultaneously imaged relative to the cell membrane location using the cyclic AMP receptor 1 (cAR1) fused to mCherry (mCherry-cAR1) as a membrane marker (Fig 23c).

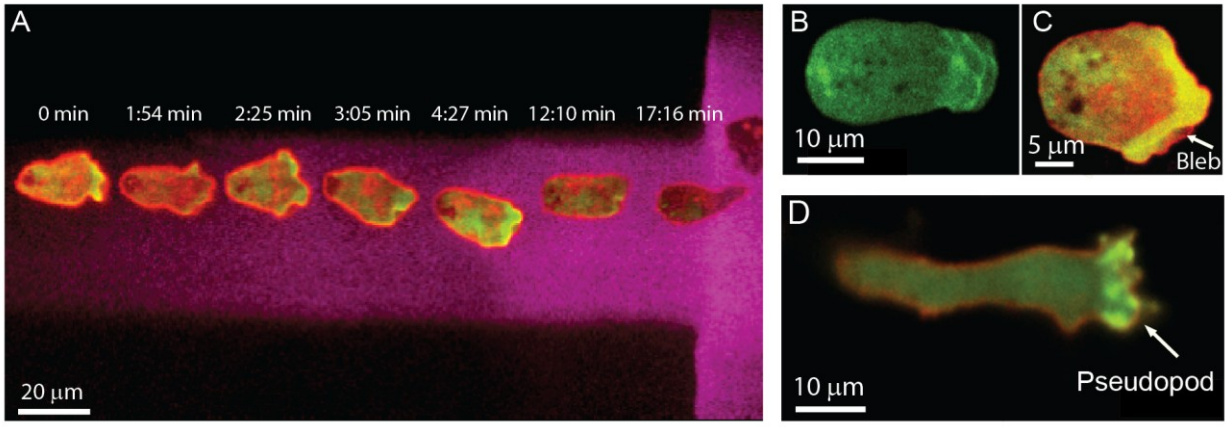

Figure 23: Cell migration in microfluidic confinement. (A) A confined *Dictyostelium* cell migrates up a cAMP gradient. The gradient is imaged using Alexa Fluor 647 hydrazide. The seven superimposed micrographs of the cell were captured (3.28 FPS) at time intervals t = 0, 1:54, 2:25, 3:05, 4:27, 12:10 and 17:16 min. (B) During bleb expansion F-actin scars remain behind and the newly formed bleb is almost devoid of F-actin. (C) When confined, blebs formed at the leading edge of a cell expressing a membrane marker (mCherry-cAR1) and F-actin reporter (GFP-LimEΔcoil). (D) Cells predominately formed pseudopods when migrating under buffer.

4.2.2 Classification of protrusions as blebs or pseudopods

As cells migrated across the confinement channel, protrusions were classified in terms of the observed actin dynamics at the cell membrane. Pseudopods expand slowly and steadily, with F-actin remaining continuously associated with the membrane as they expand (Fig 23c). Blebs, however, are rapidly expanding membrane protrusions that typically appear in less than one second (Fig 24). After the membrane detaches from the cortex, blebs leave behind an F-actin “scar”, which represents the previous cortex position (Fig 24b). The F-actin scar disappears in a few seconds while at the same time new cortex builds beneath the membrane of the bleb (Figs 24c, 24d). We classified protrusions as blebs or pseudopods depending on the presence of either an actin scar or actin at the leading edge. The blebbing activity was assessed by computing percent of blebs used compared to the total number of protrusions a cell used to transverse the confinement channel.

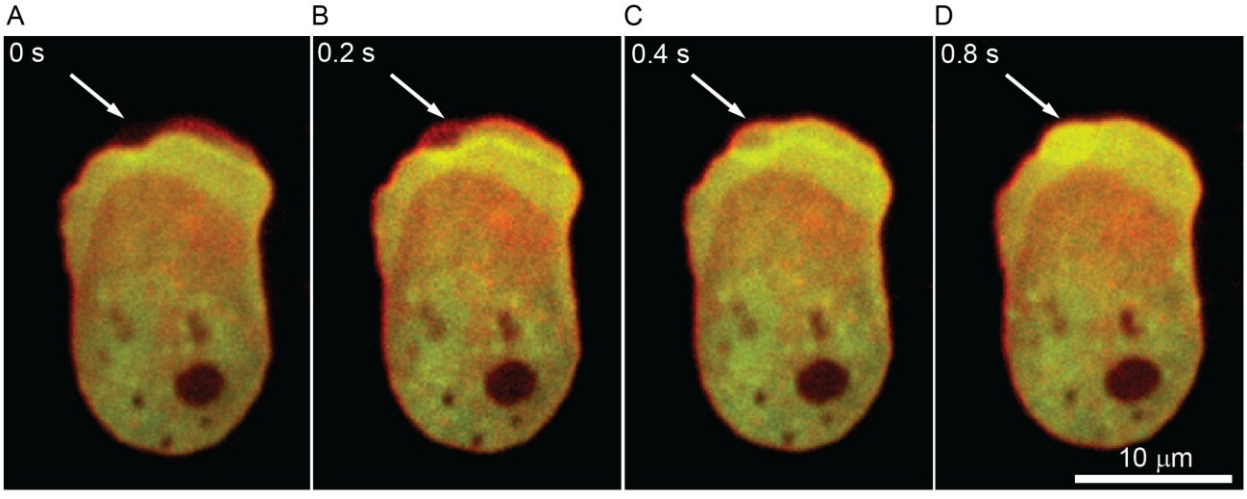

Figure 24: Blebs produced by a cell moving through a 1.7 μm microchannel. (A) A bleb forms when the cell membrane detaches from the cortex. (B) The bleb expands in

approximately 0.2 s, leaving behind a cortical F-actin scar. (C, D) Initially the bleb lacks an F-actin cortex, but it is rebuilt in less than one second. Images captured at 2.12 FPS.

Dictyostelium cells migrate using blebs when forced to move under agarose. Here, we extend these assays to microfluidic confinement channels for studying cell bleb formation. Previous work with agarose suggests that cells forced into a confined region ~ 3 μm in height will move predominately using blebs. Here, we investigated whether a mechanically restrictive agarose environment can be accurately translated into a microfluidic channel of fixed geometric height.

4.2.3 Microfluidic confinement heights

Using previous agarose overlay data as reference, we examined the blebbing behavior of *Dictyostelium* cells under different microfluidic confinement heights, varying between 1.7 μm and 3.8 μm (Fig 25).

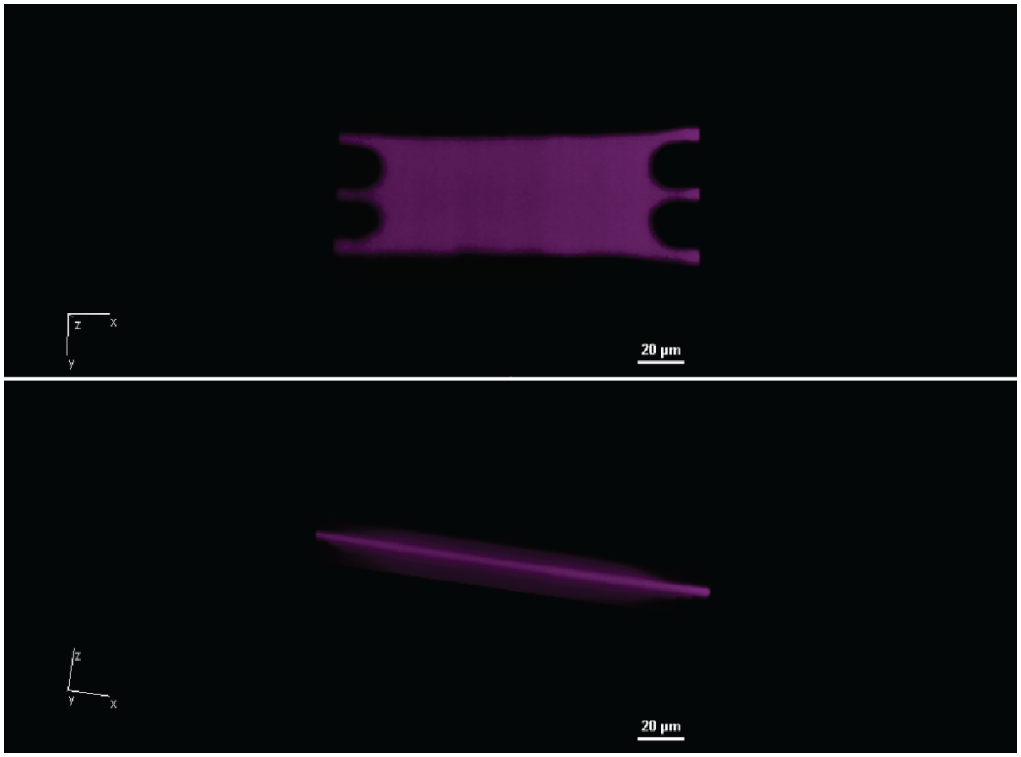

Figure 25: Top view and side view of the gradient microchannel. Confocal microscopy was used to capture z-stacks of the channels that were filled will Alexa flour 647.

Interestingly, unlike agarose where cells predominantly moved using blebs when flattened to a height of ~ 3.5 μm, we observed that cells confined to the equivalent height in a microchannel migrate using pseudopods. However, when the channel height was reduced to 2.4 μm, cells began using blebs with increased frequency. Based on these experiments, we investigated blebbing behavior using three different microchannel heights: 1.7 μm, 2.4 μm, and 3.8 μm. Each channel height was fabricated using a different microchannel mold and casting a new PDMS device.

4.2.4 Height of the confined cells expressing GFP-LimEΔcoil

We measured the microchannel mold height (channel height) and compared this with the height of confined migrating cells expressing GFP-LimEΔcoil using confocal microscopy (Figs 26a and 26b). The microchannel mold height matches the channel height with confined cells, indicating that fabricated channel height was not influenced by migrating cells and therefore cells were unable to deform the PDMS microchannel (Fig 26c). Moreover, cells were completely confined to within the given microchannel for all channel heights used in this work.

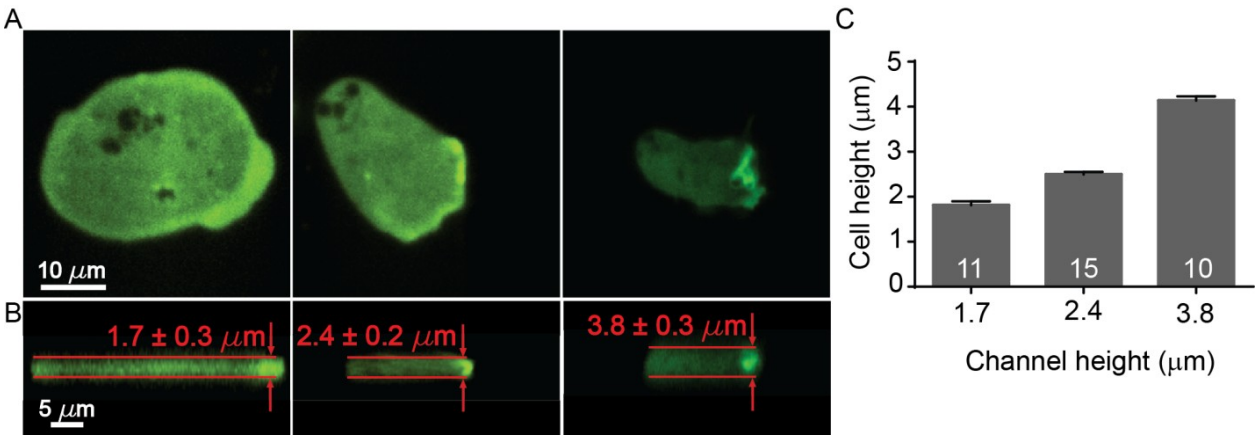

Figure 26: Cell confinement is controlled through microchannel height, as determined from confocal images. (A) Top view of cells confined using three different microchannel heights. (B) Side view of cells confined to heights of 1.7, 2.4 and 3.8 μm, as determined by using confocal microscopy. Fluorescence signal is from GFP-LimEΔcoil. (C) The measured cell height correlates with the fabricated microchannel height. Cell numbers shown on each bar. Error bars represent SEM.

4.2.5 The degree of microfluidic confinement influences the percentage of blebs utilized by the chemotaxing cells.

For each confinement experiment, developed *Dictyostelium* cells expressing mCherry-cAR1 and GFP-LimEΔcoil were seeded into a non-confining microfluidic chamber containing DB buffer. A cAMP gradient was established across the thin confinement channels and cells migrated towards the cAMP source using pseudopodia. Cells invaded the confinement channels and migrated up the cAMP gradient. Similar to previous bleb studies using agarose, the influence of microfluidic confinement on the cell protrusion mode was dramatic. Cells confined in 1.7 μm and 2.4 μm tall channels under a 20 nM/μm cAMP gradient predominantly migrated across the confinement

channel using blebs. Cells, however, confined in a 3.8-μm channel under the identical chemical gradient steepness moved largely using pseudopodia and formed only a small number of blebs (Fig 27).

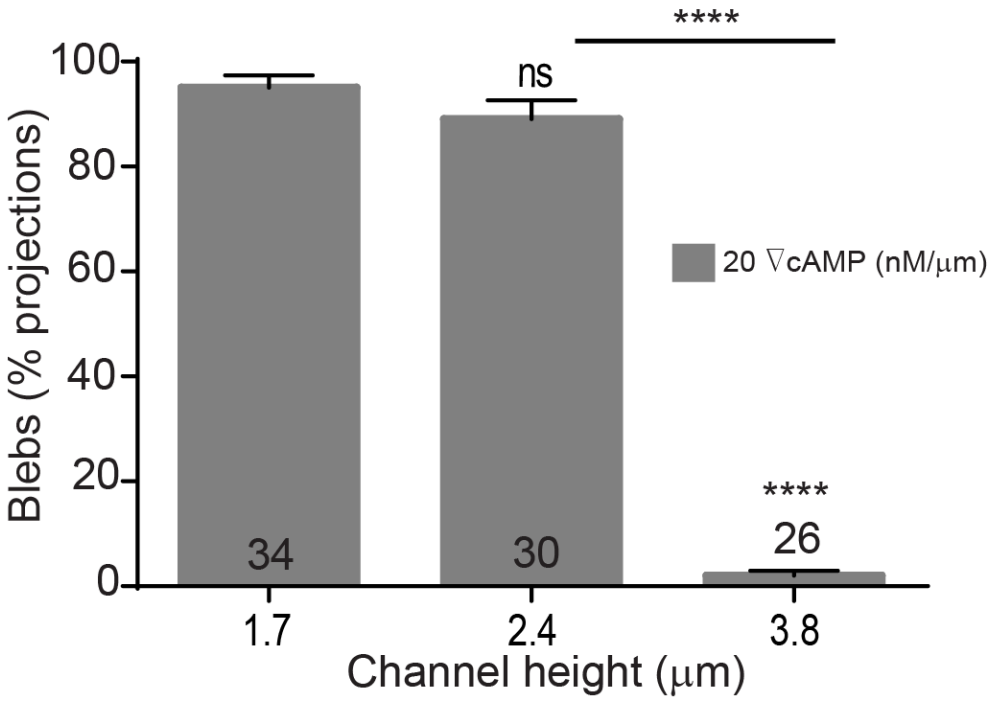

Figure 27: Cell migration is influenced by microfluidic confinement. *Dictyostelium* cells are observed as they migrate up a 20 nM/μm cAMP gradient. (A) Chemotactic cell velocity decreases as the height of the channel is reduced. (B) Blebbing increases as the height of the microfluidic gradient channel is reduced. Blebs given as percentage of total projections (pseudopods + blebs). Error bars represent SEM. The number of cells quantified shown on bars. **P ≤ 0.01, ***P ≤ 0.001, ****P ≤ 0.0001.

CHAPTER 5: INFLUENCE OF GRADIENT STEEPNESS ON CELL BLEBBING

5.1 Introduction

Chemotactic gradients can also control the position where blebs preferentially form (Zatulovskiy et al., 2014). During chemotaxis, PI3-kinase accumulates at the leading edge of migrating *Dictyostelium* cells (Manahan et al., 2004; Swaney et al., 2010). *Dictyostelium* cell blebbing is also strongly polarized up-gradient and is regulated through PI3-kinase (Zatulovskiy et al., 2014). In *PI3-kinase* null cells, where all five "type-1" PI3-kinases in the genome have been knocked out, cells migrate using significantly less blebs than parental cells (Zatulovskiy et al., 2014). Previous work also shows that the chemotactic response of *Dictyostelium* cells is dependent on gradient steepness (Song et al., 2006b).

In *Dictyostelium*, gradient steepness is an important factor in determining cell directionality and chemotactic velocity. Above a threshold gradient steepness (~10^{-3} nM/μm), the chemotactic motion of *Dictyostelium* is governed by the steepness of the applied gradient and is independent of the local cAMP concentration (Fisher et al., 1989; Jowhar et al., 2010; Song et al., 2006b). Since cAMP gradient steepness was shown previously to impact cell movement and chemotactic velocity, we investigated whether increases in cAMP steepness impacted cell bleb formation.

5.2 Results

5.2.1 The steepness of the cAMP gradient increases the blebbing frequency.

Because directedmotion of *Dictyostelium* in linear gradients was shown previously to occur when gradient steepness was greater than 10−3 nM/μm (Chan et al.), we used this threshold value as guidance for choosing the lowest gradient investigated in this work. Initially, we applied the gradient of 0.07 nM/μm (data not shown), however, the frequency of cells entering the channels was very low so we increased our gradient by one order of magnitude to 0.7 nM/μm. Based on this initial steepness, we used four different cAMP gradients in ourmicrofluidic channels: 0.7 nM/μm, 3.3 nM/μm, 13.3 nM/μm, and 20 nM/μm.We then quantified the number of blebs as a percentage of total projections (blebs + pseudopods) for cells migrating under each gradient steepness in microchannels with heights of 1.7 μm and 2.4 μm (Fig 28). The influence of gradient steepness on blebbing frequency is apparent with the proportion of blebs in cells migrating confined in a 1.7-μm channel increasing from 65% at a low steepness (0.7 nM/μm) to nearly 95% for the same cellsmoving up a 20 nM/μm cAMP gradient. Blebbing activity was measured in the same way for a channel height of 2.4 μm where cells displayed nearly identical (statistically insignificant) behavior with gradient steepness as compared to cells confined in a 1.7-μm channel (Fig 28).

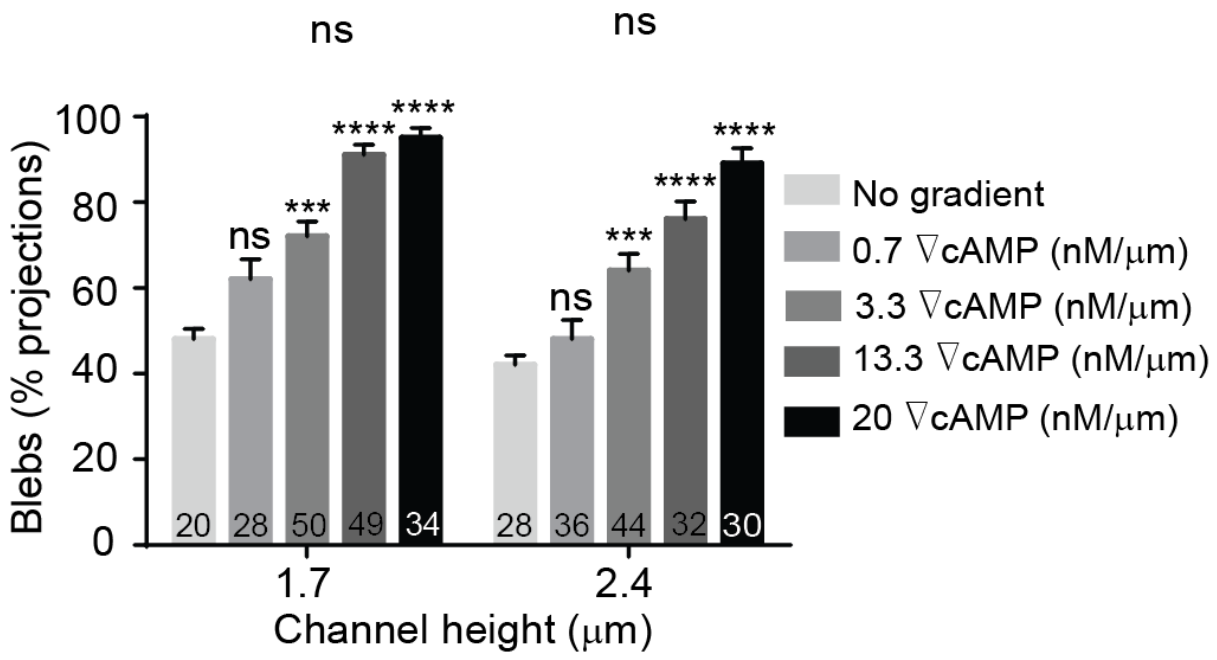

Figure 28: Bleb-driven movement is regulated by cAMP gradient steepness. The steepness of the cAMP gradient increases the blebbing frequency. Cell numbers are shown on bars. Error bars represent SEM. ***P ≤ 0.001, ****P ≤ 0.0001.

5.2.2 The local concentration of cAMP does not influence bleb driven motility.

When confined Dictyostelium cells traverse through the gradient channels they encountered a constant gradient of cAMP. However, the local concentration of cAMP is low at the inlet of the channel and has a maximum value at the high concentration outlet (Fig 29).

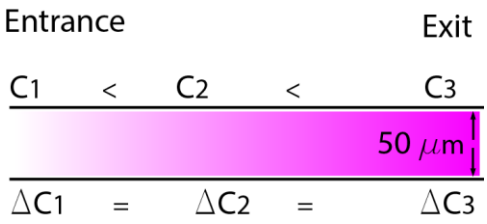

Figure 29: Illustration of the gradient michrochannel. The local concentration of cAMP increases as the cell is getting closer to the exit of the gradient channel.

To determine whether the blebbing was impacted by the local concentration of cAMP or by the relative gradient we quantified the number of blebs as a percentage of total number of protrusions (blebs + pseudopods) for cellsmigrating near the inlet and the outlet of themicrofluidic gradient channels. The linear cAMP gradient provided a constant relative gradient throughout the entire length of the confinement channels, however, the local concentration of cAMP was low at the gradient inlet and at a maximum value at the high concentration outlet (Fig 29). Results show that the percentage of blebs utilized by the cells remained the same in both low and high local cAMP concentrations (Fig 30).

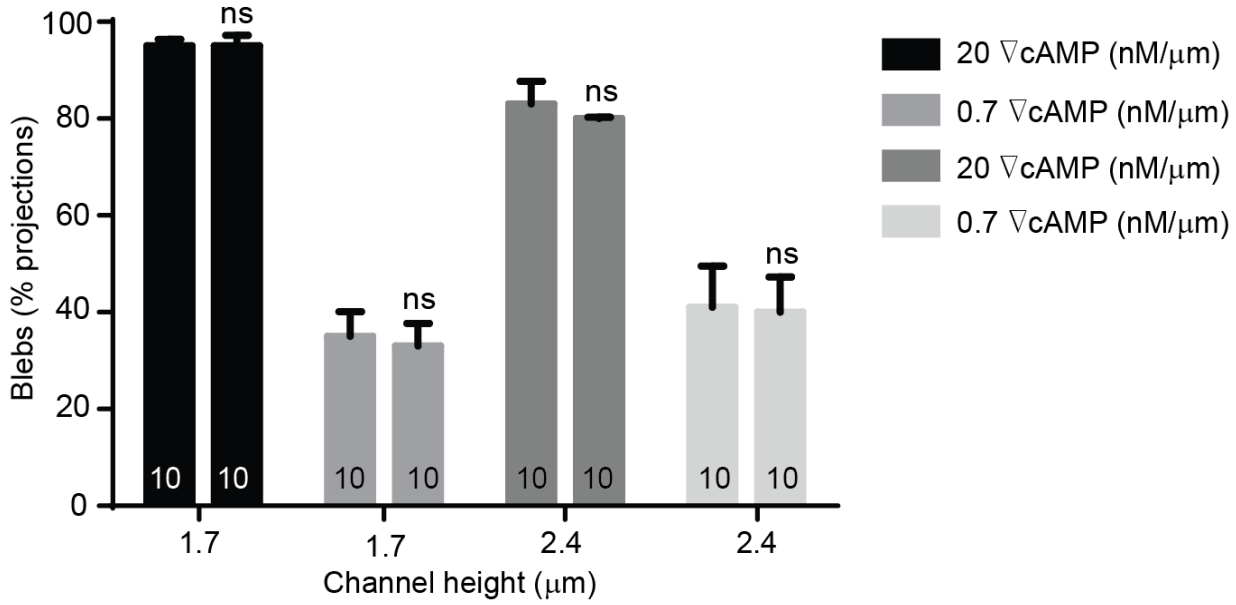

Figure 30: Bleb motility is not regulated by the absolute concentration of cAMP. (A) The percentage of blebs utilized *Dictyostelium* cells in the vicinity of the inlet and outlet of the gradient channels remained constant. The first bar in each group represents the percentage of blebs at low cAMP concentration and the second bar corresponds to the high concentration end of the gradient. Cell numbers are shown on bars. Error bars represent SEM.

5.2.3 Surface area of blebs

Next we investigated how bleb surface area is influenced by confinement height and gradient steepness. The percentage of blebs utilized by the cell was statistically the same at both channel heights of 1.7 μm and 2.4 μm but the bleb surface area is greater at 1.7 μm as compare to 2.4 μm tall channel. Our data also shows that stepper gradients led to the formation of bigger blebs. At high cAMP steepness (20 nM/μm), for example, the average bleb surface area increases from 10 μm^2 at a channel height of 2.4 μm to 15 μm^2 when cells are confined at 1.7 μm (Fig 31).

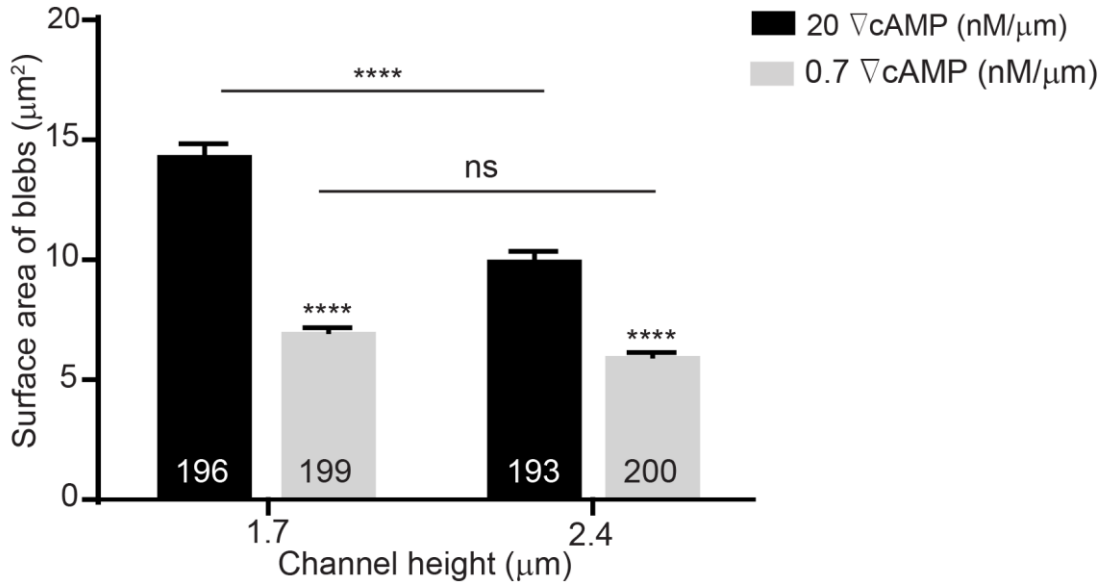

Figure 31: Increasing the cAMP gradient from 0.7 nM/μm to 20 nM/μm induces the cells to produce blebs with larger surface area. Bleb numbers are shown on bars. Error bars represent SEM. ****P ≤ 0.0001.

5.2.4 Chemotactic velocity of confined cells

Cells were loaded into a 80 μm tall channel and allowed to adhere on the glass substrate. A cAMP gradient was established by lowing development buffer through one inlet and cAMP with development buffer through the second inlet. Cells were able to detect the linear gradients and migrated towards the entrance of the thin channels. During cell migration though the gradient channels we quantified the chemotactic velocity of the chemotaxing cells.

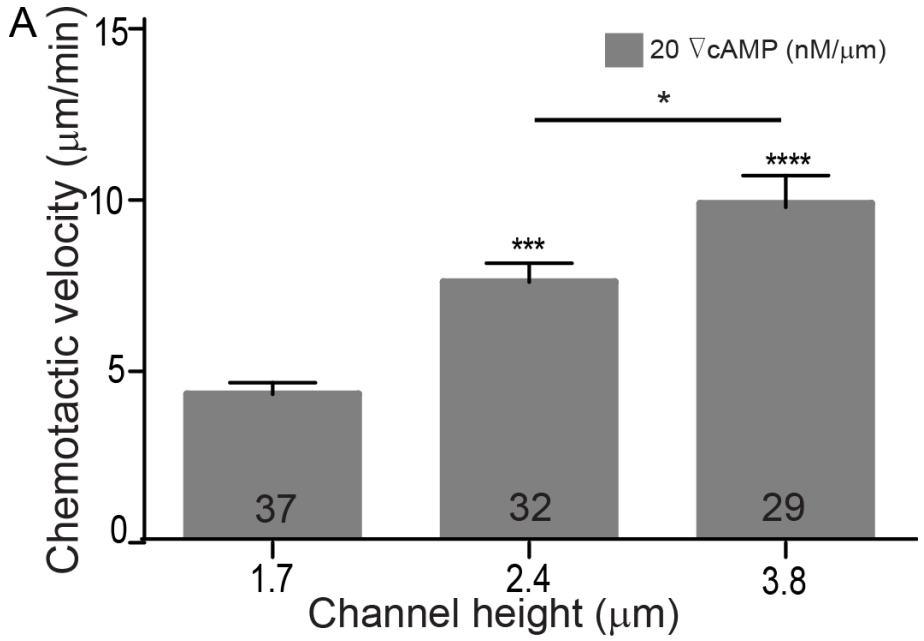

Figure 32: *Dictyostelium* cells are observed as they migrate up a 20 nM/μm cAMP gradient. (**A**) Chemotactic cell velocity decreases as the height of the channel is

reduced. Error bars represent SEM. The number of cells quantified shown on bars. ****P ≤ 0.0001.

The chemotactic cell velocity decreased by approximately 50% from10 μm/min to 5 μm/min when the confinement height reduced from 3.8 μm to 1.7 μm (Fig 32).

There are three parameters that may lead to the reduction of the chemotactic velocity:

f) The cells went on random walks.

g) The cells are experiencing a higher degree of confinement at 1.7 μm tall channel than they are at 3.8 μm channel.

h) Or it is because the cells are utilizing a higher percentage of blebs when confined in 1.7 μm tall channel than at 3.8 μm channel.

5.2.5 Cell speed

In order to eliminate one of these factors we calculated the cell speed for all four cAMP gradients and at all three different channel heights. Cell speed was observed to decrease with increasing gradient steepness in microchannels with heights of 1.7 μm and 2.4 μm. However, the cell speed remained approximately the same for cells migrating in 3.8 μm tall channels. Lastly, the cell speed remains constant for cells migrating up a low cAMP gradient, for instance 0.7 Nm/μm, at all three different channel heights (Fig 33). This proves that the chemotactic velocity is not reduced because the cells are experiencing a higher degree of confinement at 1.7 μm than they are at 3.8 μm.

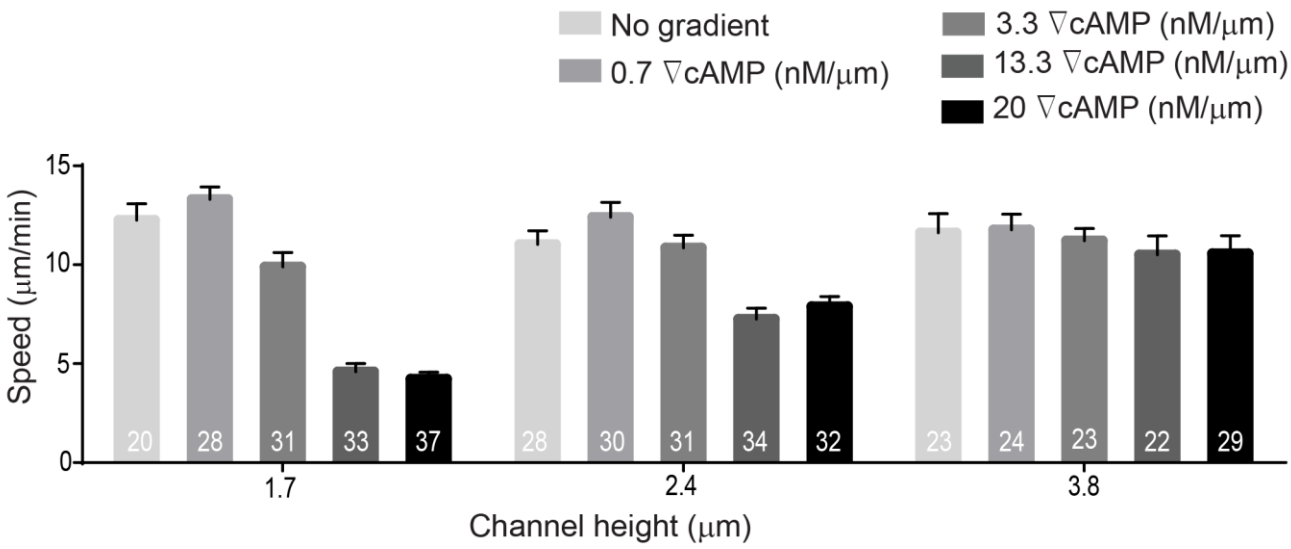

Figure 33: Cell speed is reduced when cells migrate largely using blebs. The Dictyostelium cell velocity is reduced with increasing the steepness of cAMP gradient at 1.7 μm and 2.4 μm. Under these conditions cells migrate using a larger percentage of blebs (see Fig 6). Cell velocity remains approximately constant when cells migrate in 3.8 μm-tall channels, were cells used very few blebs. The data shown are the mean ± SEM.

5.2.6 Chemotaxis index of cells under microfluidic confinement

The remaining question is; did the chemotactic velocity reduce because the cells went on random walks or because they used higher percentage of blebs at 1.7 μm than they did at 3.8 μm. To find an answer to this question we calculated the chemotaxis index of cells migrating at no gradient and at gradients that were varying between 0.7 nM/μm and 20 nM/μm at three different channel heights. When no gradient was applied the chemotaxis index was reduces. The chemotactic index does not approach zero due to the biasing influence of the microchannel side walls; cells migrate into the wall and are directed along the channel axis. When the gradient was applied, the chemotaxis index

increased and varied from 0.9 to 1 for all channel heights and cAMP gradient steepness (Fig 34). Therefore, cell velocity does not decrease due to a reduced bias towards cAMP, but because cells migrate using more blebs. This finding is consistent with previous work demonstrating that cell displacement is greater when cells migrate with pseudopods than with blebs (Corall et al.).

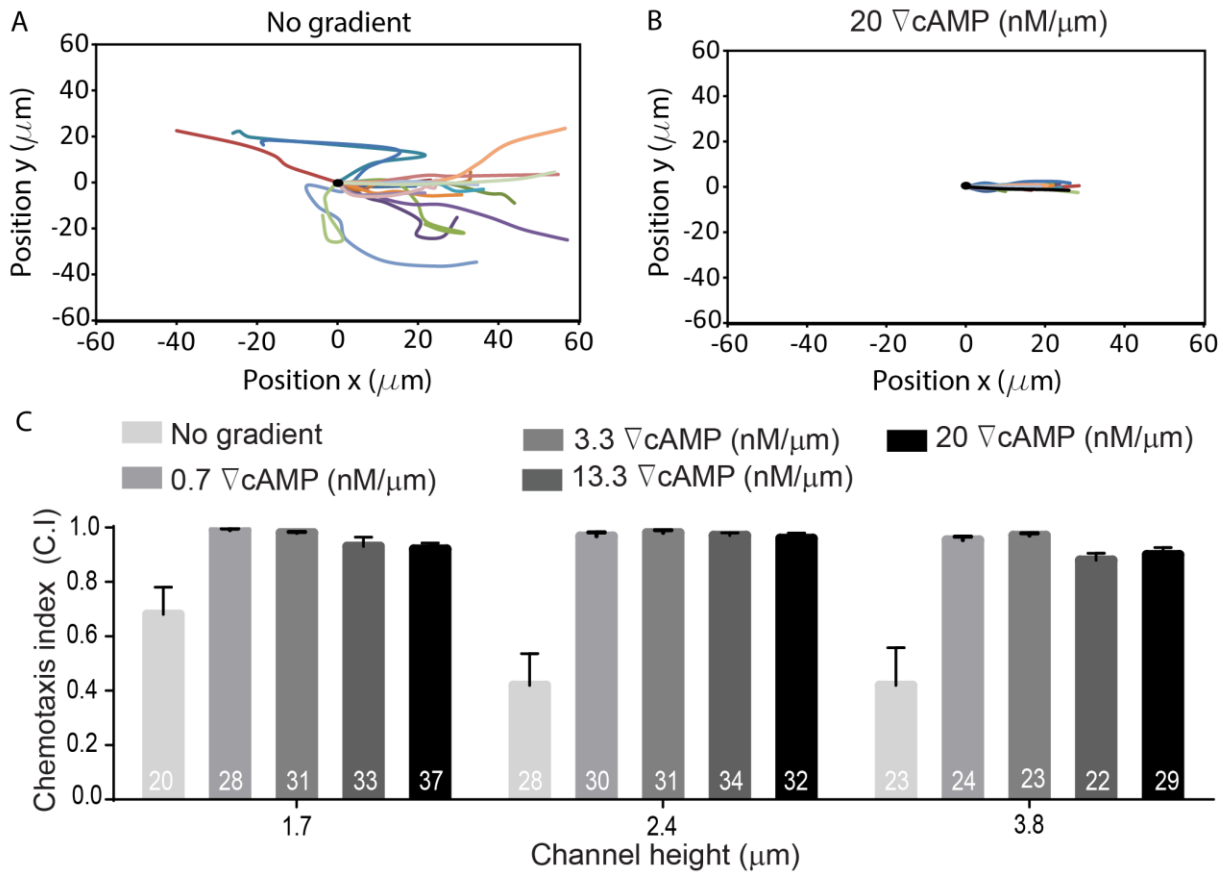

Figure 34: Chemotaxis index (C.I) of *Dictyostelium* is not influenced by microchannel height. The cell tracks for 20 cells are shown for cells chemotaxing in a 1.7 μm-tall channel in (A) no cAMP gradient and (B) a 20 nM/μmcAMP gradient. (C) The cell chemotaxis index varies from 0.9±1.0 when cells migrate in a cAMP gradient, but significantly less when no gradient is applied. The data shown are the mean ± SEM.

CHAPTER 6: MYOSIN II ACTIVITY IS INFLUENCED BY MICROFLUIDIC CONFINEMENT

6.1 Introduction

Blebbing requires sufficient intracellular fluid pressure to drive membrane expansion (Charras et al., 2005; Maugis et al., 2010; Ridley, 2011). This blebbing is mediated through myosin II-induced contraction of the cortex, where both heavy and light chain mutants are unable to bleb under buffer or agarose (Laevsky and Knecht, 2003; Paluch et al., 2006; Ruprecht et al., 2015; Zatulovskiy et al., 2014). Myosin II activity in *Dictyostelium* is stimulated by cAMP and regulated, in part, through phosphorylation of its regulatory light chain, which is simulated by cAMP signaling through downstream guanylyl-cyclases and cyclic-GMP-binding proteins. Chemotactic stimulation of *Dictyostelium* cells therefore results in a transient increase in cGMP and phosphorylation of myosin II heavy and regulatory light chains (Bosgraaf et al., 2002). Because cAMP controls where blebs form, mediates myosin II contraction, and influences *Dictyostelium* chemotactic motility (Fig 35), we sought to investigate the influence of cAMP steepness and myosin II activity on cell blebbing during cell migration in confined environments.

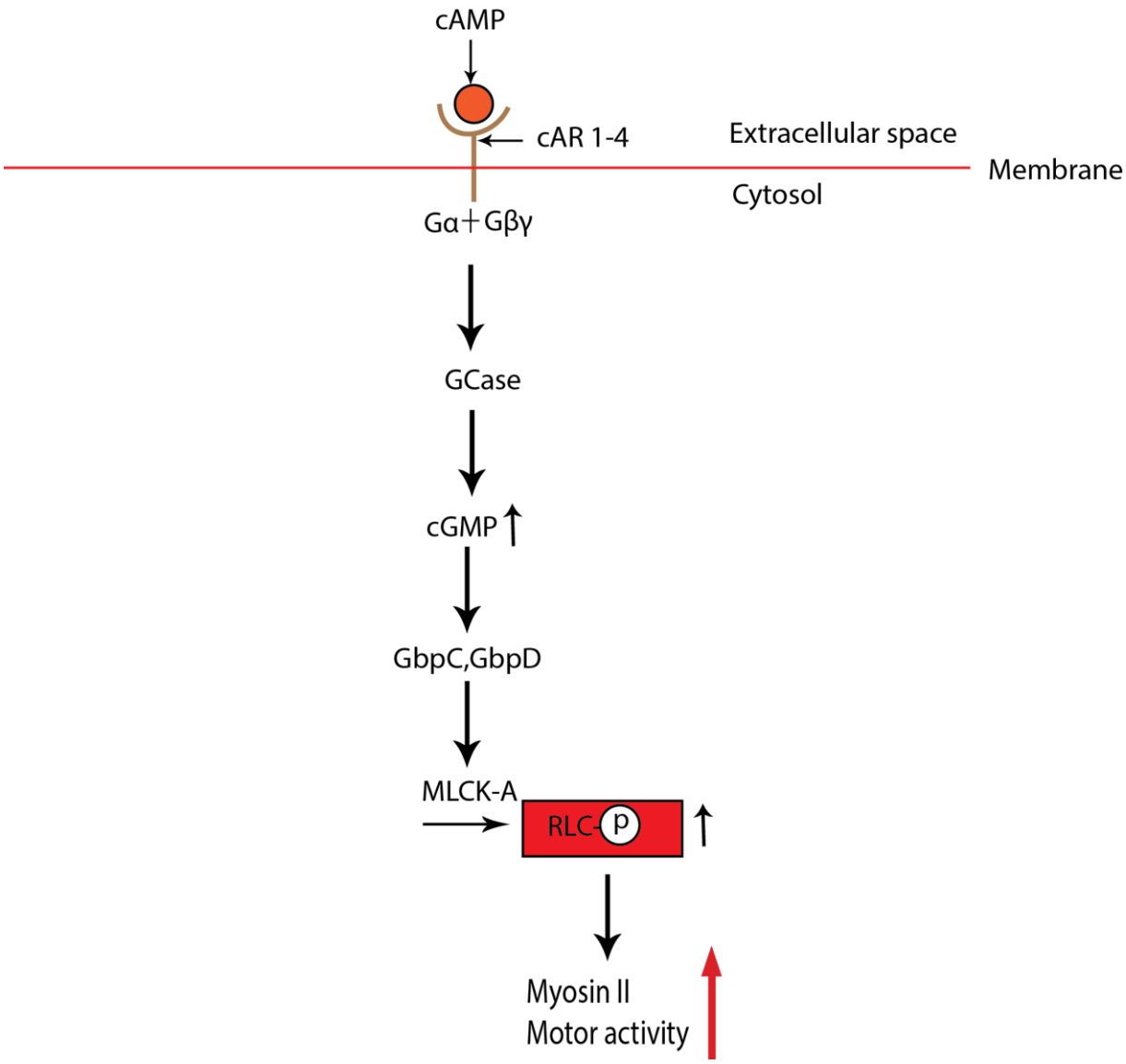

Figure 35: Myosin II activity is regulated by cAMP.

Our experiments illustrate that microfluidic confinement significantly influences the degree to which *Dictyostelium* cells move by using blebs. Previous work attributes increased blebbing activity to the mechanical resistance of the environment, which has been reported as “the force cells exert to deform the matrix” (Zatulovskiy et al., 2014). In our microfluidic device, however, we found that cells do not deform the microchannel during chemotaxis (Fig 26b). Therefore, cells do not experience mechanical resistance in

the same way as they do under agarose since no force is necessary to deform the microfluidic channel. Confinement in microfluidic channels and migration against physical resistance under agarose, however, are related to some degree in that both environments lead to an increase in intracellular pressure. During migration, confined cells experience an increase in membrane tension when compared to non-confined movement under buffer. With this increase in membrane tension, cells require sufficient cortical tension to overcome confinement stresses and migrate. To provide structural support, we hypothesized that myosin II becomes locally associated to the actin cytoskeleton in order to increase cortical tension and provide sufficient integrity (Hung et al., 2016; Laevsky and Knecht, 2003). We therefore investigated how confinement influences myosin II activity in migrating *Dictyostelium* cells.

Myosin II activity is also associated with bleb formation in *Dictyostelium.* Heavy chain null-mutants and cells treated with blebbistatin, for example, are unable to bleb (Langridge and Kay, 2006; Yoshida and Soldati, 2006; Zatulovskiy et al., 2014). A key requirement for blebbing is that the cell must produce enough internal fluid pressure to drive membrane detachment and bleb expansion. Below a critical fluid pressure, blebs cannot expand (Tinevez et al., 2009). Hydrostatic pressure is produced by myosin-II-mediated contraction of the actomyosin cortex. Myosin II provides multiple functions in the cell cortex, including promoting contractility, increasing cortical tension and viscoelasticity, and sensing and responding to mechanical stresses acting in the cytoskeletal network (Srivastava et al., 2015). The myosin II-mediated cortical tension then combines with local surface curvature, leading to hydrostatic pressure that can promote rupture of the cortical actin network or local detachment of

the plasma membrane (Blaser et al., 2006). Once the cortex is ruptured or the membrane detached, cytosol flows along the pressure gradient and forces the plasma membrane to protrude outward as an expanding bleb.

The tendency for cells to form blebs through cortical contractility suggests that cells might adapt to confinement conditions through increases in myosin activity since confined cells experience external stress from the environment and require sufficient cortical tension to overcome these forces and migrate. Interestingly, previous studies show that myosin II localizes at the cell membrane in cells undergoing chemotaxis under agarose overlay (Laevsky and Knecht, 2003) . Because there is clear evidence that myosin II plays a role in controlling membrane and cortical tension (Tinevez et al., 2009) and producing contractile forces for bleb formation, we asked whether myosin II activity increases when cells are confined and how this correlates with blebbing activity in confinement channels of differing height and with variations in the cAMP gradient steepness.

6.2 Results

6.2.1 Localization of Myosin II under microfluidic confinement

Cells expressing GFP-myosin II were filmed at 5–10 Hz while under different degrees of microfluidic channel confinement. Myosin II localized at the cell membrane when *Dictyostelium* was confined in a 1.7 μm channel (Fig 36a), and the degree of myosin II localization at the cortex decreased with increasing channel height (Figs 36b, 37a and 37c). Cells expressing cytosolic mCherry were also imaged while confined at 1.7 μm and 3.8 μm, and no localization was observed (Fig 10b and 10d). Our data shows that

microfluidic confinement promotes increased myosin II localization at the cell cortex.However, we found that the degree of translocation is not influenced by cAMP gradient steepness (Fig 36b). GFP-myosin II was measured in cells migrating in channels with 1.7, 2.4 and 3.8 μm at two different gradients: 20 nM/μm and 3.3 nM/μm. For each channel height,myosin II activity remained unaffected by changes in gradient steepness.

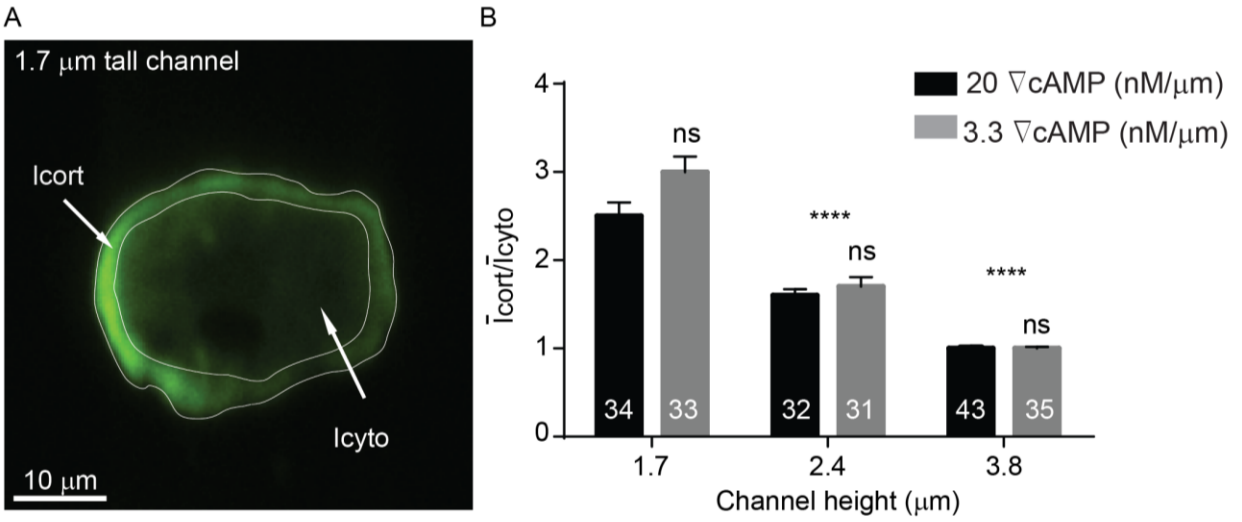

Figure 36: Myosin-II localizes to the cell cortex when cells are confined within microfluidic gradient channels. (A) Fluorescence intensity of GFP-myosin was higher at the cell cortex (Icort) than in the cytosol (Icyto). (B) The ratio of Icort/Icyto increased when the microfluidic confinement channel height was decreased from 3.8 μm to 1.7 μm. Cell numbers are shown on bars. Error bars represent SEM. ****P ≤ 0.0001.

We have shown that *Dictyostelium* cells in confined microfluidic channels move by using blebs, consistent with earlier observations under agarose and our experiments suggest that microfluidic confinement and steep cAMP gradients shift the balance between actin

polymerization and myosin contractility, leading to increased intracellular pressure and bleb formation. Because myosin II activity in *Dictyostelium* is stimulated by cAMP and regulated by phosphorylation through downstream guanylyl-cyclases and cyclic-GMP-binding proteins(vanHaastert and Kuwayama, 1997), we suggest that cortical accumulation of myosin II mediated by confinement leads to increased cortex contractility potential. This mechanical-chemical coupling is supported by previous work in zebrafish progenitor cells, which can be promoted to bleb by increasing myosin II activity through biochemical stimuli (Ruprecht et al., 2015).

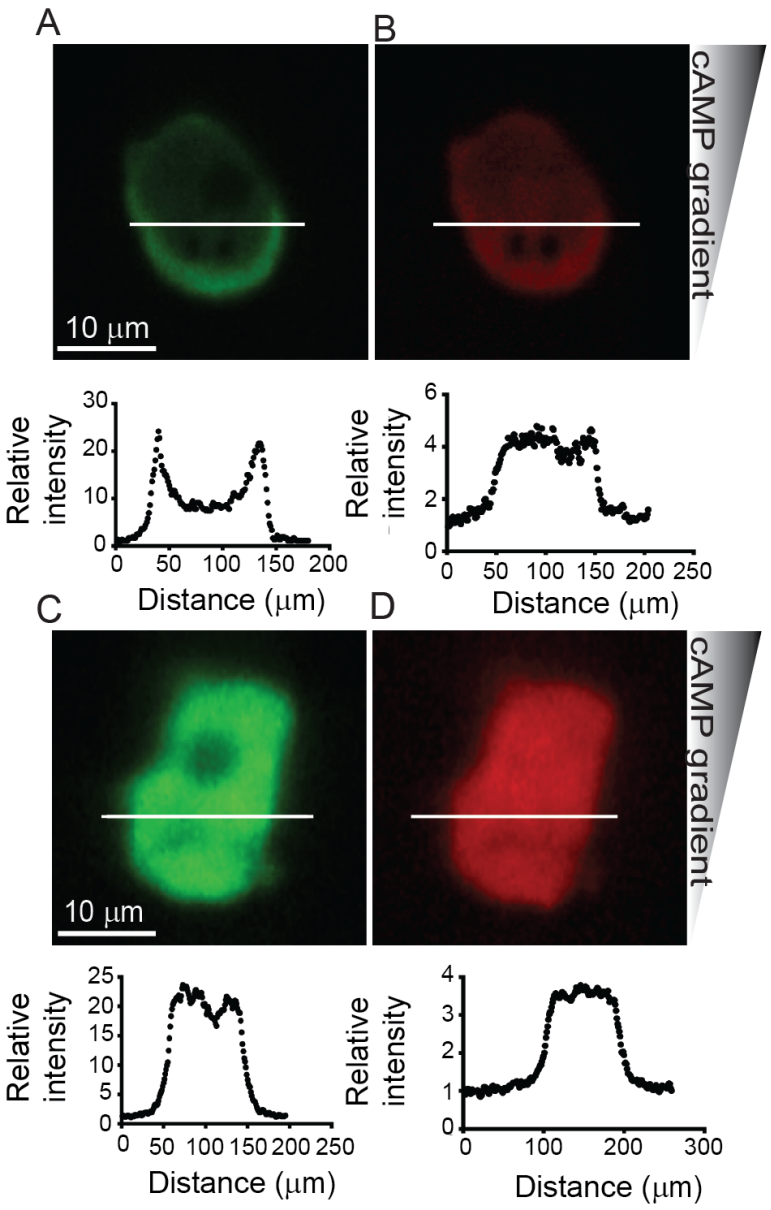

Figure 37: Myosin-II and cytosolic mCherry during migration under microfluidic confinement. (A) Myosin-II accumulates at the cortex in confined *Dictyostelium* cells, while (B) mCherry, used as a volume marker, does not show cortical/membrane enrichment at 1.7 μm. (C) Myosin-II and (D) mCherry do not concentrate at the cell cortex in confined cells at 3.8 μm. Cell numbers are shown on bars. Error bars represent SEM.

6.2.2 Myosin II-null cells

We also investigated the behavior of myo II null cells, Myo II: GFP- linkers PDM 181. These cells were not able to invade the 1.7 μm tall channels. They were extending protrusions inside the 1.7 μm tall channels but they were not able to retract their trailing edge into the channels. However, they migrated across 2.4 μm and 3.8 μm without using blebs and only using pseudopods. Moreover, when compared to a control experiment, Myo II: GFP- myo II PDM 181, cells were able to invade into all three gradient channels (Fig 38a) and used 36% blebs during migration at 2.4 μm channels and no blebs at 3.8 μm (Fig 38b). The chemotactic velocity of the myosin II null reduced as compare to the chemotactic velocity of the control cells (Fig 38a).

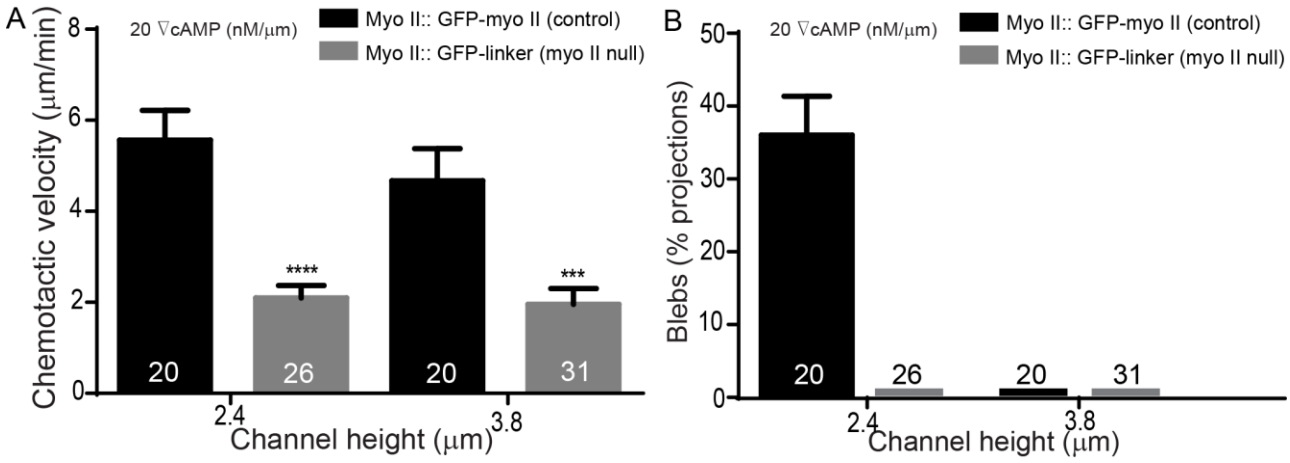

Figure 38: Myosin II-null cells could not invade the 1.7 μm.

6.2.3 Blebbistatin treated cells

When cells were treated with 25 μM blebbistatin, an inhibitor of myosin II, they used less and smaller blebs compare to untreated cells at 1.7 μm (Figs 39 and 41). The chemotactic velocity of the treated cells, however, uninfluenced (Fig 40). We speculate

that the increased percentage of pseudopodia can promote higher velocity, but the inhibition of myosin II then reduces this velocity. Therefore, these two affects counteract each other and the chemotactic velocity remains largely the same. In cells migrating in channels 3.8 μm in height where they form few blebs, blebbistatin treatment led to a reduction in the chemotactic velocity.

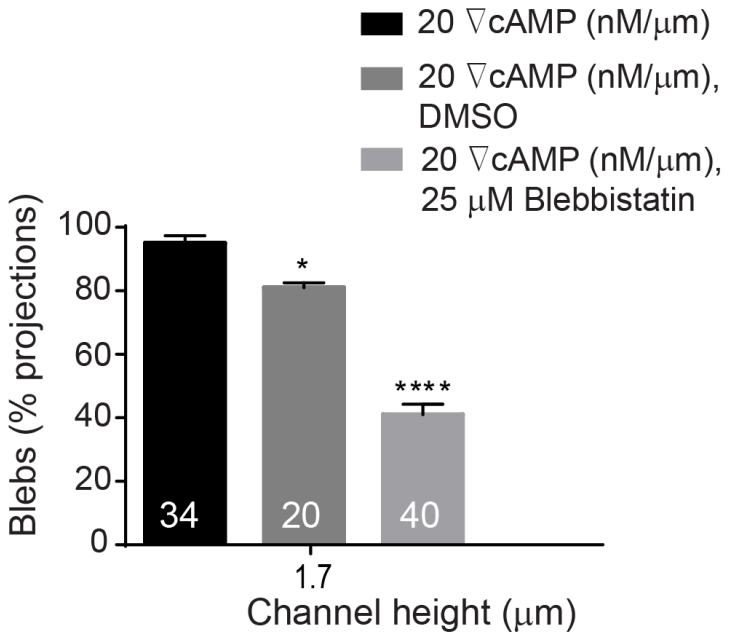

Figure 39: Effects of blebbistatin on the percentage of blebs utilized by the cells. Cells utilized higher percentage of pseudopods after treatment with blebbistatin in 1.7 μm tall channels. Cell numbers are shown on bars. Error bars represent SEM. *P ≤ 0.1, ****P ≤ 0.0001.

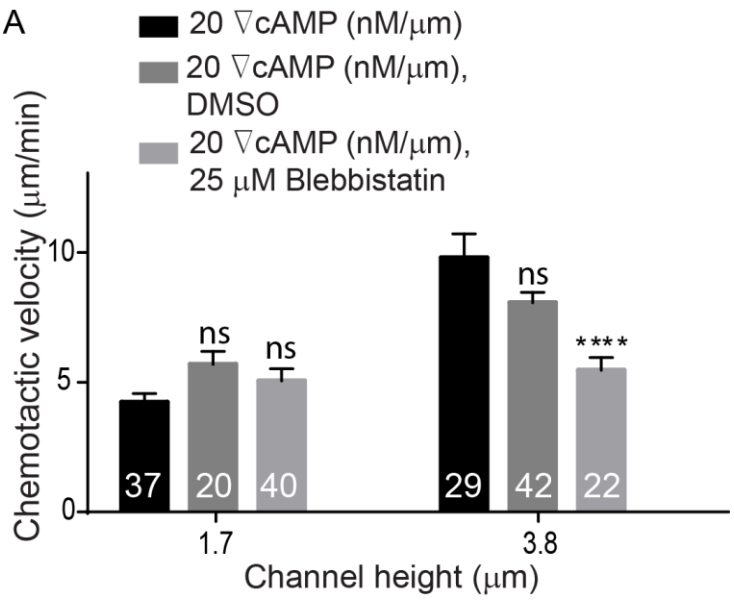

Figure 40: Effects of blebbistatin on the chemotactic velocity of cells. Blebbistatin did not impact chemotactic velocity at 1.7 μm and reduced cell velocity at 3.8 μm. Cell numbers are shown on bars. Error bars represent SEM. ****P ≤ 0.0001.

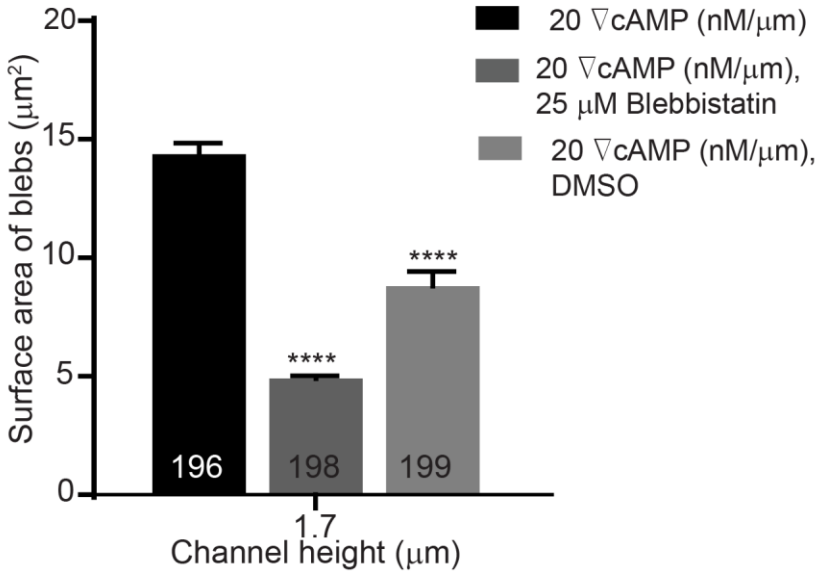

Figure 41: Blebbistatin reduced the bleb surface area. Bleb numbers are shown on bars. Error bars represent SEM. ****P ≤ 0.0001.

6.2.4 Sorbitol treated cells

Lastly, when the internal cell pressure was reduced, cells migrated with less blebs too. *Dictyostelium* cells were coerced to migrate in a high (20 nM/μm) gradient in DB buffer containing 100 mM sorbitol, which reduces the osmotic pressure drop across the membrane. We found that cells confined in 3.8 μm channels were not influenced by sorbitol. However, cells confined in 1.7 μm channels formed smaller blebs (Fig 44), migrated with a faster pseudopodia-driven velocity (Fig 43) and produced significantly fewer blebs (Fig 42).

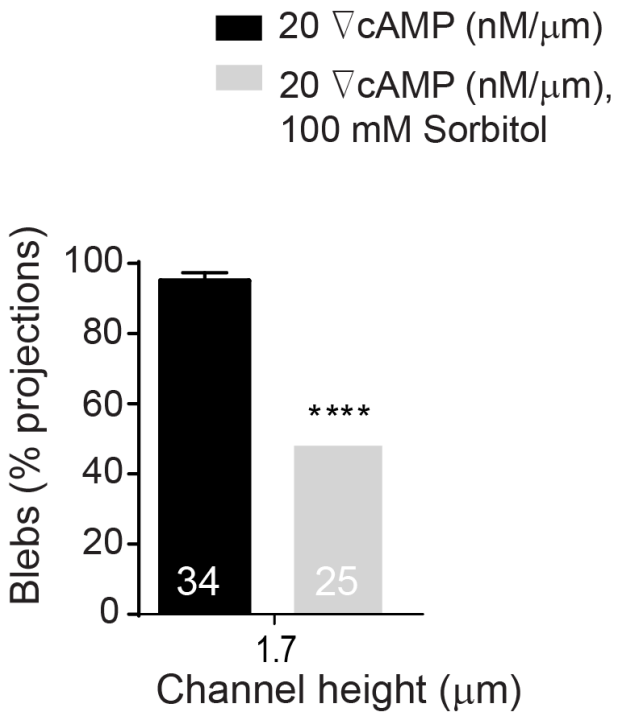

Figure 42: Effects of sorbitol on the percentage of blebs utilized by the cells. Cells utilized higher percentage of pseudopods in high osmolarity buffer in 1.7 μm tall channels. Cell numbers are shown on bars. Error bars represent SEM. ****P ≤ 0.0001.

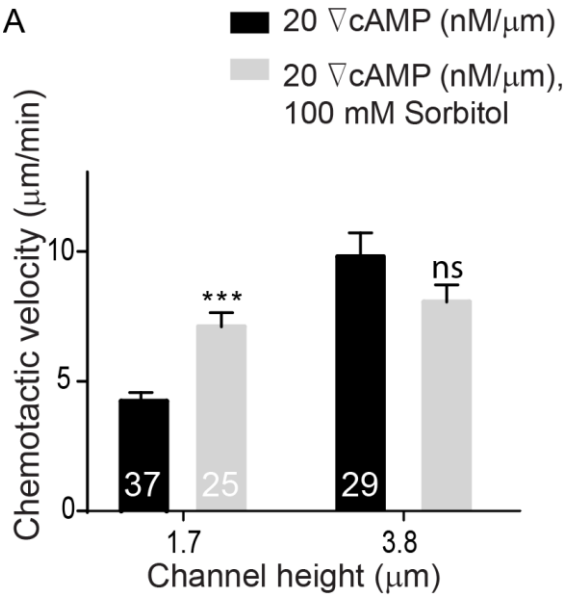

Figure 43: Effects of high osmolarity on the chemotactic velocity of cells. High osmolarity increased the cell velocity at 1.7 μm and did not impact the velocity of the cells at 3.8 μm. Error bars represent SEM. ***P ≤ 0.001.

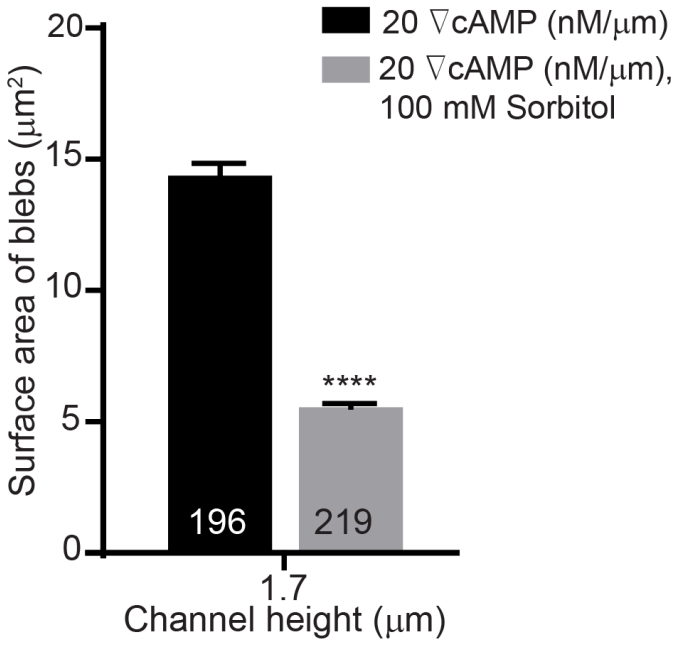

Figure 44: Sorbitol reduced the bleb surface area. Bleb numbers are shown on bars. Error bars represent SEM. ****P ≤ 0.0001.

CHAPTER 7: CONCLUSIONS

7.1 Review of findings

In this work, we offer insight into the role that confined environments can play in promoting the formation of blebs during chemotaxis. In particular, we make use of microfluidics to create confining microchannels with stable linear cAMP gradients. *Dictyostelium* cells are loaded into non-confined microchannel chambers and coerced to migrate through confined channels with a fixed width (50 μm) and varying height (1.7, 2.4, or 3.8 μm). For each confinement experiment, we quantified the rate to which cells formed blebs or pseudopods at different cAMP gradient steepness, ranging between 0.7 - 20 nM/μm. We observed that cells migrated through all channels, but the degree of confinement influenced the degree to which cells moved with blebs as is consistent with other reports conducted using agarose overlays. Blebbing was observed to increase with increasing steepness of the cAMP gradient, and cells produced larger blebs when the gradient was increased. Moreover, when the internal cell pressure was reduced using buffer containing sorbitol, cells formed smaller blebs with reduced frequency. Myosin II concentration at the cortex was seen to be independent of gradient steepness, but increased by as much as 250% when cells were coerced to migrate in channels 1.7 μm in height. Finally, inhibition of myosin by blebbistatin or through the use of Myosin II-null cells led to a reduction in both the percentage and size of blebs used by the migrating confined cells.

Based on our results, we therefore suggest that when stimulated in a steep cAMP gradient under confinement, cells are capable of contracting the cortex to a greater

extent than when non-confined due to the increased local availability of myosin II. This contraction leads to increased internal cell pressure and a greater rate of bleb formation during migration. When this internal pressure is reduced with the addition of sorbitol, blebbistatin, or through the use of Myo II–null cells, the rate of formation and size of these blebs are reduced (Fig 45).

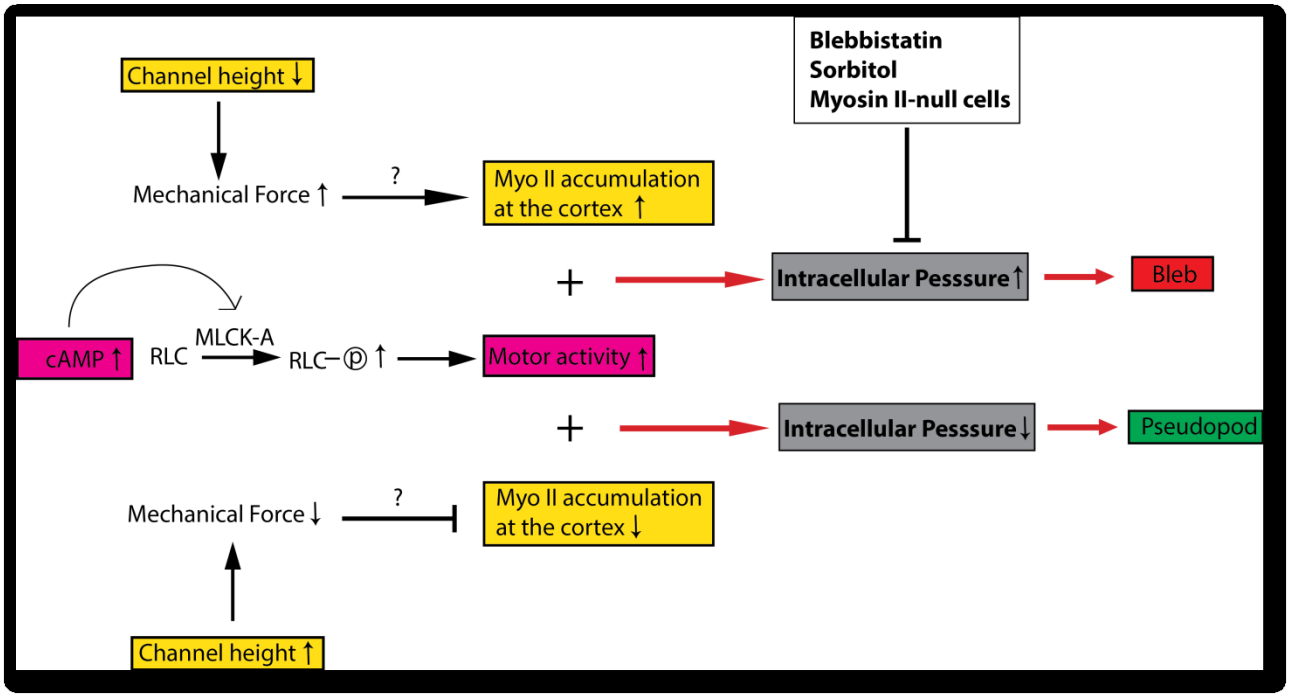

Figure 45: Schematic with conclusions based on the results.

7.2 Future work

7.2.1 Blebbing assay

In this study, we were able to increase the intracellular pressure by naturally confining the cells and by activating the myosin II through the cGMP/Myosin II pathway. The increased intracellular pressure let to an increase in the percentage of blebs utilized at the leading edge of the cells during migration. Moreover, we were able to decrease the intracellular pressure by using a high osmolarity buffer that reduced the percentage of blebs when cells migrated under the same confinement and the same gradient steepness. In future work, we propose the study of three more factors that influence bleb motility and answer the following questions.

a) How does the external pressure, which is the pressure of the buffer in which the cells are embedded, impact bleb driven motility? If we increase the extracellular pressure, will the cells use a smaller number of blebs?
b) How does the adhesiveness of the substrate influence the percentage of blebs utilized by the cells during migration in resistive microfluidic environments? If we increase the adhesion between the cells and the substrate on which the cell is crawling, will the cell stop blebbing?
c) What will happen if we reduce the membrane-cortex adhesion, by using Talin A-null cells? Will the cells bleb at taller channels as compared to the previous study?

We have performed a small number of experiments trying to answer the first question related to the external pressure. There are two ways to change the external pressure of

the cells: either increase the flow rates of the liquid solutions that are delivered at the PDMS inlets of the device or close the main outlet of the device and let pressure build up in the microfluidic chip. Based on these suggestions, we ran an experiment where we loaded the cells into the device and let them enter the gradient channels via chemotaxis. When the cell had entered the gradient channel, we closed and opened the main outlet of the device three times. We found that the cell was able to switch between the bleb driven motility and pseudopod driven movement spontaneously. When the outlet was open, the cell used blebs, and when the outlet was closed, which led to an increased external pressure, the cell utilized pseudopods. In that we have shown that the degree of confinement is important for bleb formation, we next measured the height of the PDMS channels at open and closed outlet. The channel height changed from 2 um to 2.5 µm (Fig 46) when we closed the outlet. However, we have shown that at 2.5 µm tall, channels the cells utilized a high percentage of blebs with an open outlet. Next we would like to further study why cells are using pseudopods under the same degree of confinement but with a closed outlet.

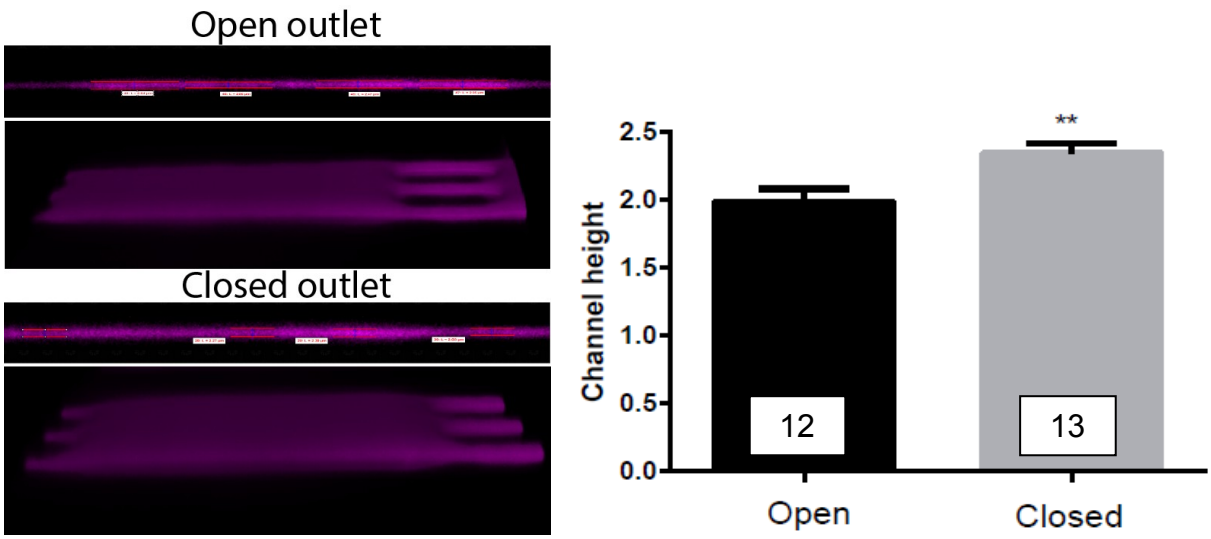

Figure 46: The height of the gradient channels increases when the main outlet of the device is closed. The channel height with a closed outlet is still in the range where the cells produce a high percentage of blebs. Channel numbers are shown on bars. Error bars represent SEM. **P ≤ 0.01.

7.2.2 Electrotaxis assay

The main focus of this work is to develop a microfluidic device for contactless electrotaxis. The latter is when the electrodes are not in contact with the buffer in which the cells are embedded. In addition, we aim to detect the uptake of the extracellular calcium from Dictyostelium cells during electrotaxis under microfluidic confinement.

We fabricated the microfluidic device through standard photolithography and soft lithography techniques. Electrodes are empty PDMS channels that we filled with a mixture of PDMS and 10% carbon black. The electrodes are separated by a 30 μm wide PDMS membrane from the channel where electrotaxis takes place. When an electric field was applied in the range of 400 V the PDMS membrane detached and the electrodes got in contact with the buffer. The latter one led to Faraday reaction (Fig 47). Therefore, in future work we will need to address this issue by developing a microfluidic system where the adhesion between the PDMS membrane and cover glass will increase.

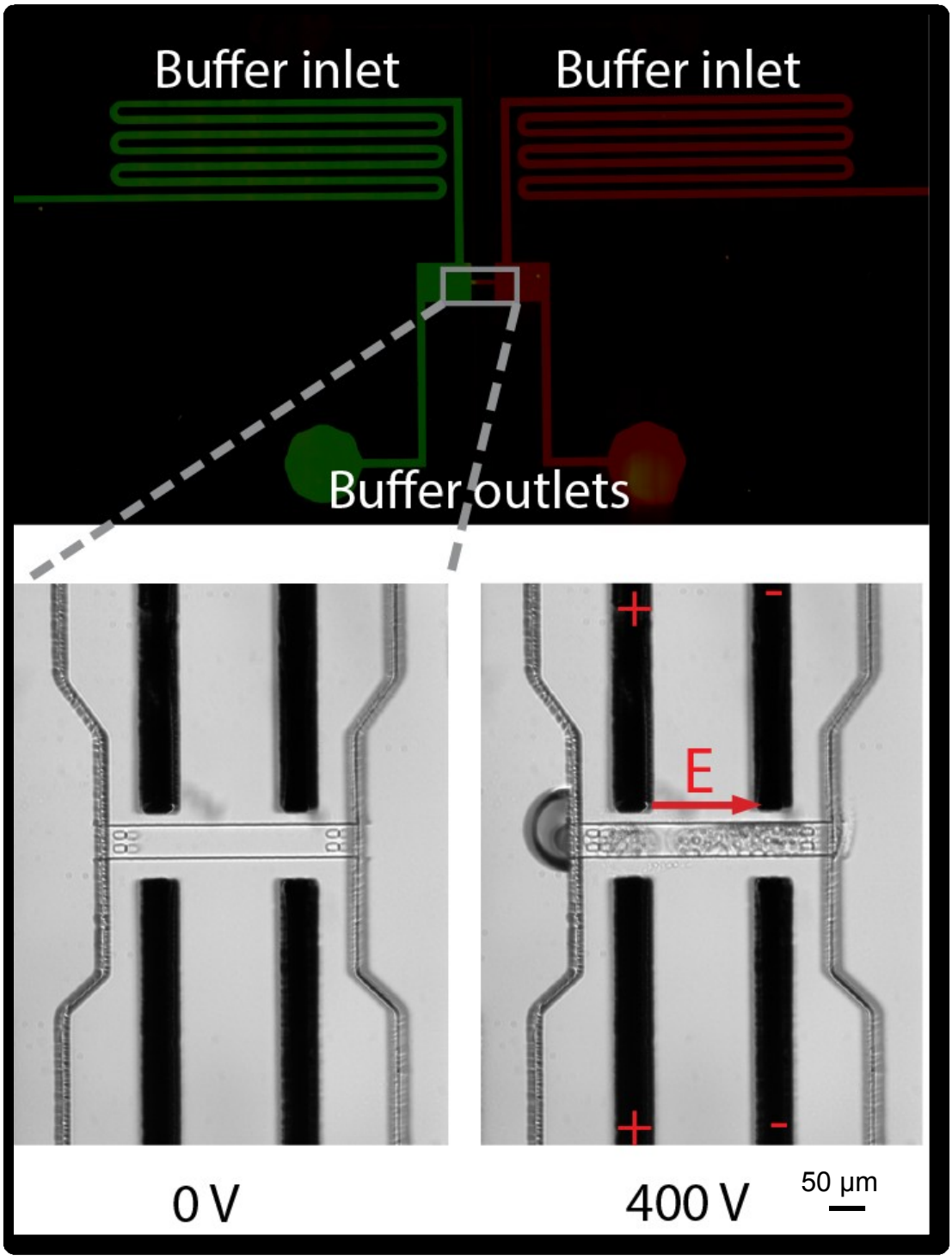

Figure 47: Microfluidic device for contactless electrotaxis. Confocal micrograph of the chip. Bightfield images depicting the impact of the electric field when the PDMS membrane, that separates the electrodes from the main channel, is detached.

During electrotaxis Dictyostelium cells uptake calcium form outside and the calcium concentration in the cytosol increases. In order for us detect the calcium uptake we utilized different fluorescent calcium indicators such as Fluo-4,AM and Fura dextran, Potassium salt, 10,000 MW, anionic. The first dye is cell permeable and the second one is not. Therefore, to load the cells with the Fura-2 dye we used a Influx pinocytic cell-loading reagent. We chose the Fura-2 dye because the Fura dextran conjugates tend to do not compartmentalize into the contractile vacuoles and remain in the cytosol. However, both calcium indicators that we used were compartmentalized in the contractile vacuoles (Fig 48). Therefore, in the future we would like to find a calcium indicator that will remain in the cytosol.

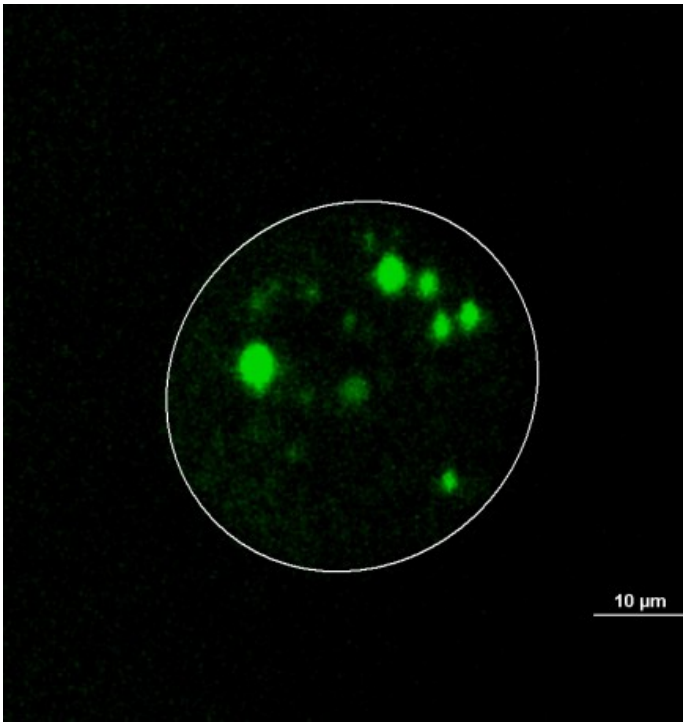

Figure 48: Confined Dictyostelium cell is loaded with Fura dextran. The calcium indicator is compartmentalized in the contractile vacuoles.

CHAPTER 8: EMULSION GENERATION IN FLOW FOCUSING MICROFLUIDIC DEVICE USING DIRECT CURRENT ELETRIC FIELD

8.1 Introduction

Over the last two decades, the controlled production and manipulation of highly uniform droplets of water-in-oil have attracted a great interest due to their wide variety of applications including the synthesis of microparticles (Zhao, 2013), enzyme activity assays (Huebner et al., 2008), reaction (Song et al., 2006a), protein expression (Fitzpatrick et al., 2006), DNA assay (Srisa-Art et al., 2007), cell encapsulation (Choi et al., 2007) and biosensing (Kim et al., 2009) (Fig 49). Different conventional methods that have been used to generate emulsions such as high pressure liquid homogenizers and microfluidizers are using turbulence to induce drop break up. These approaches provide little control over the drop size since polydisperse drops are formed. Alternatively, microfluidics appears to be one of the most dominant technologies for producing monodisperse droplets with narrow size distribution (approximately 2%). There are mainly three distinct geometrical designs of microfluidic channels for droplet generation: T-junction (Xu et al., 2006), flow focusing (Anna et al., 2003) and co-flowing (Cramer et al., 2004) (Fig 50). Flow focusing geometry is the most commonly used method for droplet generation in microfluidics and was first proposed by Anna *et al*. (Anna et al., 2003) and Dreyfus *et al*. (Dreyfus et al., 2003). In flow focusing devices, droplets are formed by injecting a discontinuous fluid phase into a central flow channel

surrounded by a second immiscible liquid in two outside channels. Both phases flow through a constriction orifice that is located downstream of the three channels. The viscous forces overcome surface tension to create uniform drops.

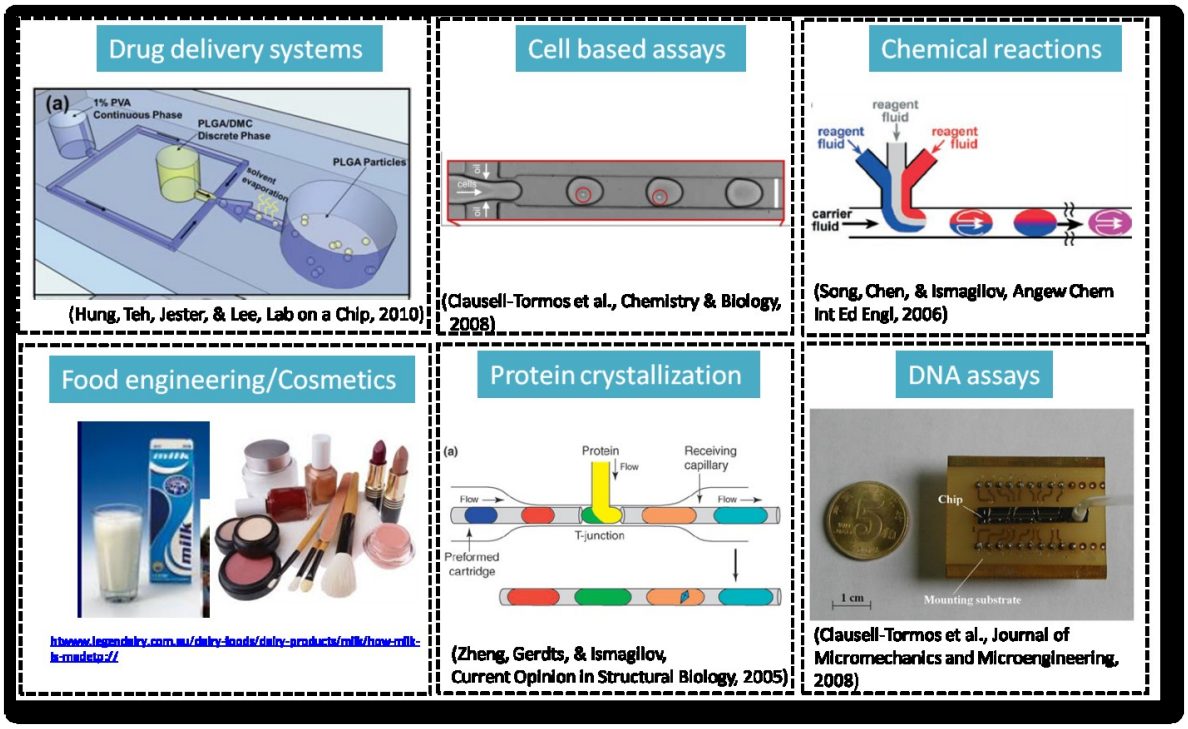

Figure 49: Applications of emulsions. Microfluidics provides an experimental platform that can be used to generate dispersions of droplets of one liquid suspended in a different immiscible liquid.

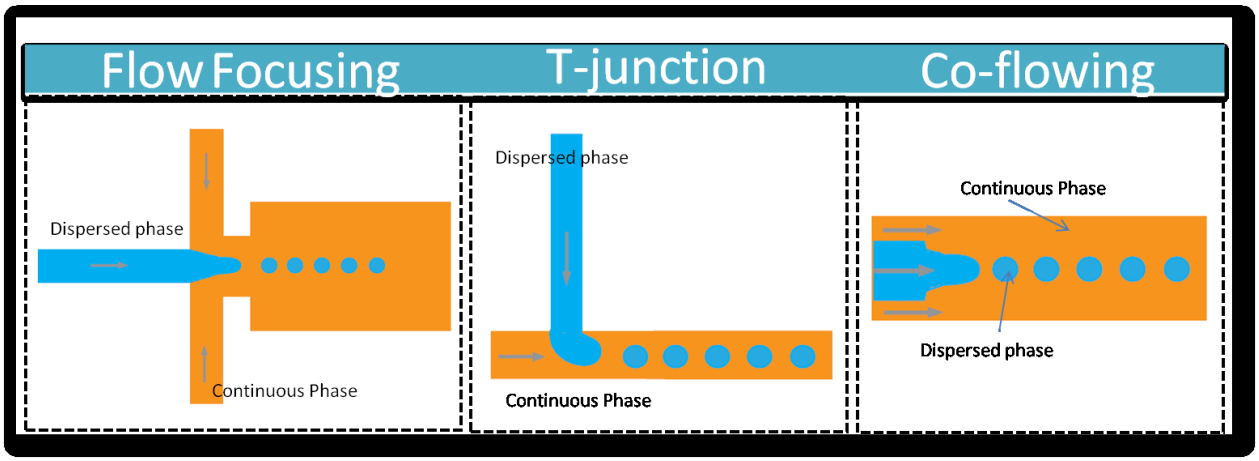

Figure 50: Different geometries of droplet generation microfluidic devices. The flow focusing, t-junction and co-flowing are the most common microfluidic geometries that have been used to produce emulsions.

The size of the droplets is controlled by the size of the microchannels, the volumetric flow rate ratios of oil and water, and fluid properties. The minimum achievable droplet size in a flow-focusing microfluidic device is limited to a range of 1-100 μm. One way to overcome such a limitation, of not being able to produce nanometer-sized droplets with a flow-focusing geometry, is to use active droplet generation methods such as electrical forces, temperature, magnetic forces, and acoustic forces (Fig 51).

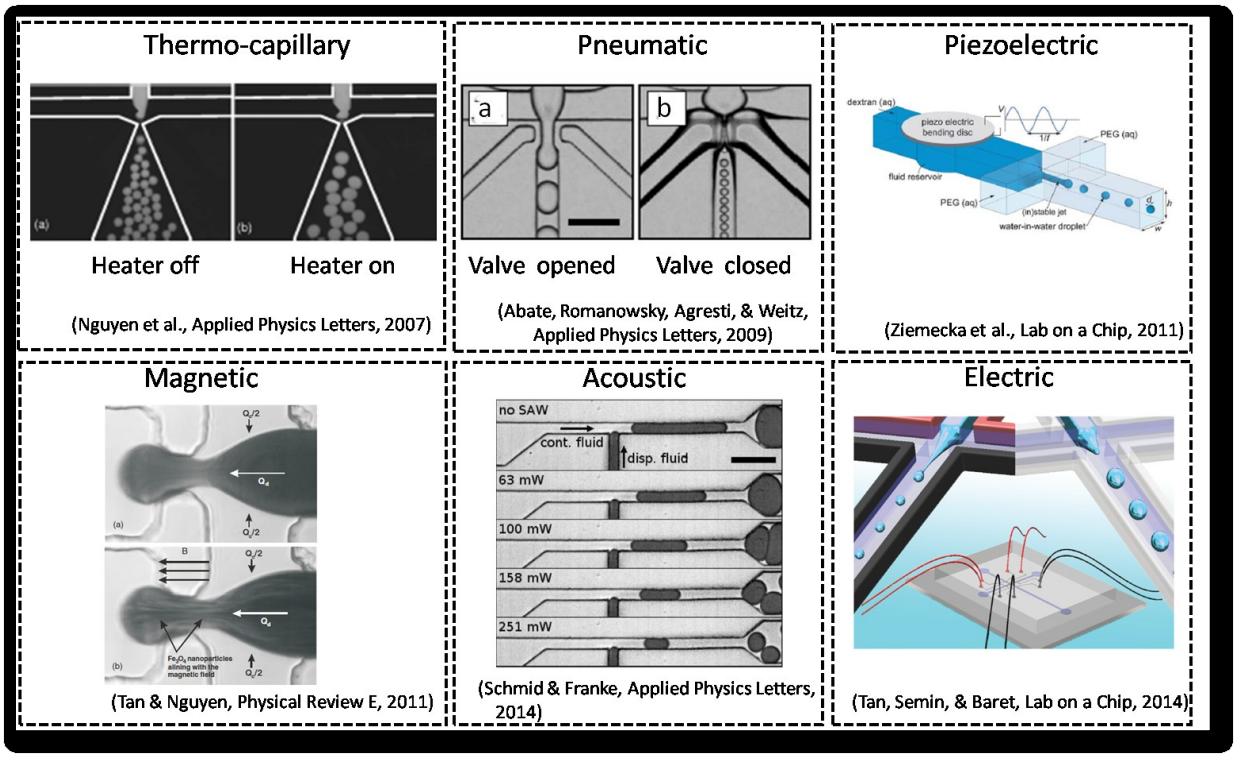

Figure 51: Active droplet generation methods. The size of the droplets can be also controlled by using an external perturbation through thermal, pneumatic, piezoelectric, magnetic, acoustic, and electrical modulation of the liquid properties.

In the present study, we consider the use of a DC electric field to actively control the size or frequencies of droplets generated in a microfluidic flow focusing device. Water-in-oil droplets are formed by focusing the dispersed phase (Milli-Q water) with the continuous phase (mineral oil with 5% Span 80), which flows from two opposing side channels. The two liquids flow through a constriction orifice located downstream of the three channels, and the dispersed phase breaks into droplets. Here, we are using 10% carbon black electrodes to deliver a DC electric field across the orifice perpendicular to the flow of both phases. The latter results in the production of droplets in the range of nanometer size. Therefore, our system provides the ability to make nanodroplets in microchannels.

8.2 Methods and Materials

8.2.1 Design and fabrication of microfluidic device

The planar flow focusing microfluidic device was fabricated using photolithography and standard soft lithography techniques. The channel geometry of the microfluidic device was designed using AutoCAD® 2014 software and printed onto a transparency mask. We spin coated a 50 um thick layer of SU-8 3050 photoresist onto a 5 inch silicon wafer, aligned the mask on top of the wafer, and then exposed them to a UV light. After chemical development, the microchannel pattern is left on the silicon mold. The flow-focusing microchannels were made of polydimethylsiloxane (PDMS) by using the replica mold technology. We poured a 10:1 ration mixture of PDMS elastomer and curing agent into the constructed mold and baked it at 85 ^{o}C for 30 min in the oven. The PDMS chips were pilled off from the mold, and a punch (Harris Uni-Core ^{TM}, tip diameter

0.75 mm) was used to create inlets and outlets in the PDMS devices. After oxygen plasma treatment, the PDMS channels were sealed using cover glass slides coated with a thin layer of PDMS to establish that the four channel walls have the same wetting features. The assembled PDMS device was baked at 85 ^{o}C for several hours to improve the PDMS bond strength and to prevent the leakage of the device. The manufactured PDMS channels have rectangular cross sections and hydrophobic walls, so oil wets them.

The microfluidic device consists of two inlets and one outlet; the width of the two inlets is 255 μm, and the outlet channel width is 969 μm with a contraction of 34 μm. The distance between the orifice and the water channel is 180 μm (Fig 52). The flow focusing channels have a height of 50 μm as measured by a profilometer (Fig 52).

Lastly, two 10% carbon black electrodes, 30 μm wide, are patterned on both sides of the orifice as microfluidic channels each separated by a thin PDMS membrane of 30 μm in thickness, from the rest of the device (Fig 52). The electrodes were made by filling the two dead end PDMS channels with a mixture of 10% carbon black, PDMS, and crosslinking agent. After fabrication, the device was baked for 24 hr. Finally, the inlet of the carbon black channels was sealed with 0.75 mm diameter copper wires, and the last ones were connected to the source and ground electrodes of an external power supply machine. This electrical connection resulted in the generation of a DC electric field through the orifice.

8.2.2 Microfluidic emulsification system

In this study, water-in-oil droplets are formed by using deionized water obtained from a Millipore purification system (18 MΩ, 0.2 micrometer filtration) as the dispersed phase

liquid. The continuous phase liquid is light mineral oil (M5904, Sigma Aldrich) mixed with $6\%_{w/w}$ non-ionic surfactant (Span 80, Sigma Aldrich). The two immiscible fluids were delivered by using a Elveflow® microfluidic flow control system (OB1 MK3) and two Elveflow® microfluidic flow sensors.

8.3 Results

8.3.1 Droplet generation in DC electric field perpendicular to the flow

Electrical control has proven to be the most reliable method for the actuation of droplet size in microfluidic systems. When the electric field is used as an external source, the droplet size is controlled by the flow rate ratio, the geometry, and size of the channels, the liquid properties, and the strength of the electric field. In this study, we are using a flow focusing device to investigate the role of the DC electric field that will be perpendicular to the flow of the dispersed phase. We performed a series of experiments where we first adjusted the strength of the DC electric field under a fixed flow rate ratio (Q_d/Q_c) of the continuous and dispersed phase, changed the flow rate ratio (Q_d/Q_c) of the continuous and dispersed phase, and last tuned the viscosity of the dispersed phase. The flow rate of the continuous phase, which consists of mineral oil with 6% span 80, is always higher than the flow rate of the disperse phase, which is water. The PMDS based channels of the device are hydrophobic, so only the dispersed phase will wet them. A high speed camera (IL5-L FASTEC) was used to capture the frequency of the droplet production (Fig 54). The forces that act at the interface during droplet formation are: viscosity force of the continuous phase, surface tension of the dispersed

phase, and electrical stress from the applied electric field at the constriction region (Fig 50). These three forces break up the water jet into drops.

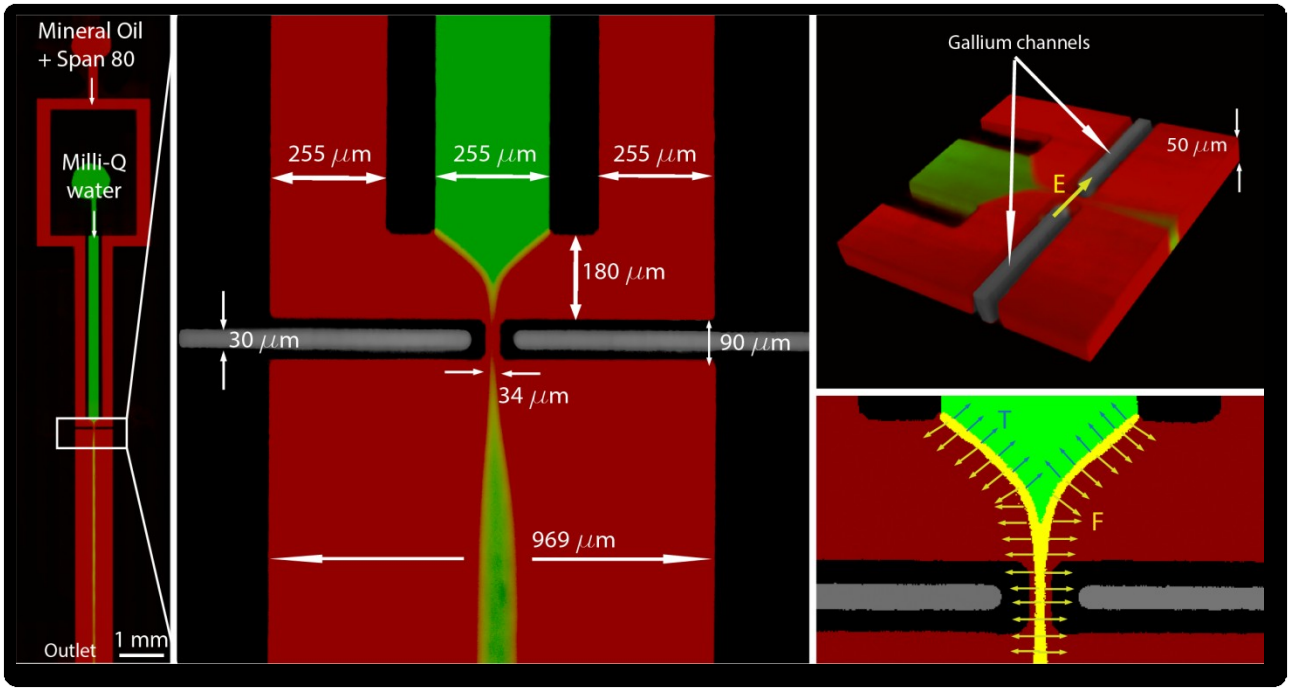

Figure 52: Confocal micrograph of the flow focusing microfluidic device. Large image of the PDMS device. Image shows the dimensions of the microchannels. 3-D image of the constriction region and the carbon black electrodes. The last micrograph depicts the forces that are exerted on the interface during droplet formation. The blue arrow represents the surface tension; the yellow arrow illustrates the force from the electric field; and the white, the viscous force from the oil that drags the water into the nozzle.

First, we decided to calculate the distribution of the electric field applied around the nozzle and to do that, we used COMSOL. Different nozzle geometries were used in order to find a nozzle design that would allow us to deliver the strongest electric field at the interface (Fig 53).

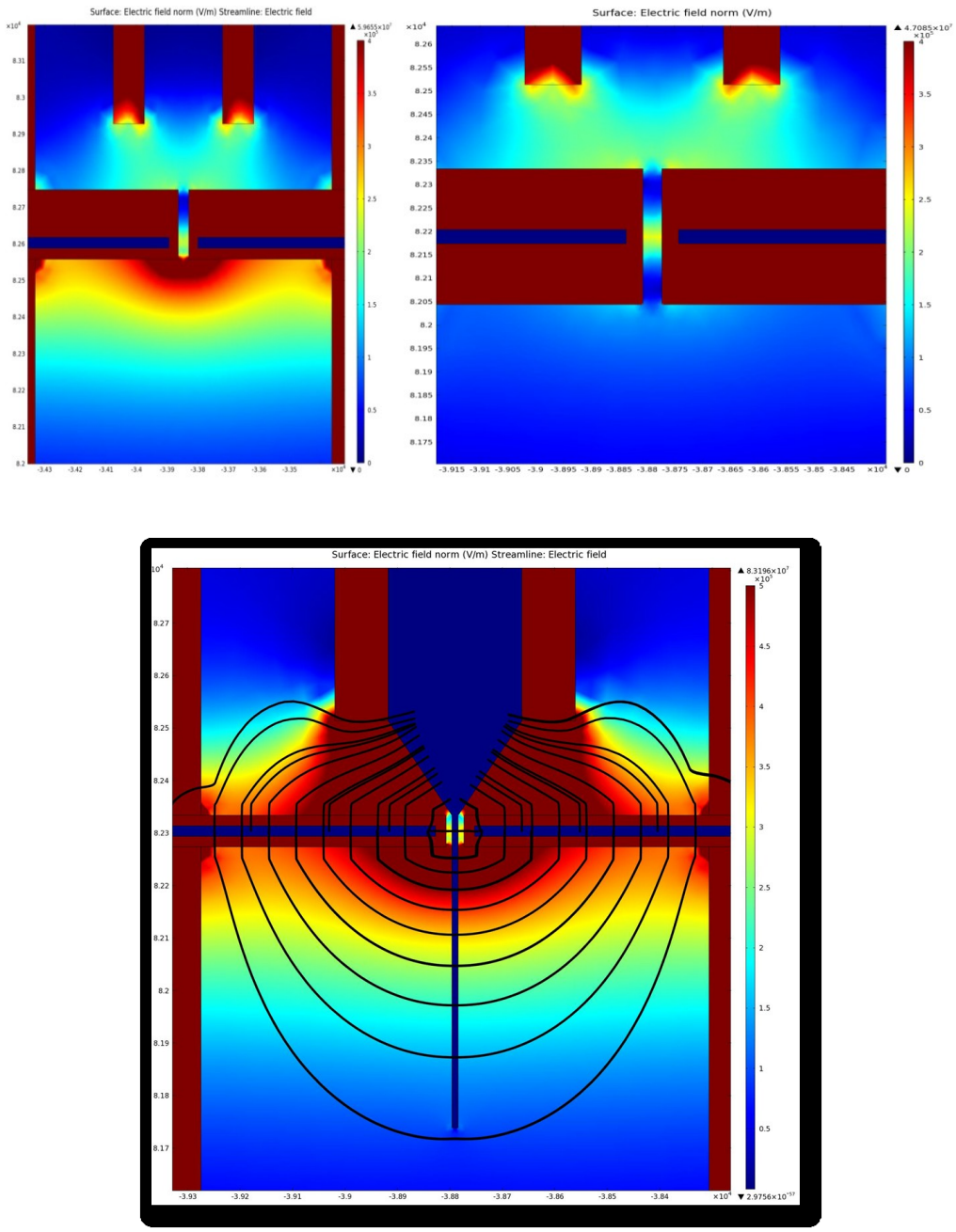

Figure 53: COMSOL was used to simulate the distribution of the electric filed at the nozzle. The black lines indicate the electric field lines.

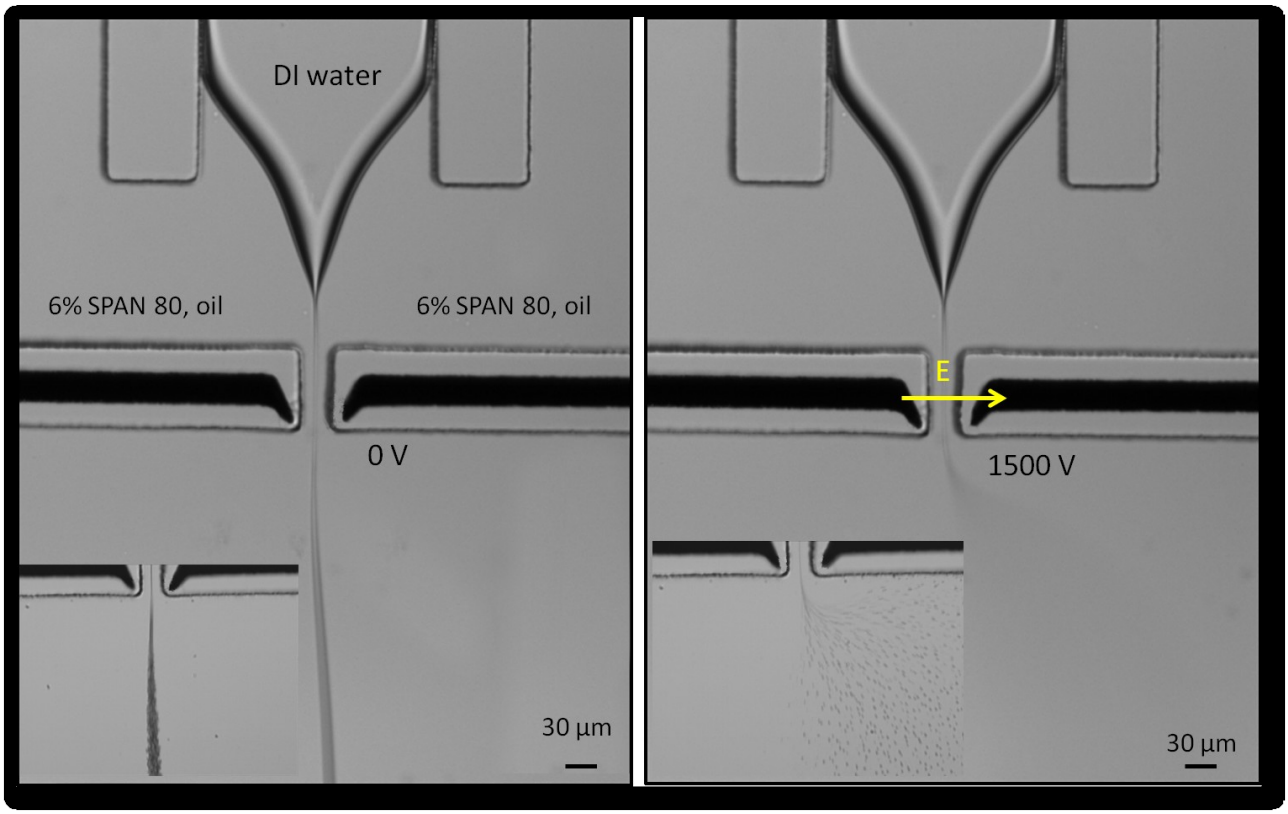

Figure 54: Flow-focusing microfluidic device. The yellow arrow depicts the direction of the applied DC electric field. The small pictures located at the bottom left corners are images taken with a high speed camera.

8.3.2 The droplet size depends on the voltage

We decided to investigate how the strength of the electric field influences the droplet size. During this set of experiments, we kept the flow rate ratio constant and changed the voltage. Results show that the droplet size decreases as the voltage increases (Fig 55). In addition, at this specific flow rate ratio, which is the smallest flow rate ratio that we can get with the particular experimental system, and at the highest voltage, we were able to generate very fine droplets in the submicron range. This droplet size could not have been achieved without the application of the electric field. Moreover, the droplet

size was measured by collecting a sample of the emulsion and analyzing it by using dynamic light scattering.

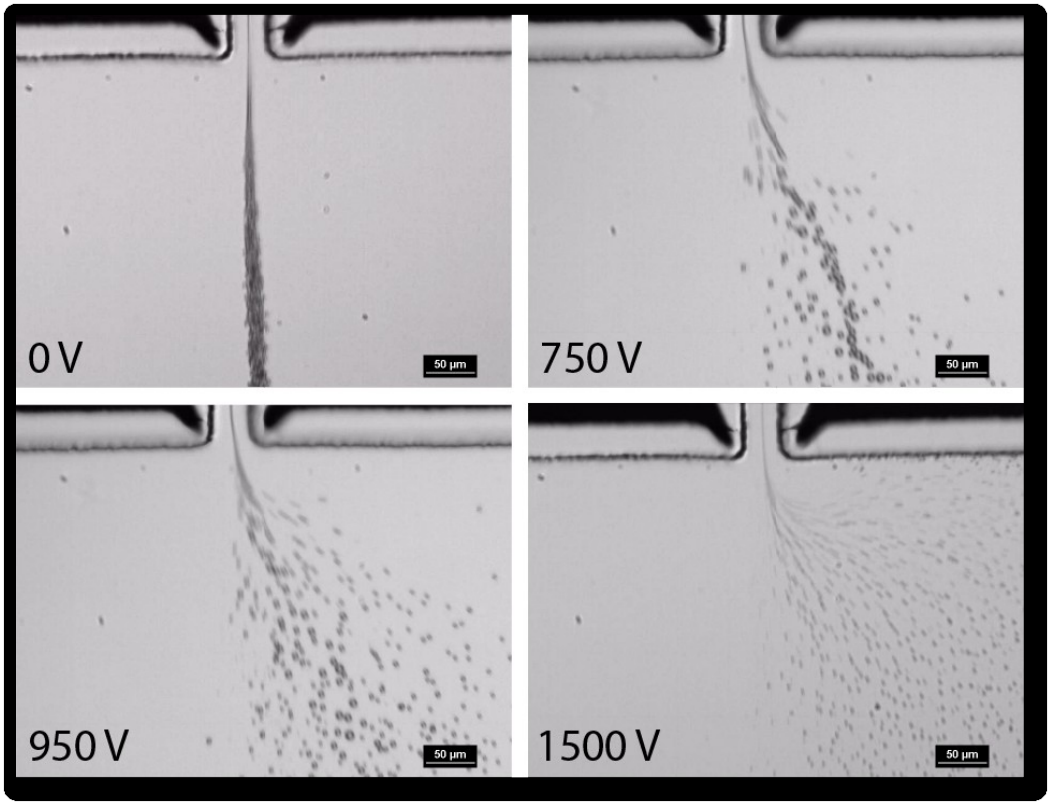

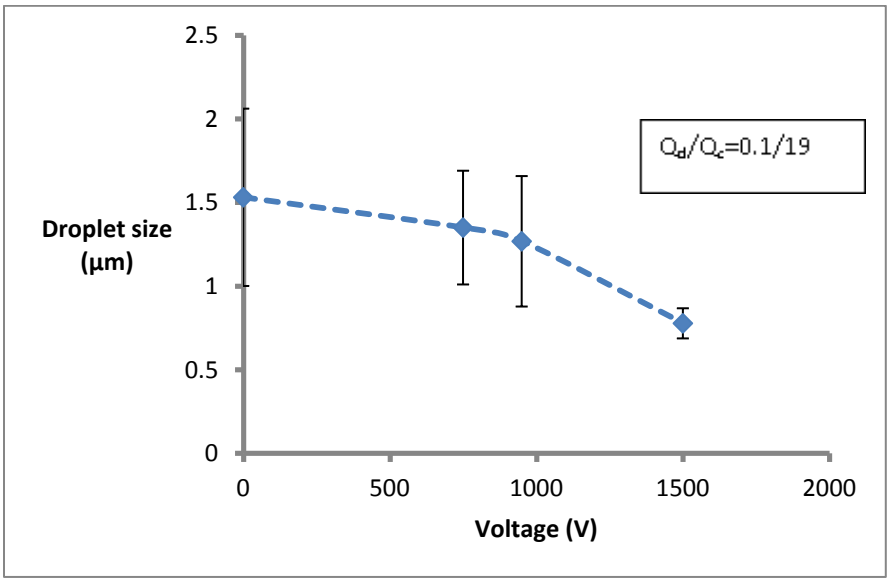

Figure 55: Submicron sized droplet generation. The droplet size is correlated to the strength of the electric field. The results from dynamic light scattering show that the droplet size decreases as the voltage increase.

8.3.3 Higher voltages needed for greater flow rate ratio

During this set of experiments, we increase the flow rate ratio to a 1/19 value in order to examine the impact of the electric field when the dispersed phase is forming a wider thread as compared to the one at the smallest flow rate ratio. A 2000 V was applied through the nozzle, this is the highest voltage that we could apply with the current piece of equipment that we have in the lab. Data show that the effect of the electric filed was not enough to break up the water thread into small droplets (Fig 56). The next chapter describes the method used to solve the issue.

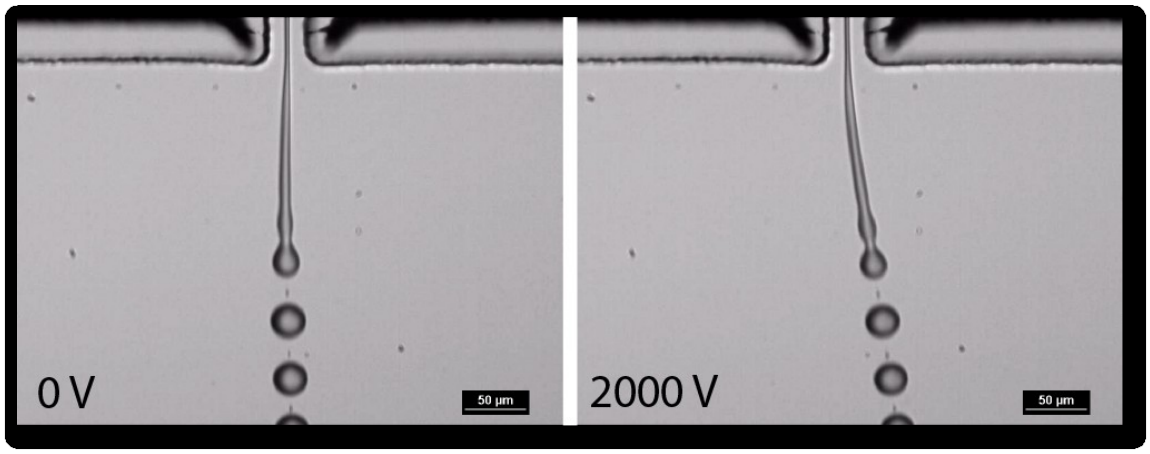

Figure 56: The electric field is not strong enough to break the water thread into droplets. The water thread was tilted to the right when the highest value of the electric field was applied.

8.3.4 Carbon Black Electrodes with Openings

In order for us to deliver a stronger electric field by applying the same potential difference, we fabricated carbon black electrodes with openings. When the carbon black electrodes were surrounded with a PDMS membrane, the resistance that the electric field encountered was high. Therefore, we decided to fabricate electrodes that contained openings and those openings, allow a stronger electric field to be delivered at the interface (Fig 57).

Results show that this design of the electrodes allowed us to deliver a stronger electric field at the interface, which was enough to break the wider thread of water into droplets (Fig 57).

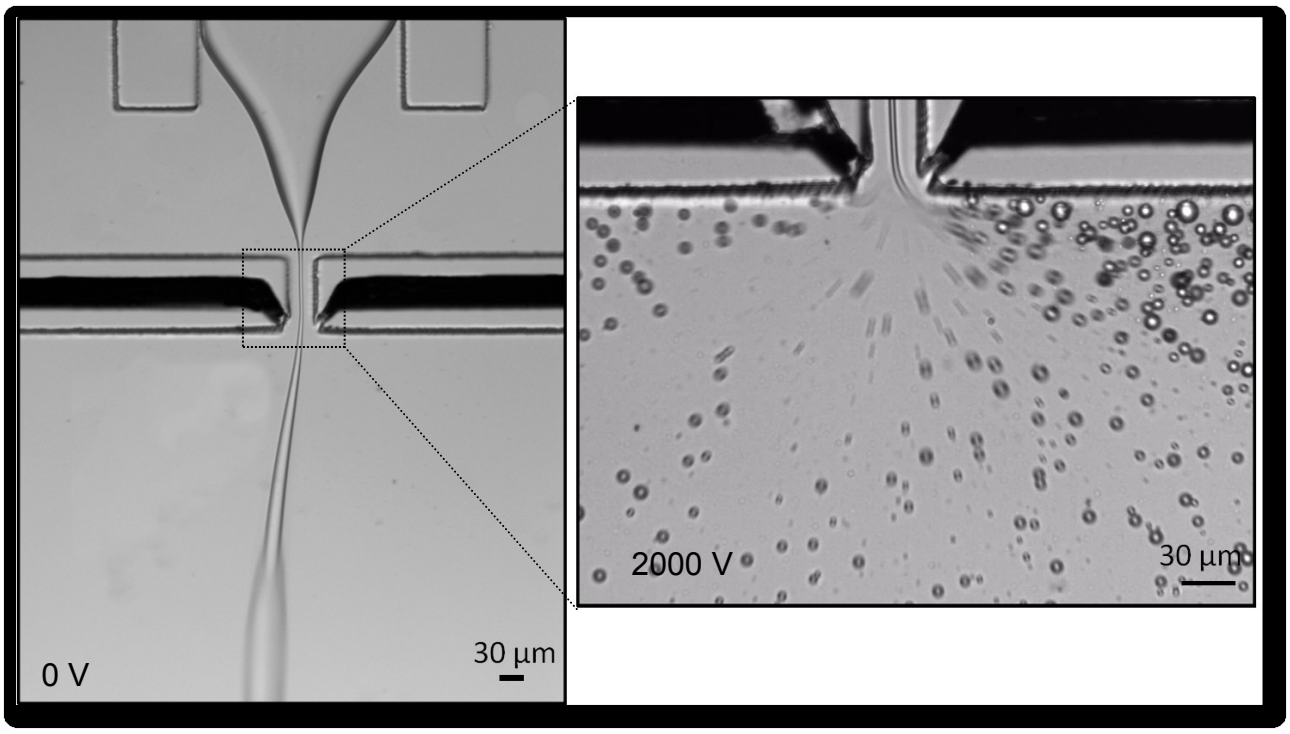

Figure 57: Carbon black electrodes with openings provide smaller resistance to the electric field.

8.3.5 Increased the Viscosity of the Disperse Phase

The parameters that we have changed so far are the flow rates ratio and the strength of the electric field. Next we decided to investigate how the system will behave if we increase the viscosity of the disperse phase. We fabricated a new pair of electrodes where each electrode contained three openings. Next we increased the viscosity of the water by dissolving 17% dextran in water. When the electric field was on, the thread of the dispersed phase close to the nozzle was oscillating, and further down the main outlet, droplets were generated (Fig 58). After observing this behavior, we decided to use the system for mixing.

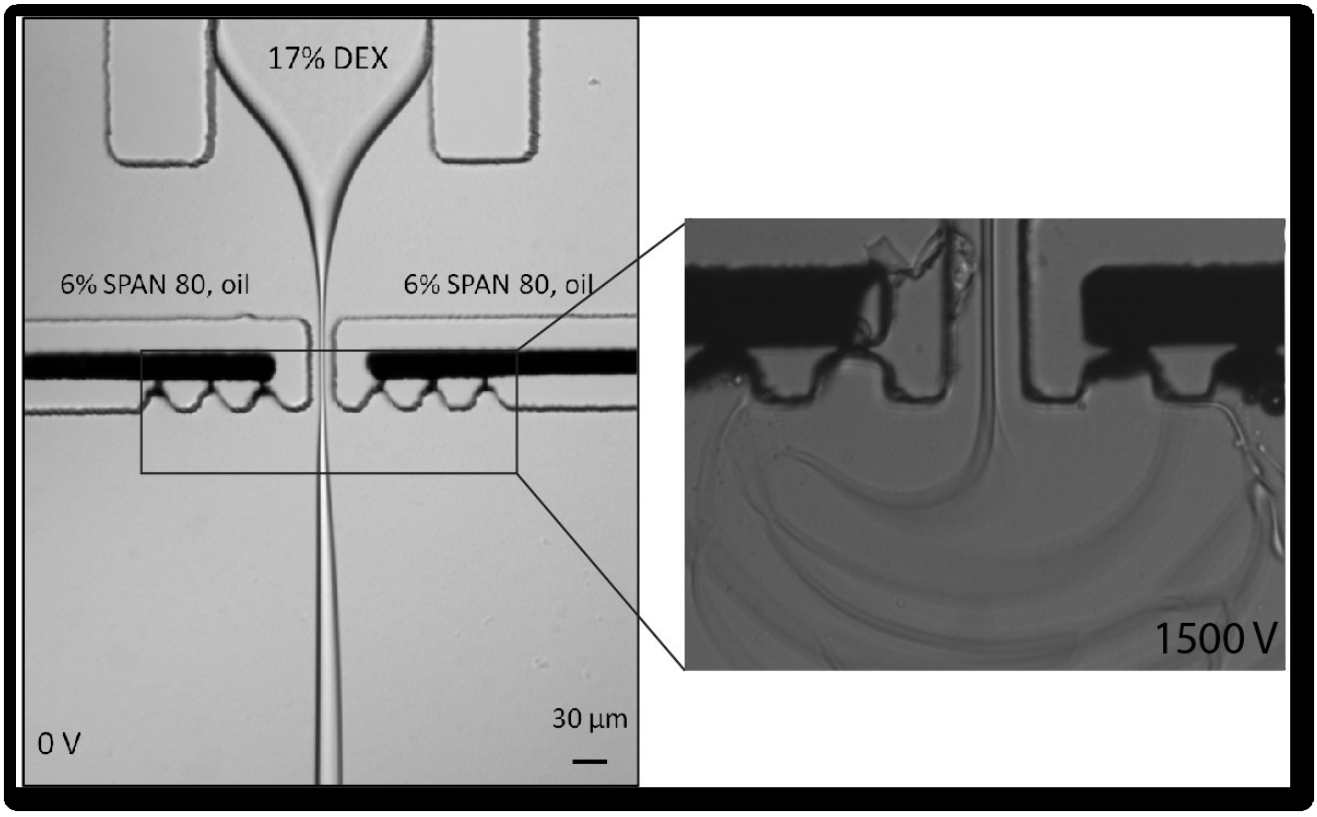

Figure 58: A whipping effect was observed when the viscosity of the dispersed phase was increased.

8.3.6 Water-in-Water-in-Oil emulsion in one step

We decided to use the whipping effect to generate double emulsions in one step. We fabricated a new device which contained three inlets in contrast with the previous devices which had two inlets. We delivered the dispersed phase, mineral oil, through one inlet, and we also delivered solutions of peg and dextran through the remaining two inlets (Fig 59). We found that when a 2000 V electric field was applied droplets of dextran-in-peg-in-oil were produced (Fig 59). Therefore, here we generated a system that can produce a double emulsion by having only one nozzle in contrast with the conventional assays that contain two constriction areas.

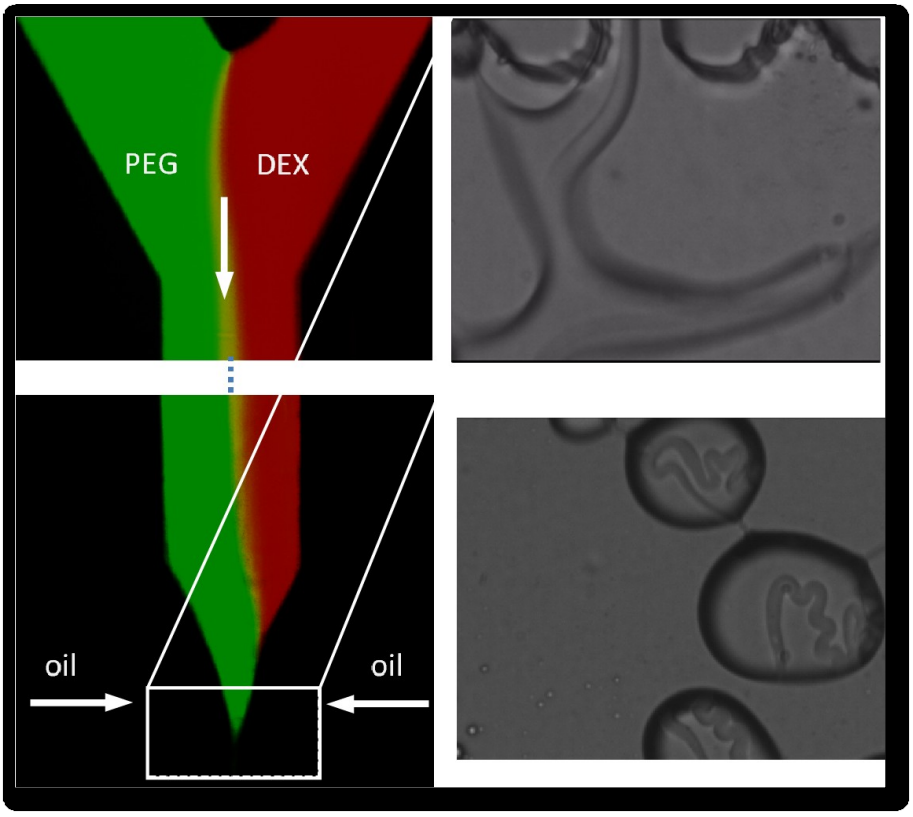

Figure 59: Generation of double emulsion W/W/O in one step. Droplets of Dextran-in-Peg-in-oil are produced by using only one nozzle

8.4 Conclusions

To summarize, our results showed that we can tune the droplet size by using DC electric field as an external source. Specifically, we found that at a constant flow rate ratio, the droplet size decreases as the strength of the electric field increases. Moreover, we were able to generate very fine droplets in the submicron range. Lastly, we developed a microfluidic device that can produce double emulsions by only containing one constriction region in contrast with conventional microfluidic devices, which contain two nozzles in order to produce double emulsions.

8.5 Future work

During all the work that is described in this chapter, we were using mineral oil as the continuous phase. Next, we decided to switch the dispersed phase with the continuous phase. Therefore, we used water as the continuous phase, and we ran into problems such as Faraday reaction occur at the points where the electrodes were in contact with the water. Another issue that we faced was that we had to generate electrodes with openings in order to deliver sufficient electric field at the interface in order to be able to break the wide water thread into small droplets. To address these issues, we propose the use of a alternate current electric field which will allow us to deliver a stronger electric field and to prevent the Faraday reactions from occurring.

REFERENCES

Ananthakrishnan, R., and A. Ehrlicher. 2007. The forces behind cell movement. *Int J Biol Sci*. 3:303-317.

Anna, S.L., N. Bontoux, and H.A. Stone. 2003. Formation of dispersions using "flow focusing" in microchannels. *Applied physics letters*.

Atencia, J., G.A. Cooksey, and L.E. Locascio. 2012. A robust diffusion-based gradient generator for dynamic cell assays. *Lab on a chip*. 12:309-316.

Bergert, M., S.D. Chandradoss, R.A. Desai, and E. Paluch. 2012. Cell mechanics control rapid transitions between blebs and lamellipodia during migration. *Proc Natl Acad Sci U S A*. 109:14434-14439.

Blaser, H., M. Reichman-Fried, I. Castanon, K. Dumstrei, F.L. Marlow, K. Kawakami, L. Solnica-Krezel, C.P. Heisenberg, and E. Raz. 2006. Migration of zebrafish primordial germ cells: a role for myosin contraction and cytoplasmic flow. *Developmental cell*. 11:613-627.

Bosgraaf, L., H. Russcher, J.L. Smith, D. Wessels, D.R. Soll, and P.J. Van Haastert. 2002. A novel cGMP signalling pathway mediating myosin phosphorylation and chemotaxis in Dictyostelium. *EMBO J*. 21:4560-4570.

Bosgraaf, L., and P.J. van Haastert. 2006. The regulation of myosin II in Dictyostelium. *European journal of cell biology*. 85:969-979.

Bozzaro, S. 2013. The model organism Dictyostelium discoideum. *Methods in molecular biology*. 983:17-37.

Bravo-Cordero, J.J., L. Hodgson, and J. Condeelis. 2012. Directed cell invasion and migration during metastasis. *Current Opinion in Cell Biology*. 24:277-283.

Breckenridge, M.T., T.T. Egelhoff, and H. Baskaran. 2010. A microfluidic imaging chamber for the direct observation of chemotactic transmigration. *Biomed Microdevices*. 12:543-553.

Cavanagh, L., and W. Weninger. 2008. Dendritic cell behaviour in vivo: lessons learned from intravital two-photon microscopy. *Immunology and cell biology*. 86:428-438.

Chan, B., P.A. VanderLaan, and V.P. Sukhatme. 2013. 6-Phosphogluconate dehydrogenase regulates tumor cell migration in vitro by regulating receptor tyrosine kinase c-Met. *Biochem Bioph Res Co*. 439:247-251.

Charras, G., and E. Paluch. 2008. Blebs lead the way: how to migrate without lamellipodia. *Nat Rev Mol Cell Bio*. 9:730-736.

Charras, G., J. Yarrow, M. Horton, L. Mahadevan, and T. Mitchison. 2005. Non-equilibration of hydrostatic pressure in blebbing cells. *Nature*. 435:365-369.

Chhabra, E.S., and H.N. Higgs. 2007. The many faces of actin: matching assembly factors with cellular structures. *Nat Cell Biol*. 9:1110-1121.

Choi, C.H., J.H. Jung, Y.W. Rhee, D.P. Kim, and S.E. Shim. 2007. Generation of monodisperse alginate microbeads and in situ encapsulation of cell in microfluidic device. *Biomedical …*.

Corall, S., T. Haraszti, T. Bartoschik, J.P. Spatz, T. Ludwig, and E.A. Cavalcanti-Adam. 2014. 1-integrin and MT1-MMP promote tumor cell migration in 2D but not in 3D fibronectin microenvironments. *Comput Mech*. 53:499-510.

Cramer, C., P. Fischer, and E.J. Windhab. 2004. Drop formation in a co-flowing ambient fluid. *Chemical Engineering Science*.

de la Roche, M.A., and G.P. Cote. 2001. Regulation of Dictyostelium myosin I and II. *Biochimica et biophysica acta*. 1525:245-261.

Dreyfus, R., P. Tabeling, and H. Willaime. 2003. Ordered and disordered patterns in two-phase flows in microchannels. *Physical review letters*.

Eichinger, L., J.A. Pachebat, G. Glockner, M.A. Rajandream, R. Sucgang, M. Berriman, J. Song, R. Olsen, K. Szafranski, Q. Xu, B. Tunggal, S. Kummerfeld, M. Madera, B.A. Konfortov, F. Rivero, A.T. Bankier,

R. Lehmann, N. Hamlin, R. Davies, P. Gaudet, P. Fey, K. Pilcher, G. Chen, D. Saunders, E. Sodergren, P. Davis, A. Kerhornou, X. Nie, N. Hall, C. Anjard, L. Hemphill, N. Bason, P. Farbrother, B. Desany, E. Just, T. Morio, R. Rost, C. Churcher, J. Cooper, S. Haydock, N. van Driessche, A. Cronin, I. Goodhead, D. Muzny, T. Mourier, A. Pain, M. Lu, D. Harper, R. Lindsay, H. Hauser, K. James, M. Quiles, M. Madan Babu, T. Saito, C. Buchrieser, A. Wardroper, M. Felder, M. Thangavelu, D. Johnson, A. Knights, H. Loulseged, K. Mungall, K. Oliver, C. Price, M.A. Quail, H. Urushihara, J. Hernandez, E. Rabbinowitsch, D. Steffen, M. Sanders, J. Ma, Y. Kohara, S. Sharp, M. Simmonds, S. Spiegler, A. Tivey, S. Sugano, B. White, D. Walker, J. Woodward, T. Winckler, Y. Tanaka, G. Shaulsky, M. Schleicher, G. Weinstock, A. Rosenthal, E.C. Cox, R.L. Chisholm, R. Gibbs, W.F. Loomis, M. Platzer, R.R. Kay, J. Williams, P.H. Dear, A.A. Noegel, B. Barrell, and A. Kuspa. 2005. The genome of the social amoeba Dictyostelium discoideum. *Nature*. 435:43-57.

Faix, J., D. Breitsprecher, T.E. Stradal, and K. Rottner. 2009. Filopodia: Complex models for simple rods. *The international journal of biochemistry & cell biology*. 41:1656-1664.

Fisher, P.R., R. Merkl, and G. Gerisch. 1989. Quantitative analysis of cell motility and chemotaxis in Dictyostelium discoideum by using an image processing system and a novel chemotaxis chamber providing stationary chemical gradients. *The Journal of cell biology*. 108:973-984.

Fitzpatrick, E., S. McBride, J. Yavelow, and S. Najmi. 2006. Microfluidic techniques for single-cell protein expression analysis. *Clinical …*.

Fletcher, D.A., and D. Mullins. 2010. Cell mechanics and the cytoskeleton. *Nature*. 463:485-492.

Friedl, P., S. Borgmann, and E.B. Brocker. 2002. Amoeboid leukocyte crawling through extracellular matrix: lessons from the Dictyostelium paradigm of cell movement. (vol 70, pg 491, 2001). *J Leukocyte Biol*. 71:377-377.

Fujiwara, I., S. Takahashi, H. Tadakuma, T. Funatsu, and S. Ishiwata. 2002. Microscopic analysis of polymerization dynamics with individual actin filaments. *Nature Cell Biology*. 4:666-673.

Gadea, G., M. de Toledo, C. Anguille, and P. Roux. 2007. Loss of p53 promotes RhoA-ROCK-dependent cell migration and invasion in 3D matrices. *J Cell Biol*. 178:23-30.

Gauthier, N., M. Fardin, P. Roca-Cusachs, and M. Sheetz. 2011. Temporary increase in plasma membrane tension coordinates the activation of exocytosis and contraction during cell spreading. *Proceedings of the National Academy of Sciences of the United States of America*. 108:14467-14472.

Goldman, R.D., S. Khuon, Y.H. Chou, P. Opal, and P.M. Steinert. 1996. The function of intermediate filaments in cell shape and cytoskeletal integrity. *Journal of Cell Biology*. 134:971-983.

Hamill, O.P., and B. Martinac. 2001. Molecular basis of mechanotransduction in living cells. *Physiological reviews*. 81:685-740.

Heuze, M.L., O. Collin, E. Terriac, A.M. Lennon-Dumenil, and M. Piel. 2011. Cell migration in confinement: a micro-channel-based assay. *Methods in molecular biology*. 769:415-434.

Huang, C.H., M. Tang, C.J. Shi, P.A. Iglesias, and P.N. Devreotes. 2013. An excitable signal integrator couples to an idling cytoskeletal oscillator to drive cell migration. *Nature Cell Biology*. 15:1307-U1108.

Huang, Y., B. Agrawal, D. Sun, J.S. Kuo, and J.C. Williams. 2011. Microfluidics-based devices: New tools for studying cancer and cancer stem cell migration. *Biomicrofluidics*. 5:13412.

Huebner, A., L.F. Olguin, D. Bratton, and G. Whyte. 2008. Development of quantitative cell-based enzyme assays in microdroplets. *Analytical …*.

Hung, W.C., J.R. Yang, C.L. Yankaskas, B.S. Wong, P.H. Wu, C. Pardo-Pastor, S.A. Serra, M.J. Chiang, Z. Gu, D. Wirtz, M.A. Valverde, J.T. Yang, J. Zhang, and K. Konstantopoulos. 2016. Confinement Sensing and Signal Optimization via Piezo1/PKA and Myosin II Pathways. *Cell reports*. 15:1430-1441.

Insall, R. 2010. Understanding eukaryotic chemotaxis: a pseudopod-centred view. *Nature reviews. Molecular cell biology*. 11:453-458.

Irimia, D., D.A. Geba, and M. Toner. 2006. Universal microfluidic gradient generator. *Analytical chemistry*. 78:3472-3477.

Irimia, D., and M. Toner. 2009. Spontaneous migration of cancer cells under conditions of mechanical confinement. *Integr Biol (Camb)*. 1:506-512.

Jeon, N.L., S.K.W. Dertinger, D.T. Chiu, I.S. Choi, A.D. Stroock, and G.M. Whitesides. 2000. Generation of solution and surface gradients using microfluidic systems. *Langmuir*. 16:8311-8316.

Jowhar, D., G. Wright, P.C. Samson, J.P. Wikswo, and C. Janetopoulos. 2010. Open access microfluidic device for the study of cell migration during chemotaxis. *Integr Biol (Camb)*. 2:648-658.

Kay, R.R., P. Langridge, D. Traynor, and O. Hoeller. 2008. Changing directions in the study of chemotaxis. *Nature reviews. Molecular cell biology*. 9:455-463.

Keenan, T.M., and A. Folch. 2008. Biomolecular gradients in cell culture systems. *Lab on a chip*. 8:34-57.

Kim, J., M. Junkin, D.H. Kim, S. Kwon, and Y.S. Shin. 2009. Applications, techniques, and microfluidic interfacing for nanoscale biosensing. *Microfluidics and …*.

Kim, S., H. Kim, and N. Jeon. 2010. Biological applications of microfluidic gradient devices. *Integrative biology : quantitative biosciences from nano to macro*. 2:584-603.

King, J.S., and R.H. Insall. 2009. Chemotaxis: finding the way forward with Dictyostelium. *Trends in cell biology*. 19:523-530.

Kolaczkowska, E., and P. Kubes. 2013. Neutrophil recruitment and function in health and inflammation. *Nat Rev Immunol*. 13:159-175.

Laevsky, G., and D.A. Knecht. 2001. Under-agarose folate chemotaxis of Dictyostelium discoideum amoebae in permissive and mechanically inhibited conditions. *Biotechniques*. 31:1140-+.

Laevsky, G., and D.A. Knecht. 2003. Cross-linking of actin filaments by myosin II is a major contributor to cortical integrity and cell motility in restrictive environments. *Journal of cell science*. 116:3761-3770.

Lammermann, T., B.L. Bader, S.J. Monkley, T. Worbs, R. Wedlich-Soldner, K. Hirsch, M. Keller, R. Forster, D.R. Critchley, R. Fassler, and M. Sixt. 2008. Rapid leukocyte migration by integrin-independent flowing and squeezing. *Nature*. 453:51-+.

Lammermann, T., and M. Sixt. 2009. Mechanical modes of 'amoeboid' cell migration. *Curr Opin Cell Biol*. 21:636-644.

Langridge, P., and R. Kay. 2006. Blebbing of Dictyostelium cells in response to chemoattractant. *Experimental cell research*. 312:2009-2017.

Lauffenburger, D.A., and A.F. Horwitz. 1996. Cell migration: A physically integrated molecular process. *Cell*. 84:359-369.

Li, J., and F. Lin. 2011. Microfluidic devices for studying chemotaxis and electrotaxis. *Trends in cell biology*. 21:489-497.

Li, L., S.F. Norrelykke, and E.C. Cox. 2008. Persistent Cell Motion in the Absence of External Signals: A Search Strategy for Eukaryotic Cells. *Plos One*. 3.

Lin, F., C.M. Nguyen, S.J. Wang, W. Saadi, S.P. Gross, and N.L. Jeon. 2004. Effective neutrophil chemotaxis is strongly influenced by mean IL-8 concentration. *Biochem Biophys Res Commun*. 319:576-581.

Liu, Y.J., L.M. Berre, F. Lautenschlaeger, and P. Maiuri. 2015. Confinement and low adhesion induce fast amoeboid migration of slow mesenchymal cells. *Cell*.

Long, T., and R.M. Ford. 2009. Enhanced transverse migration of bacteria by chemotaxis in a porous T-sensor. *Environmental science & technology*. 43:1546-1552.

Loomis, W.F., D. Fuller, E. Gutierrez, A. Groisman, and W.J. Rappel. 2012. Innate non-specific cell substratum adhesion. *Plos One*. 7:e42033.

Luo, T., K. Mohan, P.A. Iglesias, and D.N. Robinson. 2013. Molecular mechanisms of cellular mechanosensing. *Nature materials*. 12:1064-1071.

Manahan, C.L., P.A. Iglesias, Y. Long, and P.N. Devreotes. 2004. Chemoattractant signaling in Dictyostelium discoideum. *Annual Review of Cell and Developmental Biology*. 20:223-253.

Martin, P., and S.M. Parkhurst. 2004. Parallels between tissue repair and embryo morphogenesis. *Development*. 131:3021-3034.

Maugis, B., J. Brugues, P. Nassoy, N. Guillen, P. Sens, and F. Amblard. 2010. Dynamic instability of the intracellular pressure drives bleb-based motility. *Journal of cell science*. 123:3884-3892.

Mavrogiannis, N., M. Ibo, X. Fu, F. Crivellari, and Z. Gagnon. 2016. Microfluidics made easy: A robust low-cost constant pressure flow controller for engineers and cell biologists. *Biomicrofluidics*. 10:034107.

Mills, J., N. Stone, J. Erhardt, and R. Pittman. 1998. Apoptotic membrane blebbing is regulated by myosin light chain phosphorylation. *The Journal of cell biology*. 140:627-636.

Paluch, E., C. Sykes, J. Prost, and M. Bornens. 2006. Dynamic modes of the cortical actomyosin gel during cell locomotion and division. *Trends in cell biology*. 16:5-10.

Paluch, E.K., and E. Raz. 2013. The role and regulation of blebs in cell migration. *Current Opinion in Cell Biology*. 25:582-590.

Pollard, T.D., and C.C. Beltzner. 2002. Structure and function of the Arp2/3 complex. *Curr Opin Struc Biol*. 12:768-774.

Pollard, T.D., and G.G. Borisy. 2003. Cellular motility driven by assembly and disassembly of actin filaments. *Cell*. 112:453-465.

Richardson, B.E., and R. Lehmann. 2010. Mechanisms guiding primordial germ cell migration: strategies from different organisms. *Nature Reviews Molecular Cell Biology*. 11:37-49.

Ridley, A.J. 2011. Life at the leading edge. *Cell*. 145:1012-1022.

Roussos, E.T., J.S. Condeelis, and A. Patsialou. 2011. Chemotaxis in cancer. *Nat Rev Cancer*. 11:573-587.

Ruprecht, V., S. Wieser, A. Callan-Jones, M. Smutny, H. Morita, K. Sako, V. Barone, M. Ritsch-Marte, M. Sixt, R. Voituriez, and C.P. Heisenberg. 2015. Cortical contractility triggers a stochastic switch to fast amoeboid cell motility. *Cell*. 160:673-685.

Saadi, W., S.J. Wang, F. Lin, and N.L. Jeon. 2006. A parallel-gradient microfluidic chamber for quantitative analysis of breast cancer cell chemotaxis. *Biomed Microdevices*. 8:109-118.

Sahai, E. 2005. Mechanisms of cancer cell invasion. *Current opinion in genetics & development*. 15:87-96.

Sahai, E., and C. Marshall. 2003. Differing modes of tumour cell invasion have distinct requirements for Rho/ROCK signalling and extracellular proteolysis. *Nature cell biology*. 5:711-719.

Salbreux, G., G. Charras, and E. Paluch. 2012. Actin cortex mechanics and cellular morphogenesis. *Trends in cell biology*. 22:536-545.

Skoge, M., M. Adler, A. Groisman, H. Levine, W.F. Loomis, and W.J. Rappel. 2010. Gradient sensing in defined chemotactic fields. *Integr Biol (Camb)*. 2:659-668.

Song, H., D.L. Chen, and R.F. Ismagilov. 2006a. Reactions in droplets in microfluidic channels. *… chemie international edition*.

Song, L., S.M. Nadkarni, H.U. Bodeker, C. Beta, A. Bae, C. Franck, W.J. Rappel, W.F. Loomis, and E. Bodenschatz. 2006b. Dictyostelium discoideum chemotaxis: threshold for directed motion. *European journal of cell biology*. 85:981-989.

Srisa-Art, M., A.J. deMello, and J.B. Edel. 2007. High-throughput DNA droplet assays using picoliter reactor volumes. *Analytical chemistry*.

Srivastava, V., P.A. Iglesias, and D.N. Robinson. 2015. Cytokinesis: Robust cell shape regulation. *Seminars in cell & developmental biology*. 53:39-44.

Stewart, M., J. Helenius, Y. Toyoda, S. Ramanathan, D. Muller, and A. Hyman. 2011. Hydrostatic pressure and the actomyosin cortex drive mitotic cell rounding. *Nature*. 469:226-230.

Swaney, K.F., C.H. Huang, and P.N. Devreotes. 2010. Eukaryotic chemotaxis: a network of signaling pathways controls motility, directional sensing, and polarity. *Annual review of biophysics*. 39:265-289.

Tinevez, J.Y., U. Schulze, G. Salbreux, J. Roensch, J.F. Joanny, and E. Paluch. 2009. Role of cortical tension in bleb growth. *Proc Natl Acad Sci U S A*. 106:18581-18586.

Tong, Z.Q., E.M. Balzer, M.R. Dallas, W.C. Hung, K.J. Stebe, and K. Konstantopoulos. 2012. Chemotaxis of Cell Populations through Confined Spaces at Single-Cell Resolution. *Plos One*. 7:e29211.

Tozluoglu, M., A.L. Tournier, R.P. Jenkins, S. Hooper, P.A. Bates, and E. Sahai. 2013. Matrix geometry determines optimal cancer cell migration strategy and modulates response to interventions. *Nat Cell Biol*. 15:751-762.

Trinkaus, J. 1973. Surface activity and locomotion of Fundulus deep cells during blastula and gastrula stages. *Developmental biology*. 30:69-103.

Tyson, R.A., E. Zatulovskiy, R.R. Kay, and T. Bretschneider. 2014. How blebs and pseudopods cooperate during chemotaxis. *Proc Natl Acad Sci U S A*. 111:11703-11708.

vanHaastert, P.J.M., and H. Kuwayama. 1997. CGMP as second messenger during Dictyostelium chemotaxis. *Febs Lett*. 410:25-28.

Vicente-Manzanares, M., X. Ma, R.S. Adelstein, and A.R. Horwitz. 2009. Non-muscle myosin II takes centre stage in cell adhesion and migration. *Nature reviews. Molecular cell biology*. 10:778-790.

Vicente-Manzanares, M., D.J. Webb, and A.R. Horwitz. 2005. Cell migration at a glance. *Journal of cell science*. 118.

Vorotnikov, A.V. 2011. Chemotaxis: Movement, direction, control. *Biochemistry-Moscow+*. 76:1528-1555.

Wang, P., S.H. Chen, W.C. Hung, C. Paul, F. Zhu, P.P. Guan, D.L. Huso, A. Kontrogianni-Konstantopoulos, and K. Konstantopoulos. 2015. Fluid shear promotes chondrosarcoma cell invasion by activating matrix metalloproteinase 12 via IGF-2 and VEGF signaling pathways. *Oncogene*. 34:4558-4569.

Willard, S.S., and P.N. Devreotes. 2006. Signaling pathways mediating chemotaxis in the social amoeba, Dictyostelium discoideum. *European journal of cell biology*. 85:897-904.

Wirtz, D., K. Konstantopoulos, and P.C. Searson. 2011. The physics of cancer: the role of physical interactions and mechanical forces in metastasis. *Nat Rev Cancer*. 11:512-522.

Wolf, K., I. Mazo, H. Leung, K. Engelke, U. von Andrian, E. Deryugina, A. Strongin, E.-B. Bröcker, and P. Friedl. 2003. Compensation mechanism in tumor cell migration: mesenchymal-amoeboid transition after blocking of pericellular proteolysis. *The Journal of cell biology*. 160:267-277.

Xu, J.H., S.W. Li, J. Tan, Y.J. Wang, and G.S. Luo. 2006. Preparation of highly monodisperse droplet in a T-junction microfluidic device. *AIChE journal*.

Yoshida, K., and T. Soldati. 2006. Dissection of amoeboid movement into two mechanically distinct modes. *Journal of cell science*. 119:3833-3844.

Zatulovskiy, E., R. Tyson, T. Bretschneider, and R.R. Kay. 2014. Bleb-driven chemotaxis of Dictyostelium cells. *J Cell Biol*. 204:1027-1044.

Zhao, C.X. 2013. Multiphase flow microfluidics for the production of single or multiple emulsions for drug delivery. *Adv Drug Deliver Rev*. 65:1420-1446.

CURRICULUM VITAE

Markela Ibo

116 West University Parkway, Baltimore, MD 21210
Phone: 443-509-3149
Email: mibo1@jhu.edu

PROFILE

- A self-motivated Ph.D. candidate in Chemical and Biomolecular Engineering with five years of multidisciplinary research experience in bioengineering, microfluidics, biochemistry, emulsion technology, molecular and systems biology.
- Extensive understanding of experimental design, analytical and quantitative skills with strong record of productivity.
- Strong organizational and interpersonal skills. Managed multiple projects independently and through collaborations. Delivered multiple technical presentations to audiences with different backgrounds.
- Excited to acquire new knowledge and expertise in order to make a positive impact on changing patients' lives.

EDUCATION

Johns Hopkins University (Baltimore, MD) **Aug 2011- Feb 2017**
Ph.D. Chemical and Biomolecular Engineering (ChemBE) **(Expected)**

Aristotle University of Thessaloniki (Thessaloniki, Greece) **Aug 2006 - Jul 2011**
B.E. Chemical Engineering

- Awarded a three-year fellowship for academic excellence.

WORK EXPERIENCE AND COMMUNITY SERVICE

JHU Engineering Innovation Program (Baltimore, MD) **Jun 2016 - Jul 2016**
Instructor

- Taught various engineering disciplines where students earned JHU credit and developed problem-solving skills.

MedImmune – AstraZeneca (Gaithersburg, MD) **Jun 2015 - Aug 2015**
Drug Delivery and Device Development Group Intern

- Received MedImmune summer intern award. Presenter: Gail Wasserman.
- Conducted research on lipid particle generation for sustained delivery of proteins.

WISE - Women in Science and Engineering Program (Baltimore, MD) **Dec 2014 - May 2016**
Instructor

- Mentored Garrison Forest High School students in engineering.
- Designed laboratory project and assisted with their final presentations.

Science and Technology Program (Baltimore, MD) **July 2013**

Instructor

- Collaboratively taught Benjamin Stoddard Middle School students hands-on laboratory techniques.

Gagnon Laboratory (Baltimore, MD)

Captain **Nov 2011 - Present**

- Develop and operate laboratory; reduce expenses; improve productivity.

RESEARCH EXPERIENCE

JHU – GAGNON LABORATORY (Baltimore, MD) **Dec 2011 - Present**

Cell migration through physically confined microfluidic environments.

- Directed at understanding how physical cues (i.e., confinement, fluid shear stress or electric fields) regulate cell responses pertinent to cancer metastasis, inflammation, embryogenesis, and wound healing.
- Used Polydimethylsiloxane (PDMS) device to examine locomotion of Dictyostelium Discoideum in resistive microfluidic environments.
- Collaborated with ROBINSON LABORATORY, JHU School of Medicine.
- Concluded that cells moving in confined space use different mechanism due to accumulation of mechanoenzyme
  Myosin II at cell cortex.

Generation of water-in-oil-in water emulsion in a microfluidic flow focusing device.

- Studied emulsion generation in microfluidic devices to be used for particle synthesis for biomedicine applications.
- Concluded that droplets in the submicron range could be produced via fragmentation of thin thread of water by applying electric field.

Undergraduate Diploma Thesis (Thessaloniki, Greece) **Sep 2010- May 2011**

- Studied flow and energy transport in porous media by computational fluid dynamics techniques.

CONFERENCES

- **Oral presentation:** Submicron emulsion generation in flow focusing microfluidic devices by using direct current electric field. American Institute of Chemical Engineers (AIChE) 2016 **(San Francisco, CA).**

- **Poster Presentation:** Blebbing of Dictyostelium Discoideum Under Microfluidic Confinement; Advances in Microfluidics & Nanofluidics 2013 **(Notre Dame, IN)**.
- **Attended:** ITP 2012 - 19th International Symposium, Exhibit & Workshops on Electro- and Liquid Phase-separation Techniques **(Baltimore, MD).**

PUBLICATIONS

1) **Ibo M,** Srivastava V, Robinson D, Gagnon Z; *Cell Blebbing in Confined Microfluidic Environments*. **Plos one.**
(Published).
2) Mavrogiannis N, **Ibo M,** Fu X, Crivellari F, Gagnon Z; *Microfluidics made easy: A robust low-cost constant pressure flow controller for engineers and cell biologists.* **Biomicrofluidics.** 2016, 10, 034107.
3) Fu X, Mavrogiannis N, **Ibo M,** Crivellari F, Gagnon Z; *Microfluidic Free-flow Zone Electrophoresis and Isotachophoresis Using Carbon Black Nano-composite PDMS Sidewall Membranes.* **Electrophoresis.** 2016, 00, 1-8.
4) **Ibo M**, Gagnon Z; *Microfluidic Fabrication of Multivesicular Liposomes for Sustained Delivery of Proteins.*
(In preparation).

EXPERTISE

- **Broad knowledge of engineering, biology and microfluidics**
Worked in collaborative multidisciplinary environment. Performed research that encompasses cell motility, design of novel microfluidic devices, biophysics, electrokinetics, and emulsion generation techniques.
- **Biology**
Cell culture, cell transformation, chemotaxis, electrotaxis, flowtaxis, drug response studies, and cellular signaling.
- **Microfluidic techniques**
Design fault-tolerant microfluidic assay devices, PDMS device fabrication, operation of microfluidic devices, syringe pumps, and pressure control instrumentation.
- **Data analysis**
Statistical analysis methods by using GraphPad Prism.
- **Software**
ImageJ, Adobe Illustrator, Comsol Multiphysics, GraphPad Prism, AutoCAD, NIS elements, and Microsoft office suite.
- **Microscopy**
Fluorescence microscopy, Brightfield, and swept field confocal.
- **Emulsion technologies**
Multivesicular liposome (MVL) formation techniques, water-in-oil droplets, and aqueous two phase system (ATP) droplets.
- **Particle sizing methods**
Dynamic light scattering (DLS), laser particle size analyzer (HORIBA).
- **Protein-based assays**

Sodium dodecyl sulfate polyacrylamide gel electrophoresis (SDS-PAGE), size-exclusion chromatography (SEC), and nanodrop UV/VIS spectrophotometer.

LANGUAGE SKILLS

- Fluent in Greek, Albanian, and English.